NASA CONTRACTOR REPORT

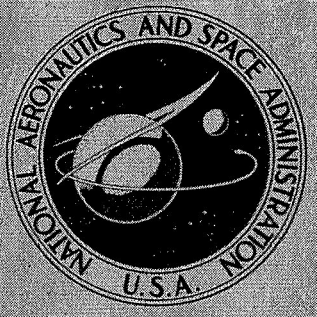

NASA CR-1753

NASA CR-1753

MANNED VEHICLE SYSTEMS ANALYSIS BY MEANS OF MODERN CONTROL THEORY

by David L. Kleinman and Sheldon Baron

Prepared by
BOLT BERANEK AND NEWMAN, INC.
Cambridge, Mass. 02138
for Electronics Research Center

NATIONAL AERONAUTICS AND SPACE ADMINISTRATION • WASHINGTON, D. C. • JUNE 1971

1. Report No.	2. Government Accession No.	3. Recipient's Catalog No.
NASA CR-1753		

4. Title and Subtitle	5. Report Date
MANNED VEHICLE SYSTEMS ANALYSIS BY MEANS OF MODERN CONTROL THEORY	June 1971
	6. Performing Organization Code
7. Author(s) David L. Kleinman and Sheldon Baron	8. Performing Organization Report No.
9. Performing Organization Name and Address Bolt Beranek and Newman Inc. 50 Moulton Street Cambridge, Massachusetts 02138	10. Work Unit No.
	11. Contract or Grant No. NAS12-104
12. Sponsoring Agency Name and Address National Aeronautics and Space Administration Washington, D. C. 20546	13. Type of Report and Period Covered Contractor Report
	14. Sponsoring Agency Code

15. Supplementary Notes

16. Abstract

Modern control and estimation theory is used to provide a framework for the analysis of manned-vehicle systems. By assuming that the human behaves "optimally" in some sense, subject to his inherent psychophysical limitations, a quantitative model is developed for the response characteristics of the human operator. The resultant model can be used to predict task performance, scanning behavior and frequency domain characteristics. The model is described in detail and is used to predict experimentally measured quantities in both single and multi-axis compensatory tracking tasks. Remarkable agreement between measured and predicted quantities is obtained, demonstrating the value and potential of the optimization approach to manned-vehicle systems analysis.

17. Key Words (Selected by Author(s))
Man-machine systems analysis
Human response theory
Optimal control theory
Compensatory tracking

18. Distribution Statement
Unclassified - unlimited

19. Security Classif. (of this report)	20. Security Classif. (of this page)	21. No. of Pages	22. Price
Unclassified	Unclassified	194	$3.00

* For sale by the National Technical Information Service, Springfield, Virginia 22151

TABLE OF CONTENTS

LIST OF ILLUSTRATIONS

LIST OF ILLUSTRATIONS (cont)

LIST OF ILLUSTRATIONS (cont)

LIST OF ILLUSTRATIONS (cont)

INTRODUCTION

The operation of vehicles that transport men and materiel is still largely under the control of people. Research in human response theory, or in that aspect of the theory commonly referred to as "manual control," is aimed at developing the data, models and procedures that will allow such human-controlled vehicles to be designed in an efficient manner. For some time now, Bolt Beranek and Newman Inc. has been conducting a comprehensive program in manual control research. An essential part of this program has been a series of theoretical studies performed under contract to NASA-ERC (NAS12-104). The basic goal of these efforts was the development of models of the human operator that could be systematically and easily used to predict pilot behavior and system performance in complex control tasks. This report presents the latest results of these theoretical studies and reflects our current status with respect to achieving the above goal.

Modern research in manual control had its origins in the 1940's. Until recently, the efforts were based primarily on statistical communications theory and on what has become known as classical control theory. As might be expected, most of the work was devoted to obtaining an understanding of human control behavior in the performance of relatively simple tasks. Typically, the controller's task was one of compensatory tracking, involving a single display indicator and a single control input. The work of Russell [1], Elkind [2], McRuer and Krendel [3] and McRuer, Graham, Krendel and Reisner [4], resulted in a set of quasi-linear models that were surprisingly adept at predicting human behavior in this simple but important class of problems. In essence, this work indicated that the human controller attempted to adopt a control strategy that would result in closed-loop performance

comparable to that of a good feedback control system. The work is well summarized in the excellent report of McRuer, et.al. [4].

Attempts to analyze more complex manual control systems began about 1960. For the most part these efforts concentrated on the problem of developing linear models for the human controller in multivariable, multi-display situations. As regards this problem, two basic approaches have been emerging. The earlier approach, developed primarily by McRuer and his colleagues [5,6], seeks to extend the methods and insights developed for single-axis studies to the multivariable case. Their approach is based on classical multiloop control theory and relies heavily on judgements concerning the closed-loop system structure.

While multiloop analysis has been applied to manual control problems with reasonable success in several instances (See, e.g., References 7 and 8.), difficulties and limitations arise in employing it in a systematic fashion. Rather, one relies on intuition and a good deal of "artistry" in applying the multiloop methods, particularly when pilot control is involved.

The second approach to human controller modelling is rooted in modern control and optimization theory. It is based on the assumption that the human controller is "optimal" in some sense. The notion of the optimality of the human operator is not a new one. Several researchers have attempted to exploit this general idea in the development of models of human control behavior. Some of the more recent attempts have been made by McRuer, et.al. [9], Elkind, et.al. [10] and Burchfiel, Elkind and Miller [11].

McRuer, et.al. [9] attempted to use an inverse optimal control approach to pilot modelling. This was motivated by an

attempt to remove some of the engineering artistry associated with the use of their verbal adjustment rules for the quasi-linear model. The approach also has merit from the point of view that the pilot is minimizing some subjective cost functional. Unfortunately, they report little success with this approach, probably because of the inherent difficulty of the inverse problem. They report better success in using optimal control theory in a model matching scheme where the model to be matched is the so-called "crossover model." They conclude that optimal control theory and the crossover models can be used effectively to develop a pilot-describing function appropriate to a particular controlled element. It is important to understand that this approach does not really exploit the full potential of modern control theory. The crossover model is a single loop model and when one is confronted with multivariable problems this approach will encounter the same difficulties as multiloop analysis.

Elkind, et.al. [10] used modern optimization theory to predict human behavior in a multivariable tracking task, corresponding to a V/STOL vehicle in hover. The results of that study were quite promising. Predicted controller gains were within a factor of two of measured gains. Techniques for determining variables of importance were suggested and partially verified. Pilot sampling behavior was also predicted with reasonable accuracy although the prediction scheme left something to be desired. Predictions of performance scores were not very good. This was primarily due to the fact that controller remnant was neglected.

Burchfiel, Elkind and Miller [11] attempted to evaluate the hypothesis of human operator optimality in a preliminary study conducted under this contract. They compared human operator behavior with that of an optimal controller in a simple control task

involving a quadratic optimization criterion. Good agreement between human and optimal controller behavior was obtained with differences between the two behaviors accounted for by assuming that the human optimized a slightly different (subjective) cost functional.

We have also used a modern control theory approach in the model development to be described in this report. Our basic assumption is that the well-trained, well-motivated human operator behaves in an optimal manner, *subject to his inherent limitations and constraints*. We are attempting to pursue this assumption to its logical conclusions. Thus, we derive a model for the human operator that contains elements that compensate optimally for his inherent limitations. Indeed, these compensating elements along with the methods for representing the human's limitations are the unique and crucial features of the model.

There are several reasons for choosing to work within a modern control framework. The powerful state-space techniques associated with modern control are ideally suited to the study of multivariable systems. The systematic manner in which these techniques can be applied to multi-input, multi-output systems suggests that many of the difficulties in using multiloop analysis with a "man in the loop" might be overcome.

The approach also facilitates modular development of the human operator model, so that the model can grow "gracefully" as more facets of human behavior are considered and understood. Thus, we have been able to use the same approach to extend the model to account for visual scanning, task interference and operator workload [12]. This was possible because of the single conceptual framework provided by the optimality hypotheses.†

†The hypothesis implies that we always seek a normative model. That is, we attempt to determine what the human should do, given his limitations and the requirements of the task. The fact that this assumption works so well, when the human is properly trained, is convincing evidence of human capability and adaptability.

In this report we first present the theoretical basis for the model of the human operator along with all the equations necessary for its use. Results for some simple control tasks that demonstrate the model's validity are also presented. Then, we examine the sensitivity of model and system outputs to changes in parameters of the model. Next, the model is used to analyze a more complex task related to hover control of VTOL-type vehicles. Preliminary studies to extend the model along with suggestions for further work follow. A manual for the use of computer programs that implement the model is included as an Appendix.

THEORETICAL DEVELOPMENT

In this chapter the mathematical and conceptual developments that underscore our modern control approach to human operator modeling are presented. Since much of the mathematical details of the problem have appeared elsewhere [13], only the major equations that serve to describe the model will be presented, with reference made to any lengthy derivations.

We begin by discussing the class of manual control problems for which the model is designed. Representations of various human limitations are incorporated and their effects are discussed. For simplicity, we analyze first the case where there is no scanning of instruments. Next, the case where the human is free to scan is presented and a means for predicting average sampling behavior is derived within the overall optimization framework.

Single-Axis Control — No Scanning

Vehicle dynamics and display. — A simplified representation of the pilot-vehicle-display system considered is shown in Fig. 1. The human operator's basic task is to control, in some prescribed way, a dynamical system that is subject to external random disturbances. One or more system outputs $\underline{y}(t) = \text{col}[y_1(t), y_2(t) \ldots y_m(t)]$ may be of concern, and it is assumed that they are presented continuously to the human via some visual display or instrument panel.†

For simplicity, we assume that the human manipulates a single (scalar) control u(t) through which he can exercise control over

†We examine situations in which visual cues dominate. However, there is no apparent mathematical restriction that would prohibit the consideration of motion or kinesthetic cues.

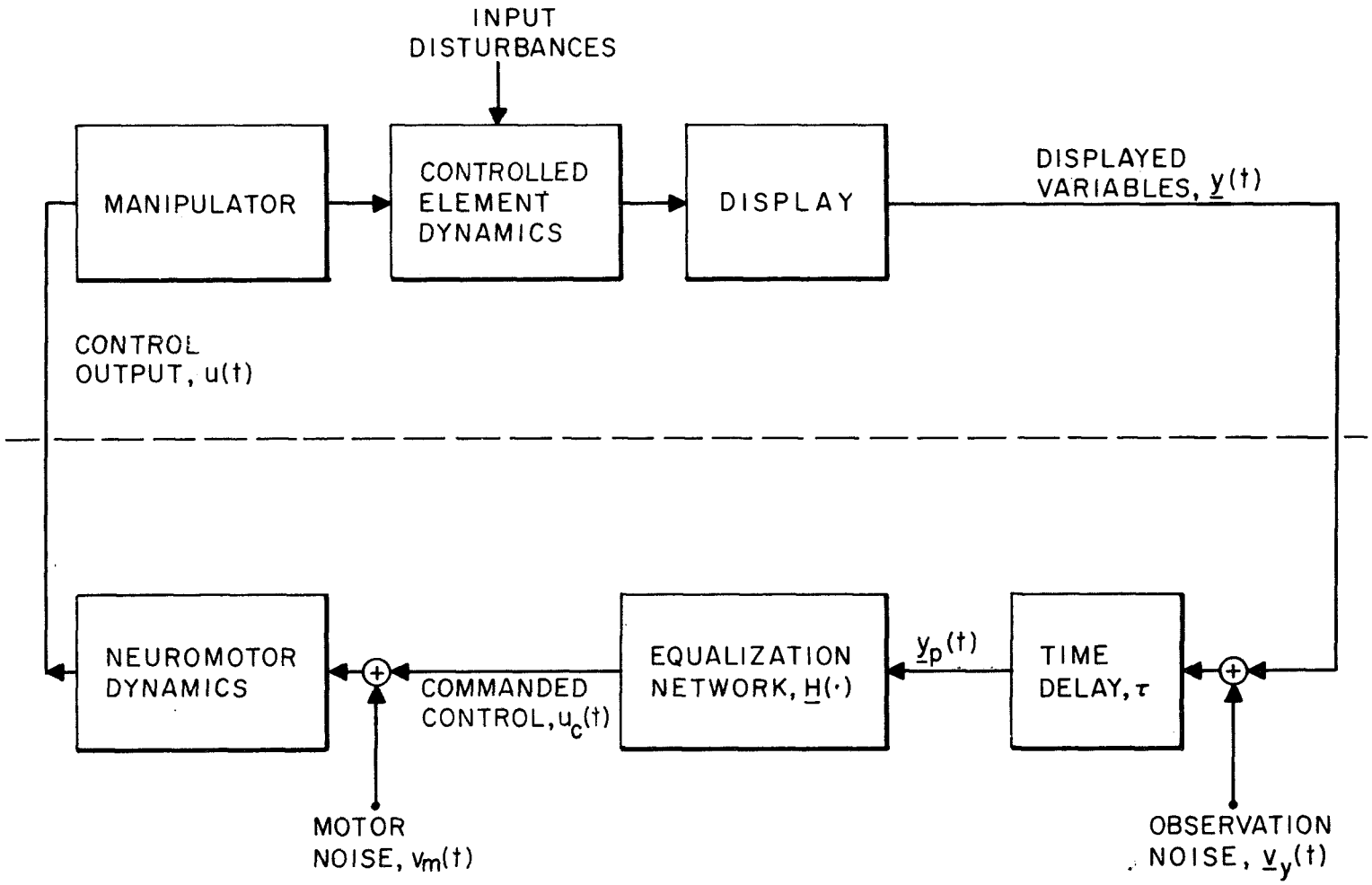

FIG.1 SIMPLIFIED MODEL OF THE HUMAN CONTROLLER IN A MULTIVARIABLE, SINGLE-CONTROL TRACKING SITUATION.

the vehicle. The equalization network $\underline{H}(\cdot)$ of Fig. 1 represents the means by which the human attempts to optimize his control strategy for a given situation. Thus, $\underline{H}(\cdot)$ is dependent on the system being controlled and on the control task. The more general case, where the human may have several control manipulators, is mathematically, a simple extension of the single control case.

It is assumed that the system dynamics, which may include actuator and sensor dynamics, are described by the linear[†], time-invariant equations of motion

$$\dot{\underline{x}}(t) = \underline{A}\,\underline{x}(t) + \underline{b}\,u(t) + \underline{w}(t) \tag{1}$$

where the n-vector $\underline{x}(t)$ represents the vehicle state, $u(t)$ is the human's control input to the system, and where $\underline{w}(t)$ represents random external disturbances. $\underline{w}(t)$ is assumed to be a vector of independent, zero-mean, gaussian white-noises with autocovariance

$$E\{\underline{w}(t)\underline{w}(\sigma)\} = \underline{W}\delta(t-\sigma) \tag{2}$$

i.e.,

$$E\{w_i(t)w_j(\sigma)\} = \begin{cases} w_{ii}\delta(t-\sigma) & i=j \\ 0 & i\neq j \end{cases}$$

In most physical situations the disturbances that act directly on the system are represented by colored noises with rational power-

[†]We do not consider any system nonlinearities in the present context. However, certain types of nonlinearities may be included. A discussion is presented in a later chapter.

density spectra. This situation is included mathematically within Eq. (1), where additional states are introduced that arise from various noise-shaping filters. If n_c such states are associated with the noise process, $\underline{A}$, $\underline{b}$ and $\underline{W}$ will have the following structure

$$\underline{A} = \left[\begin{array}{c|c} \underline{A}_{11} & \underline{0} \\ \hline \underline{A}_{21} & \underline{A}_{22} \end{array}\right] \qquad \underline{b} = \left[\begin{array}{c} \underline{0} \\ \hline \underline{b}_1 \end{array}\right] \qquad \underline{W} = \left[\begin{array}{c|c} \underline{W}_{11} & \underline{0} \\ \hline \underline{0} & \underline{0} \end{array}\right]$$

where $\underline{A}_{11}$ is $n_c \times n_c$, $\underline{A}_{21}$ is $(n-n_c) \times n_c$, etc.

The displayed variables $y_1(t),\ldots,y_m(t)$, $m \leq n$ are linear combinations of the vehicle states and may be correlated or linearly independent. Thus,

$$\underline{y}(t) = \underline{C}\ \underline{x}(t) + \underline{d}\ u(t) \tag{3}$$

where $\underline{C}$ is an mxn constant matrix.

Generally, the components of $\underline{y}(t)$ will be some subset of the system states; it is not necessary to assume that all states are explicitly displayed. We shall assume, however, that if a quantity is displayed explicitly to the human controller, he can also extract the rate of change of that quantity[†] [14]. Thus, $\underline{y}(t)$ will contain those system variables explicitly displayed to, as well as those implicitly derived by, the human.

[†] It is assumed that the human is not able to extract higher derivative information, nor can he estimate the time integral of a displayed variable.

Control task representation. – It is assumed that the control task is adequately reflected in the human's choice of a feedback control $u(\cdot)$ which, in the steady-state, minimizes the cost functional

$$J(u) = E\left\{\sum_{i=1}^{n} q_i x_i^2 + r\, u^2 + g\, \dot{u}^2\right\} \quad ; \; g>0 \tag{4}$$

on the basis of the information obtained from viewing the display.

A quadratic performance index of this type represents a natural extension of the classical manual control compensatory tracking experiments in which the subject was usually instructed to minimize mean-squared error. It was chosen here because of its physical appeal, its mathematical tractability and the resulting analytic simplfications it provides.

The cost functional weightings $q_i \geq 0$, $r \geq 0$ and $g>0$ in Eq. (4) may be either objective (specified by the experimenter or designer) or subjective (adopted by the human in performing and relating to the task). Clearly, the selection of any subjective cost weightings is a nontrivial matter and is tantamount to mathematically quantifying the human's control objectives. In some simple cases this can be accomplished a priori, since the actual weightings may often correspond to the objective weightings. However, in more complex multivariable situations, representative relative values of q_i, r and g may have to be elicited by model-data matching procedures or by questionnaire.

One approach to determine the weightings is to regard the human as attempting to minimize a prespecified error criteria

subject to the constraints of keeping one or more secondary system quantities within some desired tolerances. In this case, the subjective weightings may be viewed as Lagrange multipliers that are adjusted to satisfy the constraints imposed by the human (because of habit or desire). For example, consider a helicopter station-keeping task where it is desired to minimize mean-squared position error. It is most likely that a trained pilot in performing this task will not cause the helicopter to pitch excessively (or too rapidly) and will try to keep the pitch variance within some tolerance. This tendency will be reflected in a subjective weighting on the mean-squared pitch (or pitch rate).

The nonzero control rate weighting g is a central element in our optimal control model. As indicated, this term may represent an objective or a subjective weighting on control rate. It should be noted, for example, that rapid control movements are rarely made by trained pilots. Alternatively, this term could be used to account indirectly for the physiological limitations on the rate at which a human can effect control action. Regardless of which of the above interpretations one adopts, one would expect the g weighting to be an adjustable parameter of the model. We shall return to this point shortly.

Human limitations. — Any reasonable mathematical model of the human operator must include within its framework the various psychophysical limitations inherent in the human. Our model contains time-delay, controller "remnant" and a representation of "neuromotor" dynamics as limitations, as indicated in Fig. 1. Possible nonlinear or discontinuous controller behavior is not considered. In Fig. 1, the various internal time-delays associated with visual, central processing and neuro-motor pathways have been combined and conveniently represented by a lumped equivalent perceptual time-delay τ. No approximation to this explicit delay (e.g., Padé network) is necessary in the model's development or application.

We assume that the various sources of inherent human randomness are manifested as errors in observing displayed outputs and in executing intended control movements. Thus, observation noise and motor noise are lumped representations of "remnant." They are shown in Fig. 1 and have been discussed at length in Levison [14] These noises represent the combined effects of random perturbations in human response characteristics, time variations in response parameters, and random errors in observing system outputs and inputs.

Preliminary evidence had indicated that it would be extremely difficult to differentiate experimentally between motor noise and observation noise and that combining them into an "equivalent" observation noise seemed a perfectly valid procedure. For the time being we shall adopt this procedure, but we shall see later why this approach requires modification.

In the model of Fig. 1 an "equivalent" observation noise vector is thus added to $\underline{y}(t)$. A single noise $v_{y_i}(t)$ is associated with each output $y_i(t)$. Recent studies of controller remnant [14] have shown that over a wide range of tracking tasks, the injected noises $v_{y_i}(t)$ i=1,...,m are closely approximated by independent white-noise processes with autocovariances

$$E\left\{v_{y_i}(t)v_{y_i}(\sigma)\right\} = V_{y_i}\cdot\delta(t-\sigma) \;;\quad i=1,2,\ldots,m$$

or

$$E\left\{\underline{v}_y(t)\underline{v}_y'(\sigma)\right\} = \underline{V}_y\cdot\delta(t-\sigma) \tag{5}$$

In general, a numerical determination of the (diagonal) noise covariance matrix $\underline{V}_y$ will depend, among other things, on the relevant features (quality, type and form) of the display panel and on where the human is fixating, i.e., whether he is viewing a

quantity foveally or peripherally. This fact will be used later in extending the model to include visual scanning constraints.

In summary then, the human perceives

$$\underline{y}_p(t) = \underline{y}(t-\tau) + \underline{v}_y(t-\tau) = \underline{C}\ \underline{x}(t-\tau) + \underline{v}_y(t-\tau) \qquad (6)$$

a delayed, noisy replica of the system output. $\underline{y}_p(t)$ is processed by the human (by means of some equalization network) to yield a "commanded" control input $u_c(t)$. This later quantity is in turn operated on by the "neuro-motor" dynamics, $H_n(\cdot)$ to give the resultant control input $u(t)$.

We do not include "neuro-motor" dynamics directly among the inherent limitations of the human operator. Recall, however, that we have included a term that depends on control rate in our cost $J(u)$. Rynaskii and Whitbeck [15] have shown that the inclusion of this term results in a first-order lag being introduced in the optimal feedback controller. Thus, the control-rate weighting g could be used to account for the lag often attributed to the neuro-motor system (although there is no a priori reason to make this analogy). In any event, an analogy of this type may prove useful in helping to choose numerical values for g based on human performance data concerning neuro-muscular lags.

Model structure. – Within the above framework, the human's control characteristics are determined by the solution of a well-defined optimal linear regulator problem with time-delay and observation noise. This optimization problem has been solved by Kleinman [16] for the case when $g=0$. The results for nonzero g are found in [13] or [17].

It has been shown that the control $u^*(t)$ which minimizes $J(u)$, conditioned on the observations $\underline{y}_p(\cdot)$, is generated by the linear feedback law

$$\tau_N \dot{u}^*(t) + u^*(t) = -\underline{\ell}^* \hat{\underline{x}}(t) \equiv u_c(t) \tag{7}$$

where $\hat{\underline{x}}(t)$ is the best estimate of the system state $\underline{x}(t)$ based on the observed data $\underline{y}_p(\sigma)$, $\sigma \leq t$. τ_N and the optimal gains $\underline{\ell}^*$ depend <u>only</u> on the given system parameters $\underline{A}$, $\underline{b}$ and on the cost functional weightings. Moreover, for given values of q_i and r there is a one-to-one correspondence between g and τ_N: the smaller g, the smaller is τ_N.

The parameters $\underline{\ell}^*$ and τ_N are obtained numerically from

$$\tau_N = 1/\lambda_{n+1} \ , \ \ell_i^* = \tau_N \lambda_i \ ; \ i=1,2,\ldots,n \tag{8}$$

where $\underline{\lambda} = (\lambda_1,\lambda_2,\ldots,\lambda_{n+1})$ is obtained from

$$\underline{\lambda} = \underline{b}_0' \underline{K}_0/g \tag{9}$$

and $\underline{K}_0$ is the unique positive definite solution of the n+1 dimensional Riccati equation

$$\underline{A}_0'\underline{K}_0 + \underline{K}_0\underline{A}_0 + \underline{Q}_0 - \underline{K}_0\underline{b}_0\underline{b}_0'\underline{K}_0/g = \underline{0} \tag{10}$$

with $\underline{Q}_0 = \text{diag}(q_1,q_2,\ldots,q_n,r)$; $\underline{b}_0 = \text{col}[0,0,\ldots,0,1]$ and

$$\underline{A}_0 = \left[\begin{array}{c|c} \underline{A} & \underline{b} \\ \hline \underline{0} & 0 \end{array}\right] \tag{11}$$

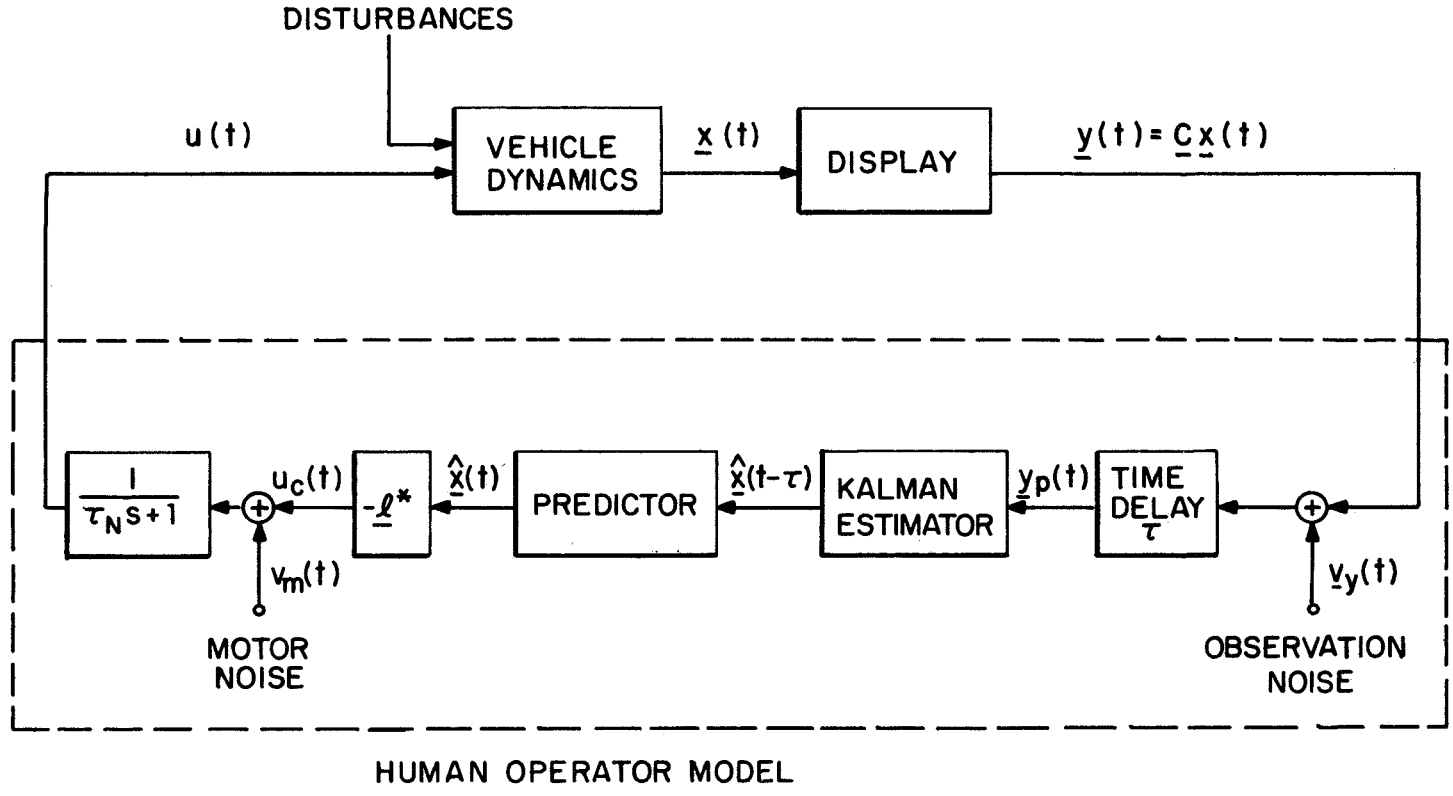

FIG.2 CONTROL THEORETIC MODEL OF OPTIMAL HUMAN BEHAVIOR.

As shown in the overall closed-loop system of Fig. 2, the optimal estimate $\underline{\hat{x}}(t)$ is generated from $\underline{y}_p(t)$ by the cascade combination of a Kalman filter and a least-mean-squared predictor.† The filter and the predictor are linear dynamic elements that require for their implementation a model of the dynamic system (1), or put another way, an internal model of the environment. The Kalman estimator models the human's deduction of system states from displayed information while the predictor models the human's compensation for his inherent time delay. The combination of estimator, predictor and gains represents the optimal model's equalization network corresponding to the $\underline{H}(\cdot)$ of Fig. 1.

Effects of motor noise. — Before proceeding further with the model, we explain the need for motor noise $v_m(t)$ and show how the above results become modified with its inclusion.

The problem lies in the estimator portion of the model. In the absence of motor noise the optimal model has perfect knowledge of the control input $u^*(t)$. It is then apparent that in some situations the Kalman filter will perform linear operations upon $u^*(t)$ in order to generate perfect estimates of some system states. As an example for which this is true consider the system governed by the equations

$$\begin{aligned} \dot{x}_1 &= x_2 + w & y_{p1} &= x_1 + v_1 \\ \dot{x}_2 &= u & y_{p2} &= x_2 + v_2 \end{aligned} \tag{12}$$

For simplicity we set $\tau=0$.

†This feedback structure is fixed. However, the various feedback parameters depend functionally and numerically on $\underline{A}, \underline{b}, \underline{C}, \underline{W}, \underline{V}_y, q_1, r, g$.

It is easy to show in this case that the Kalman filter can obtain a perfect estimate of $x_2(t)$, i.e., $\hat{x}_2(t) \equiv x_2(t)$, by simply "ignoring" the noisy observation $y_{p2}(t)$ and deriving $\hat{x}_2(t)$ by direct integration of $u^*(t)$.

In general, the model will obtain a perfect estimate of any state that is related only to the control $u^*(t)$. (In cases where input disturbances enter the dynamical system in parallel with $u^*(t)$ such a situation will not pervail.) This ability to perform perfect estimation is a limitation with the model as it presently exists.

It is relatively clear that the sources of the limitation are: (1) the estimator employs a perfect representation of the system and can integrate exactly; and (2) the estimator knows the control input $u^*(t)$ exactly. Obviously, the human operator enjoys neither of these advantages, nor did we postulate that such was the case. We did, however, lump all sources of remnant into an observational process. It is now apparent that this procedure breaks down in certain instances.

The most direct way of overcoming the problem is to include an injected motor noise, as well as an observation noise as human limitations. This construct would certainly prevent the model from having perfect knowledge of the control input.† Unfortunately, we presently do not know how to measure an injected motor noise directly. Furthermore, the best method for including such a noise in the model is not immediately obvious. As a first approximation we have included motor noise in our human operator model in the

†An injected motor noise is, in some respects, equivalent to an imperfect system model in the estimator.

manner indicated in Fig. 2. A gaussian white-noise $v_m(t)$ is added directly to the "commanded control" $u_c(t)$ with

$$E\{v_m(t)v_m(\sigma)\} = V_m \cdot \delta(t-\sigma) \tag{13}$$

thus corresponding to the simplified model of Fig. 1.†

With the inclusion of $v_m(t)$, the control theoretic model of human response becomes modified. However, it is assumed that the model retains the control structure that was obtained in the absence of motor noise. Thus the human's control input is assumed to be generated by

$$\begin{aligned} \tau_N \dot{u}(t) + u(t) &= u_c(t) + v_m(t) \\ u_c(t) &= -\underline{\ell}^* \hat{\underline{x}}(t) \end{aligned} \tag{14}$$

where τ_N and $\underline{\ell}^*$ are determined by Eqs. (8)-(11) as before.†† $\hat{\underline{x}}(t)$ again denotes the best estimate of $\underline{x}(t)$ conditioned on the observations $\underline{y}_p(\sigma), \sigma \leq t$.

The estimate $\hat{\underline{x}}(t)$ is obtained from the cascade combination of a Kalman filter and a predictor, that must be modified to include the additional noise term $v_m(t)$. We define the "augmented" state vector $\underline{\chi}(t) = [\underline{x}(t), u(t)]$ where, by combining Eqs. (1) and (14), $\underline{\chi}(t)$ satisfies

---

†An alternate representation of motor noise that has more physical appeal is presented in a later chapter.

††The ramifications of this assumption have yet to be investigated. The assumption is intuitively tenable since V_m will always be small relative to $E\{u_c^2\}$. However, from a purely theoretical viewpoint, the control strategy (14) no longer minimizes $J(u)$ (since $E\{\dot{u}^2\}$ is undefined) and must be regarded as a "suboptimal" control law.

$$\dot{\underline{\chi}}(t) = \underline{A}_1\underline{\chi}(t) + \underline{b}_1 u_c(t) + \underline{w}_1(t) \tag{15}$$

with $\underline{w}_1(t) = [\underline{w}(t),\ v_m(t)/\tau_N]$, $\underline{b}_1 = [0,\ldots,0,\tau_N^{-1}]$ and

$$\underline{A}_1 = \left[\begin{array}{c|c} \underline{A} & \underline{b} \\ \hline 0 & -\tau_N^{-1} \end{array}\right] \tag{16}$$

The Kalman filter generates $\hat{\underline{\chi}}(t-\tau)$, the least-mean-square estimate of the delayed state $\underline{\chi}(t-\tau)$ from

$$\dot{\hat{\underline{\chi}}}(t-\tau) = \underline{A}_1\hat{\underline{\chi}}(t-\tau) + \underline{\Sigma}_1\underline{C}_1'\underline{V}_y^{-1}[\underline{y}_p(t)-\underline{C}_1\hat{\underline{\chi}}(t-\tau)] + \underline{b}_1 u_c(t-\tau) \tag{17}$$

where $\underline{C}_1 = [\underline{C}:\underline{d}]$ and where $\underline{\Sigma}_1$ is the covariance of the estimation error $\underline{e}(t-\tau) = \underline{\chi}(t-\tau)-\hat{\underline{\chi}}(t-\tau)$. $\underline{\Sigma}_1$ satisfies the Variance Equation

$$\underline{0} = \underline{A}_1\underline{\Sigma}_1 + \underline{\Sigma}_1\underline{A}_1' + \underline{W}_1 - \underline{\Sigma}_1\underline{C}_1'\underline{V}_y^{-1}\underline{C}_1\underline{\Sigma}_1 \tag{18}$$

with $\underline{W}_1 = \mathrm{diag}[w_{11},\ldots,w_{nn},V_m/\tau_N^2]$.

The predictor generates the best estimate $\hat{\underline{\chi}}(t) = [\hat{\underline{x}}(t),\hat{u}(t)]$ from the estimator output $\underline{p}(t) \equiv \hat{\underline{\chi}}(t-\tau)$ according to the equation

$$\begin{aligned} \hat{\underline{\chi}}(t) &= \underline{\xi}(t) + e^{\underline{A}_1\tau}[\underline{p}(t) - \underline{\xi}(t-\tau)] \\ \dot{\underline{\xi}}(t) &= \underline{A}_1\underline{\xi}(t) - \underline{b}_1\underline{\ell}^*\hat{\underline{x}}(t) \end{aligned} \tag{19}$$

Thus, the human operator model remains linear with the introduction of motor noise. Its basic structure remains the same as in Fig. 2; however, its detailed structure is now different as a

result of $v_m(t)$. (If $V_m \to 0$ it is straightforward to show that $(\underline{\Sigma}_1)_{n+1,n+1} \to 0$, i.e., $\underline{u}(t)$ becomes estimated perfectly.)

Model outputs. — Once the optimization problems associated with the model are solved it becomes possible to predict various facets of human controller behavior as might be measured in experiment. In this section we discuss these model predictions and present equations useful in applying the control theoretic model to the study of actual man-machine systems.†

Immediately obtainable within the optimization context is a closed form expression for the covariance of $\underline{\chi}(t)$. (See Reference 16 for a derivation.) Thus,

$$\underline{X} = E\{\underline{\chi}(t)\underline{\chi}'(t)\} = e^{\underline{A}_1\tau}\underline{\Sigma}_1 e^{\underline{A}_1'\tau} + \int_0^\tau e^{\underline{A}_1\sigma}\underline{W}_1 e^{\underline{A}_1'\sigma}d\sigma$$

$$+ \int_0^\infty e^{\overline{\underline{A}}\sigma}e^{\underline{A}_1\tau}\underline{\Sigma}_1\underline{C}_1'\underline{V}_y^{-1}\underline{C}_1\underline{\Sigma}_1 e^{\underline{A}_1'\tau}e^{\overline{\underline{A}}'\sigma}d\sigma \quad (20)$$

where $\overline{\underline{A}} = \underline{A}_1 - \underline{b}_1\hat{\underline{\ell}}$, $\hat{\underline{\ell}} = (\underline{\ell}^*,0)$.

Since $\underline{\chi} = (\underline{x},u)$ the variances of system quantities are thus given by

$$E\{x_i^2(t)\} = \underline{X}_{ii} \qquad \text{for } i=1,2,\ldots,n$$

$$E\{y_i^2(t)\} = (\underline{C}_1\underline{X}\underline{C}_1')_{ii} \qquad \text{for } i=1,2,\ldots,m \quad (21)$$

$$E\{u^2(t)\} = \underline{X}_{n+1,n+1}$$

†A concise summary of model inputs and outputs is found in Appendix B.

and,neglecting the explicit white noise component of $\dot{u}(t)$.

$$E\{\dot{u}^2(t)\} = \underline{\lambda}\ \underline{X}\ \underline{\lambda}' \tag{22}$$

Equations (20-22) explicity show the manner in which the human's limitations affect overall closed-loop performance. These variances can be measured easily in an experimental situation.

As we have noted earlier, the optimal feedback controller is linear and time-invariant; its structure being expressed in the time-domain by Eqs. (15-19). This structure can therefore be expressed equally well in the frequency-domain by a transfer vector relating $\underline{y}$ to u, i.e.,

$$u(s) = \underline{h}(s)\ \underline{y}(s) \tag{23}$$

Various expressions for $\underline{h}(s)$ can be derived from Eqs. (15-19) or from block diagram manipulations. One such expression is

$$\underline{h}(s) = -\frac{\hat{\underline{\ell}}}{\tau_N s+1}\left[(s\underline{I}-\hat{\underline{A}})\int_0^{\tau} e^{(s\underline{I}-\underline{A}_1)\sigma}d\sigma\,(s\underline{I}-\overline{\underline{A}}) + s\underline{I}-\hat{\underline{A}}+\underline{b}_1\hat{\underline{\ell}}\right]^{-1}\cdot\underline{\Sigma}\underline{C}_1'\underline{V}_y^{-1} \tag{24}$$

where $\hat{\underline{A}} = \underline{A}_1 - \underline{\Sigma}_1\underline{C}_1'\underline{V}_y^{-1}\underline{C}_1$ and $\hat{\underline{\ell}} = (\underline{\ell}^*,0)$. Equation (24) is particularly interesting since it explicitly shows how the time-delay τ modifies the optimal feedback controller.

An alternate expression for $\underline{h}(s)$ that is more amenable to computation is given by

$$\underline{h}(s) = -\frac{\hat{\underline{\ell}}}{\tau_N s+1}\left[e^{(\underline{A}-s\underline{I})\tau}(s\underline{I}-\hat{\underline{A}})^{-1} \cdot \underline{\Sigma}_1\underline{C}_1'\underline{V}_y^{-1}\right] \cdot (1+D)^{-1} \tag{25}$$

where

$$D = \hat{\underline{\ell}}\left\{e^{(\underline{A}-s\underline{I})\tau}\left[(s\underline{I}-\hat{\underline{A}})^{-1} - (s\underline{I}-\underline{A})^{-1}\right] + (s\underline{I}-\underline{A})^{-1}\right\}\underline{b}_1 \tag{26}$$

These equations simplify greatly for computation since $\underline{b}_1 = (0,0,\ldots,0,\tau_N^{-1})$.

The elements $h_1,h_2,\ldots,h_m$ of $\underline{h}(s)$, called the "internal" transfer functions are not experimentally measurable, but in cases where there is a single input noise disturbance, i.e., $\underline{w}(t) = \underline{w} \cdot \xi(t)$, a closed-loop describing function relating the control $u(t)$ to any single output, say $y_i(t)$, can be easily measured. Experimentally, this is accomplished by recording the time histories of y_i and u, and computing the Fourier transforms $y_i(\omega)$ and $u(\omega)$ to obtain

$$h_{ie}(\omega) = \left[\frac{u(\omega)}{y_i(\omega)}\right]_e \tag{27}$$

A theoretical expression for this "equivalent" transfer function can be obtained in several ways. Since there is only one input noise, a convenient method is to take the ratio of the portion of $u(s)$ and $y_i(s)$ that relate directly to the input disturbance $\underline{w}$. Thus, from Eqs. (1), (3) and (23),

$$u(s) = \underline{h}(s)\underline{y}(s) = \underline{h}\ \underline{V}_1\ u(s) + \underline{h}\ \underline{V}_2\ \xi(s) \tag{28}$$

or

$$u(s) = \frac{\underline{h}\ \underline{V}_2}{1-\underline{h}\ \underline{V}_1}\ \xi(s) \tag{29}$$

where

$$\underline{V}_1 = \underline{C}(s\underline{I}-\underline{A})^{-1}\underline{b}+\underline{d},\ \underline{V}_2 = \underline{C}(s\underline{I}-\underline{A})^{-1}\underline{w} \tag{30}$$

Since u(t) and $\xi(t)$ are both scalars,

$$y_i(s) = \underline{V}_{1i}\ u(s) + \underline{V}_{2i}\ \xi(s). \tag{31}$$

Substituting for u(s) and forming the ratio u/y_i gives the result

$$h_{ie}(s) = \frac{\underline{h}\ \underline{V}_2}{\underline{V}_{1i}\ \underline{h}\ \underline{V}_2 + \underline{V}_{2i}(1-\underline{h}\ \underline{V}_1)} \tag{32}$$

Note that if $\underline{V}_2 = \underline{V}_1 \cdot \delta(s)$ where $\delta(s)$ = scalar (a condition that is satisfied if, for example, the input forcing function is added in parallel with the control signal u(t)) then Eq.(32) reduces to

$$h_{ie}(s) = \frac{\underline{h}(s)\underline{V}_1(s)}{\underline{V}_{1i}(s)} \tag{33}$$

This is a particularly interesting expression since $\underline{h}\ \underline{V}_1$ is the open-loop transfer function (corresponding to the familiar Y_pY_c) which, at least in simple cases, is identical to $\underline{h}_{ie}\ \underline{V}_{1i}$.

The model can also serve to predict the power spectral density of any signal in the closed-loop system. Moreover, since this system is linear, any power density spectrum can be considered as the sum of two parts: one arising from $\underline{w}(t)$, i.e., input-related, and the other arising from the noise sources $\underline{v}_y(t)$ and

$v_m(t)$, i.e., remnant related. The pertinent equations for power density are obtained† by substituting $u(s) = \underline{h}\,\underline{C}\,\underline{x} + \underline{h}\,\underline{v}_y + \frac{v_m}{\tau_N s+1}$ in Eq. (1) and performing the simple matrix manipulations. The resultant expressions are (positive frequencies only)

$$\underline{\Phi}_{xx}(\omega) = \frac{1}{\pi}\left[\underline{\Phi}_{xx_c}(\omega) + \underline{\Phi}_{xx_r}(\omega)\right] \tag{34}$$

where

$$\begin{aligned}\underline{\Phi}_{xx_i}(\omega) &= \underline{\Gamma}(\omega)\underline{W}\,\underline{\Gamma}'(-\omega)\\ \underline{\Phi}_{xx_r}(\omega) &= \underline{\Gamma}(\omega)\underline{b}\left[\underline{h}(\omega)\underline{V}_y\underline{h}'(-\omega) + \frac{V_m}{\tau_N^2\,\omega^2+1}\right]\underline{b}'\underline{\Gamma}'(-\omega)\end{aligned} \tag{35}$$

$$\underline{\Gamma}(\omega) = [j\omega\underline{I}-\underline{A}-\underline{b}\,\underline{h}\,(\omega)\underline{C}]^{-1} \tag{36}$$

$\underline{\Phi}_{xx_i}$ and $\underline{\Phi}_{xx_r}$ are, respectively, the input (i.e., $\underline{w}(t)$) and remnant-related portions of the $\underline{x}$ spectrum. Similarly,

$$\begin{aligned}\underline{\Phi}_{yy_i}(\omega) &= \underline{C}\,\underline{\Phi}_{xx_i}(\omega)\underline{C}'\\ \underline{\Phi}_{yy_r}(\omega) &= \underline{C}\,\underline{\Phi}_{xx_r}(\omega)\underline{C}'\end{aligned} \tag{37}$$

$$\begin{aligned}\Phi_{uu_i}(\omega) &= \underline{h}(\omega)\,\underline{\Phi}_{yy_i}(\omega)\underline{h}'(-\omega)\\ \Phi_{uu_r}(\omega) &= \underline{h}(\omega)\,\underline{\Phi}_{yy_r}(\omega)\underline{h}'(-\omega) + \frac{V_m}{\tau_N^2\,\omega^2+1} + \underline{h}(\omega)\underline{V}_y\underline{h}'(-\omega)\end{aligned} \tag{38}$$

†Setting $\underline{d}=\underline{0}$ for simplicity.

The integral (over ω) of any of the above quantities gives the total remnant and/or correlated power in any desired signal. The total power is, of course, given by Eq.(21).

Since the system is linear it is simple to reflect the remnant processes $v_y(t)$ and $v_m(t)$ into a single (mathematically) equivalent noise process $r(t)$ injected onto a particular output, say y_j. This approach of combining all sources of remnant has been used for measuring remnant in cases where there is a single input noise disturbance [14]. The expression derived in [14] for injected remnant power (regarded as a single noise on $y_j(t)$) is†

$$\Phi_{rr_j}(\omega) = \frac{1}{\pi} \cdot \frac{\Phi_{uu_r}(\omega)}{\Phi_{uu_i}(\omega)} \cdot |\underline{V}_{2j}(\omega)|^2 . \tag{39}$$

$\Phi_{rr_j}(\omega)$ can be computed easily by substituting Eqs.(38)&(30) into Eq.(39). Theoretical predictions are thus available of yet another standard measure of human response in tracking tasks.

Model application. — In this section the procedure that one would use in applying the foregoing model to predict human operator performance is discussed. It is assumed that the parameters $\underline{A},\underline{b},\underline{C},\underline{W}$ that specify the input-output characteristics of the system to be controlled are given. Similarly, the cost functional weightings q_i, r on state and control variances are assumed specified. As discussed previously, the specification of subjective weightings may be a nontrivial matter.

† Note that from an experimental point of view, only power measurement of $u(t)$ are needed to compute Φ_{rr_j}. One does not need an expression for $\underline{h}(s)$.

In order to apply the optimal control model it is necessary to know the human response parameters τ, τ_N, $\underline{V}_y$, V_m. Reasonable approximations to these quantities are often available. For example, published data in the manual control field [4] indicates that typical values for the effective time-delay are τ=.15-.25 sec. The analogy between τ_N and the "neuro-motor" time-constant is useful in helping to choose a value for τ_N. Human performance data concerning neuro-muscular lags indicates that τ_N is of the order τ_N = .1-.3 with $\tau_N \approx .1$ being typical [3].

The determination of numerical values for $\underline{V}_y$ and V_m is presently a difficult task. These quantities depend on the nature of the display, the physical environment, as well as on intrinsic human properties. One encouraging result has been found, however [14]. Over a wide range of foveal viewing conditions, each white observation noise $v_{yi}(t)$ has a covariance that is, on the average, about .01π times the variance of its associated output $y_i(t)$.† Thus

$$(\underline{V}_y)_{ii} = \pi\rho_i \, E\{y_i^2\} \; ; \; i=1,2,\ldots,m \tag{40}$$

where the observation-noise-ratio, ρ_i = .01. Thus, $v_{yi}(t)$, when normalized with respect to the variance σ_{yi}^2, has a positive frequency power density level of -20 dB.

The motor noise, $v_m(t)$, which is added to the "commanded" control $u_c(t)$, is <u>assumed</u> to have a covariance

†This is indicative of an underlying multiplicative noise process of the form $v_{yi}(t) = \xi_i(t)y_i(t)$ where $\xi_i(t)$ is a white-noise. This multiplicative aspect of observation noise is discussed in Reference 14.

$$V_m = \pi\rho_m \, E\{u_c^2\} \tag{41}$$

Values for the motor-noise-ratio, ρ_m, have been obtained from model-matching analysis of some simple tracking tasks. We found, typically, ρ_u=.003 (corresponding to a normalized motor noise of approximately -25 dB), although a further study of motor-noise is warranted.

The sources of human randomness are thus modelled by additive white-noises, each of whose covariance scales (with factor ρ_i or ρ_m) with the variance of the quantity to which it is associated. From a mathematical viewpoint this representation introduces a subtlety in the theoretical developments. The (sub)optimality of the control law (14) depended on the separability of estimation and control processes, i.e., on $\underline{\Sigma}_1$ being independent of $u_c(t)$. If the noise covariances are given by Eqs. (40-41), then $\underline{\Sigma}_1$ depends on the control, and separability cannot be guaranteed. This point is too complex to be investigated within the scope of this report. However, it seems plausible to assume that even if (14) is nonoptimal, it is a reasonable suboptimal (separable) control law, provided the noise covariances are suitably adjusted.

Once the value of τ_N is specified, it is a simple matter to choose a "control rate weighting" g in Eq. (4) such that the corresponding gains $\underline{\lambda}$ determined by Eqs. (8)-(11) have $\tau_N=1/\lambda_{n+1}$ as required. Next, values of $\underline{V}_y$ and V_m are adjusted in such a way that when the variances (20) are computed:

$$\begin{aligned} \frac{(\underline{V}_y)_{ii}}{\pi E\{y_i^2\}} &= \rho_i \; ; \; i=1,2,\ldots,m \\ \\ \frac{V_m}{\pi E\{u_c^2\}} &= \rho_m \end{aligned} \tag{42}$$

Since the noise-ratios ρ_i and ρ_m have been designated as both inputs and outputs of our model, (inasmuch as they depend on the solution to the Variance Equation (18)),the adjustment process requires several iterations on $\underline{V}_y$ and V_m. We thus solve a sequence of optimization problems in which we choose values for $\underline{V}_y$ and V_m and compute the resultant noise-ratios. The sequence is terminated when values for the covariances are found such that the computed noise-ratios are equal to the pre-specified noise-ratios.†

When the model has been adjusted to the requisite values of ρ_i and ρ_m (or $\underline{V}_y$ and V_m) numerous outputs can be obtained that serve to predict different facets of human response as discussed in the preceding section. An interactive computer program, Human Response Analyzer III (HRA3), has been developed for accomplishing these predictions. A manual describing in detail the program and its usage is included as Appendix B. The manual contains an example (along with actual computer type-out) that explicitly shows the manner in which one uses the model.

Model validation. – To validate the model and to illustrate the procedure for applying it, model predictions are compared with data obtained from a set of manual control experiments. Each of these experiments consisted of a compensatory tracking task in which the human controller was provided with a single manipulator and was given an explicit display of system error, e, (a scalar). The controller could therefore obtain error rate, $\dot{e}$, directly by observing the velocity of the display indicator. Figure 1 contains a block diagram of the control situation.

†A new solution to the problem that allows for direct specification of the noise-ratios is presented in a later chapter. This alleviates the need for on-line iterations.

Three sets of vehicle dynamics were investigated: pure gain (k), velocity control (k/s), and acceleration control (k/s^2). The system input disturbance was composed of a set of sinusoids whose amplitudes were chosen to approximate a rational power spectral density function. For k/s and k/s^2 dynamics, a simulated first-order noise spectrum having a break frequency of 2 rad/sec was applied as a velocity disturbance to the vehicle. For the experiments with k dynamics, a simulated second-order noise spectrum having a break frequency of 2 rad/sec was applied as a position disturbance. In all cases the subjects were instructed to minimize mean-squared system error. The experimental conditions are described in more detail in **References 12 and 17.**

In the theoretical analysis of each of the three cases, the cost functional (4) was taken to be of the form

$$J(u) = E\{e^2\} + g\, E\{\dot{u}^2\} \tag{43}$$

The normalized observation noises on error and error rate were adjusted to -20 dB (white noise power density level) corresponding to foveal viewing conditions. Normalized motor noise was universally adjusted to -25 dB. Nominal values of τ and τ_N were .15 and .1 sec, respectively. τ_N was adjusted by picking an appropriate control rate weighting, g.

k/s Dynamics (k=1)

If $x_1(t)$ denotes the noise disturbance and $x_2(t)$ denotes the system error, e, then

$$\dot{x}_1(t) = -2x_1(t) + w_1(t) \tag{44}$$

$$\dot{x}_2(t) = x_1(t) + u(t)$$

where $w_1(t)$ is white noise with covariance $w_{11} = 8.8$ (so as to yield a required value of $E\{x_1^2\} = 2.2$). The system outputs (i.e., "displayed" quantities) y_1 and y_2 were respectively error (x_2) and error rate ($\dot{x}_2 = x_1 + u$).

The analysis was conducted with $g = .00017$ so as to yield $\tau_N = .08$ sec (slightly below nominal).† The nominal effective time-delay τ=.15 sec was taken. Next, as outlined in the preceding section, values of V_{y1},V_{y2} and V_m were chosen which corresponded to normalized white noise power density levels of -20, -20, and -25 dB, respectively. The variances which result from these noise values constitute the prediction of closed-loop performance. Table 1 contains the experimental and theoretical values of mean-squared error, error rate and control input. Both sets of numbers correspond to within 10 percent.

Having specified all of the model's parameters, Eq. (25) was used to determine the human's transfer function. Since there are two displayed quantities y_1 and y_2 and a single control input u,

$$u(s) = h_1(s)y_1(s) + h_2(s)y_2(s) \tag{45}$$

The transfer functions $h_1(s)$ and $h_2(s)$ are not directly measurable but a closed-loop describing function relating control to error can be measured. Since $y_2(s) = sy_1(s)$, this "equivalent" transfer between u and y_1 is given by

$$\left[\frac{u}{y_1}\right]_e = h_{1e} = h_1 + sh_2 \tag{46}$$

†It was found that $\tau_N = .08$ resulted in slightly better agreement with experimental quantities than did $\tau_N = .1$.

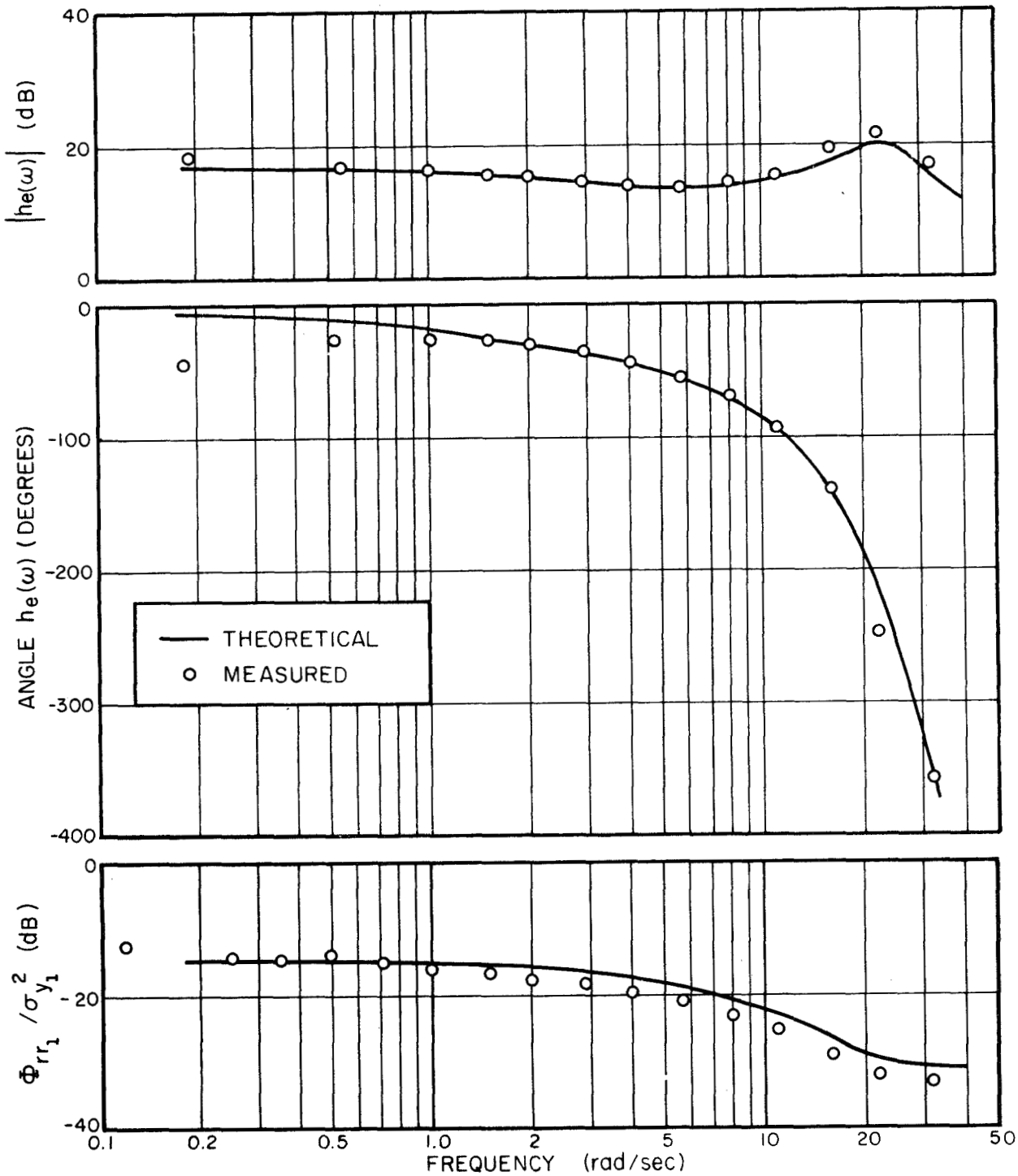

FIG.3 MEASURED AND PREDICTED FREQUENCY DOMAIN MEASURES, k/s DYNAMICS (Average of four subjects)

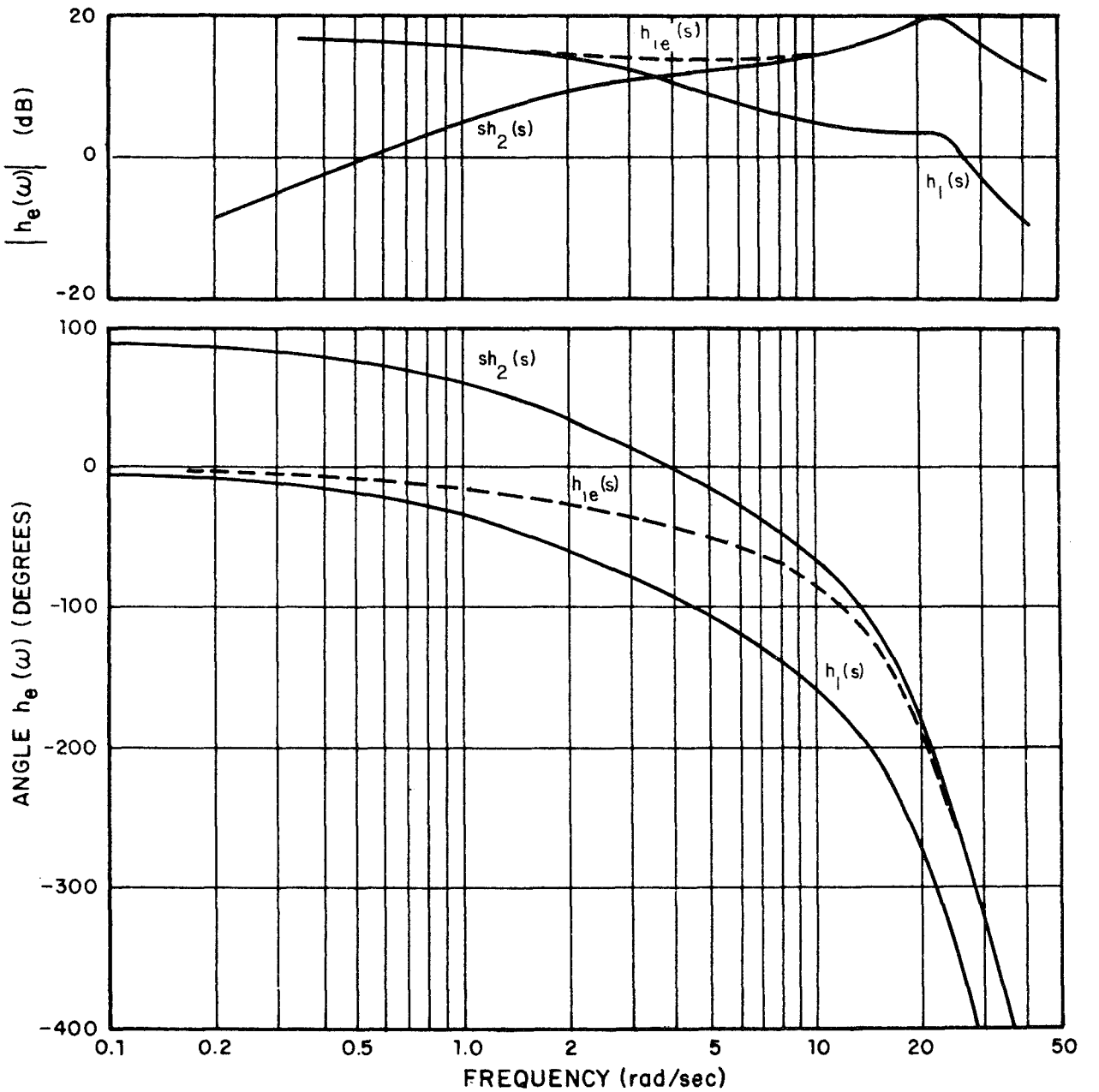

FIG.4 INTERNAL AND EQUIVALENT DESCRIBING FUNCTIONS k/s DYNAMICS

Figure 3 shows a comparison of the measured and predicted describing functions for this example (crossover frequency is at $\omega_c = 4.8$ rad/sec). The measured and predicted equivalent injected remnant spectra (39) (reflected and normalized to system error) are also shown in Fig. 3. As can be seen, the predicted results are in remarkable agreement with the measured data.

The manner in which the model's "internal" transfers $h_1(s)$, $h_2(s)$ combine to give $h_{1e}(s)$ is shown in Fig. 4. Note that the major contribution of h_1 is at low frequencies (i.e., below crossover) while that of h_2 is at high frequencies (beyond crossover). This is intuitively expected since at low [high] frequencies the human responds primarily to position [rate] information.

k/s^2 Dynamics (k=1)

The system state equations are (x_1 = noise, x_2 = error)

$$\dot{x}_1(t) = -2x_1(t) + w_1(t) \tag{47}$$

$$\dot{x}_2(t) = x_3(t) + x_1(t)$$

$$\dot{x}_3(t) = u(t)$$

$w_1(t)$ has covariance $w_{11} = .217$ to give $E\{x_1^2\} = .054$. The two output quantities are $y_1 = x_2$, $y_2 = x_3 + x_1$ = error rate.

The analysis was conducted as for k/s dynamics. τ_N was set to .1 sec by picking $g = 7 \times 10^{-5}$. The time delay τ was .21 sec. Observation and motor noise levels were adjusted to their requisite values.

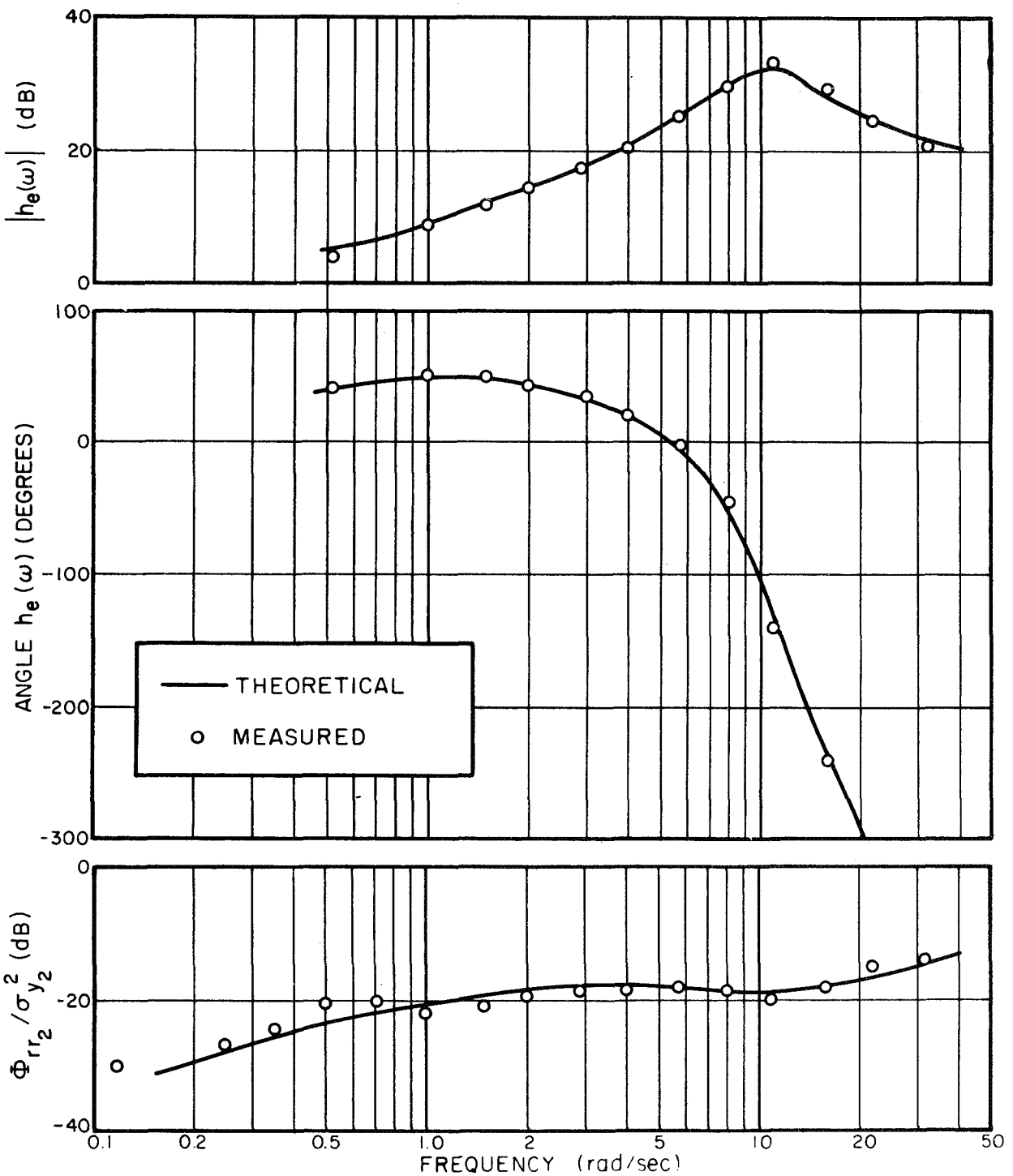

FIG.5 MEASURED AND PREDICTED FREQUENCY DOMAIN MEASURES k/s^2 DYNAMICS (Average of three subjects)

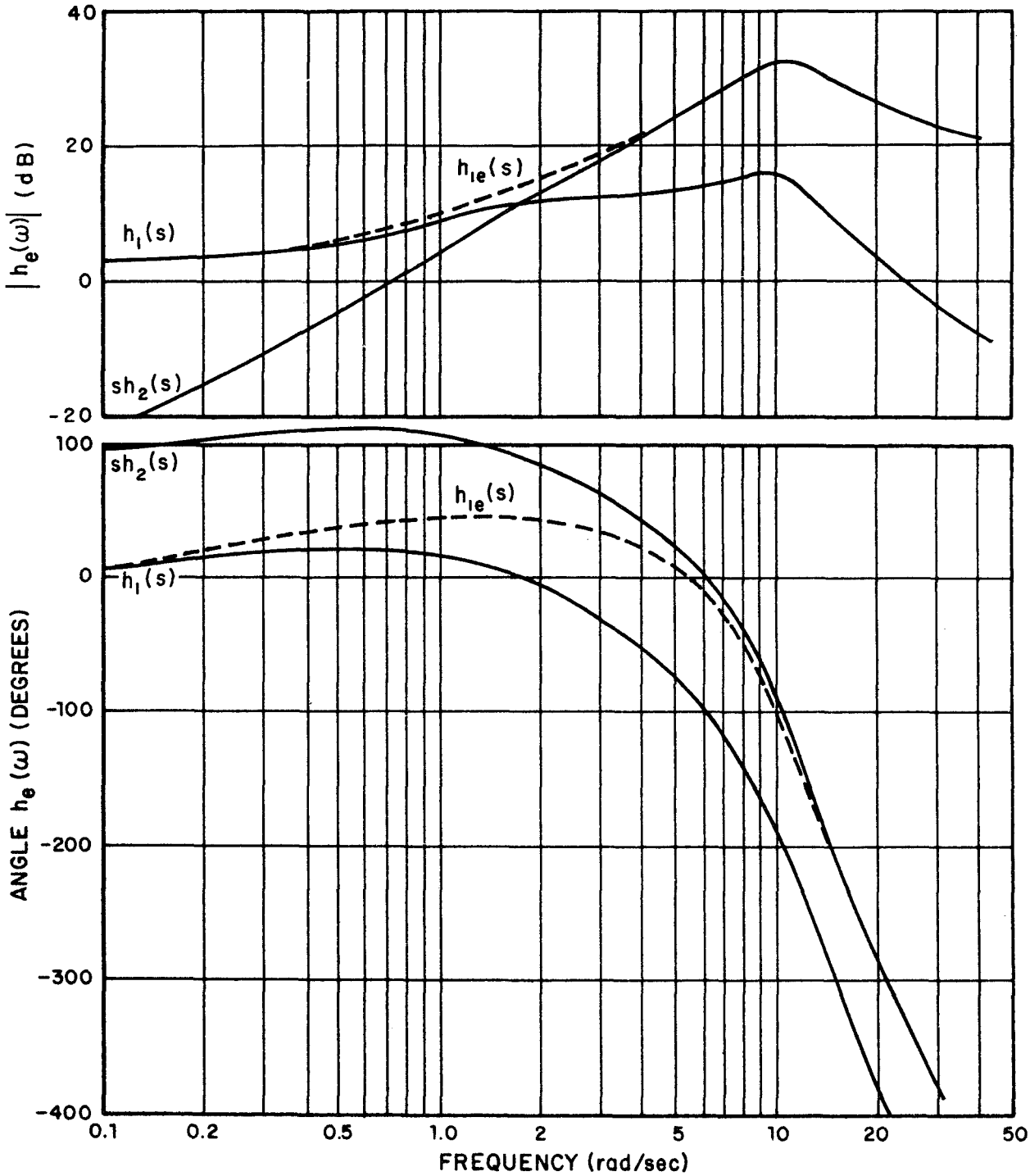

FIG.6 INTERNAL AND EQUIVALENT DESCRIBING FUNCTIONS, k/s^2 DYNAMICS

Table 1

Measured and Theoretical Human Performance

Parameters			M.S. Error		M.S. Error Rate		M.S. Control	
System	τ_N	τ	Meas.	Theor.	Meas.	Theor.	Meas.	Theor.
k/s	.08	.15	.13	.12	3.1	3.06	4.2	3.83
k/s^2	.10	.21	.014	.014	.10	.11	1.43	1.28
k	.11	.15	.13	.14	4.8	5.3†	.53	.54

The resultant closed-loop performance, equivalent human describing function and remnant spectrum (reflected to error rate) are compared with the corresponding experimentally obtained quantities in Table 1, and Fig. 5. The internal describing functions $h_1(s)$ and $h_2(s)$ for this case are plotted in Fig. 6. Again, we see that at low frequencies $h_{1e}(s) \approx h_1(s)$, while at high frequencies $h_{1e}(s) \approx sh_2(s)$, indicating the manner in which displayed information is used in generating the control input.

k Dynamics (k=1)

In order to reduce high frequency noise, the pure gain dynamics were approximated by a filter $f(s) = 40/(s+40)$. The time constant τ_N was set to .1 sec and the time delay to .15 sec. Observation and motor noises were adjusted to their respective levels. The comparison of theoretical and measured quantities is given in Table 1 and Fig. 7.

†In the measurement frequency range $\omega<32$ rad/sec.

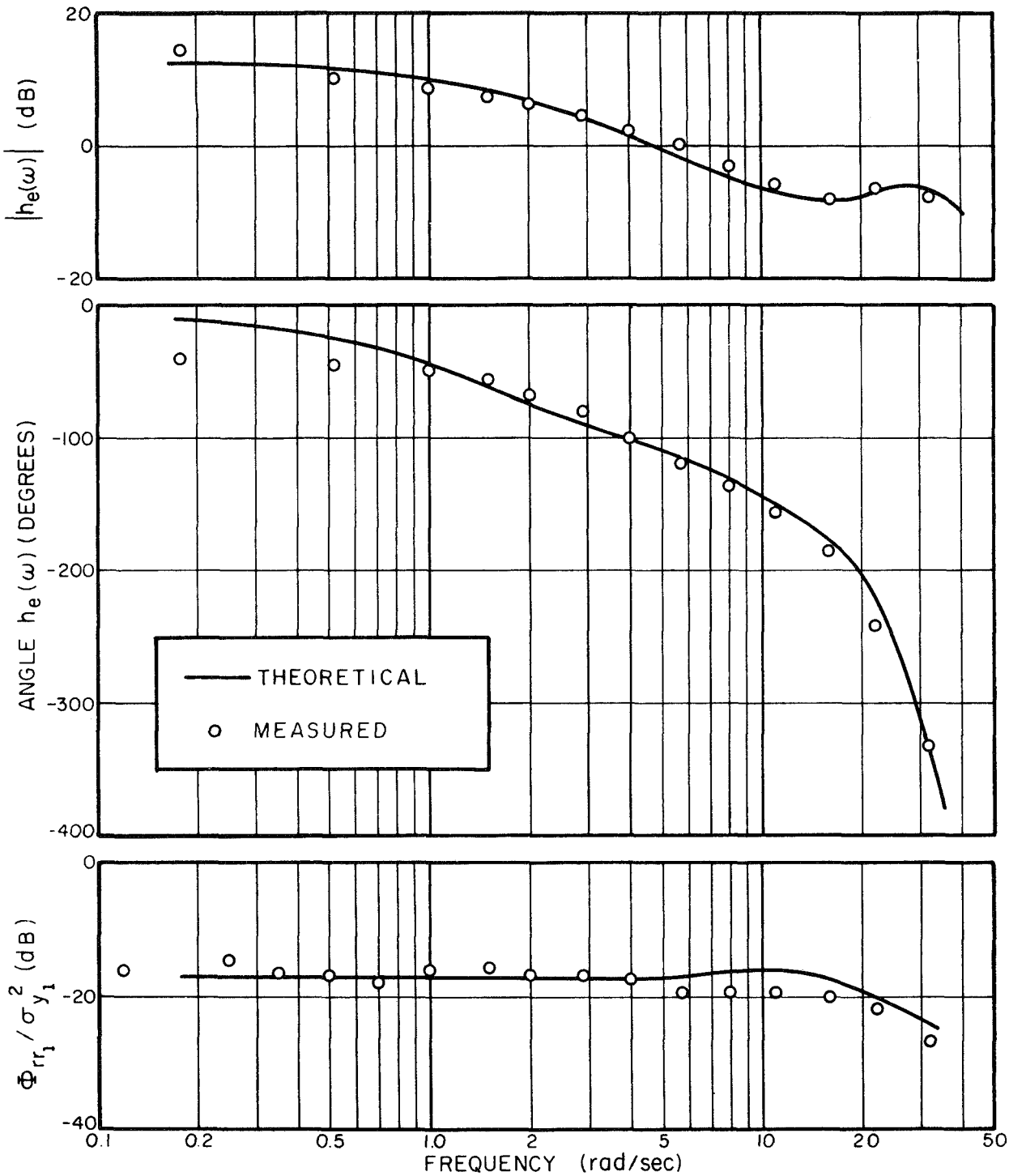

FIG.7 MEASURED AND PREDICTED FREQUENCY DOMAIN MEASURES, k DYNAMICS (Average of three subjects)

The remarkable agreement between predicted and measured quantities as demonstrated above is extremely encouraging and underscores our modern control theory approach to human operator studies. The model was capable of accurately predicting and/or reproducing various properties of human response in simple tracking tasks, using relatively few parameters. Of course the model does not tell us whether observed characteristics of the human's response (e.g., the high-frequency resonant peaks) are implemented by muscles in the arm or in the head. However, the model does suggest reasons why these characteristics are present. For our purposes, understanding why is usually more important than understanding where.

Single-Axis Control — Scanning

We now discuss the modifications to the above results when there are multiple instruments and scanning among instruments is allowed. We shall remain within our conceptual optimization framework to develop and solve an "optimal sampling problem".[18]

Preliminaries. - Recall that in developing our model of the human operator, a white observation-noise vector $\underline{v}_y(t)$ is associated with the output process $\underline{y}(t)$. The noises $v_{yi}(t)$ depend parametrically on the various display features and (in cases where there are several instruments to monitor) on the fixation point of the eye, represented mathematically herein by ω. Thus, parametrically

$$\underline{v}_y(t) = \underline{v}_y(\omega,t) \tag{48}$$

$$\underline{V}_y = \underline{V}_y(\omega)$$

Numerical values for the covariance matrix $\underline{V}_y(\omega)$ will depend on where the human operator is fixating (i.e., whether he is viewing an instrument foveally or peripherally).

We define a scanning strategy as a method for picking the fixation point of the eye at different time instances, i.e., a procedure for choosing $\omega(t)$. We shall assume that there are k instruments to be viewed. Therefore, at any time t the human is fixating on one of the instruments or else is switching his foveal attention between instruments.† These possibilities are denoted

†Since the human's fixation point cannot be changed instantaneously we associate a finite transition time with any saccade. Typically t_o = .1-.15 sec.

by letting $\omega(t) = j$, $j=1,2,\ldots,k$ or $\omega(t) = 0$, respectively. Note that $\omega(t)$, so defined, is piecewise constant and over any time interval may be represented by a sequence of values of the form $\{1,0,3,0,2,0,3,\ldots\}$.

When the fixation point of the eye varies with time, the observation-noise covariance matrix $\underline{V}_y(\omega(t))$ will also vary with time. However, for each (constant) value of $\omega=0,1,\ldots,k$ we associate a constant covariance matrix $\underline{V}_y(0)$, $\underline{V}_y(1),\ldots,\underline{V}_y(k)$. These matrices are diagonal since the observation-noise processes $v_{yi}(\omega)$ are assumed independent. If $\underline{V}_y(i)$ is the covariance matrix corresponding to $\omega=i$ then the j-th diagonal element $[\underline{V}_y(i)]_{jj}$ is the noise covariance associated with viewing $y_j(t)$ while fixating display i. The matrix $\underline{V}_y(\omega(t))$ is thus piecewise constant, i.e.,

$$\underline{V}_y(\omega(t)) = \underline{V}_y(i) \qquad \text{if } \omega(t) = i \tag{49}$$

Each of the matrices $\underline{V}_y(i)$ have elements corresponding to viewing each of the displayed quantities $y_i(t)$ on a continuous basis. Some of these elements will correspond to foveal viewing and others to peripheral viewing. However, the signals on the fixated instrument will generally have lower observation-noise levels associated with their readings; this influences scanning behavior.

In formulating the method for predicting scanning behavior it is assumed that the matrices $\underline{V}_y(i), i\neq 0$ are given. This is a nontrivial assumption since precise quantitative determination of these values is a difficult task. However, in some cases a coarse approximation to $\underline{V}_y(\omega)$ suffices (see Ref. 17). Finally, the elements of $\underline{V}_y(0)$ are assumed to be infinite, i.e., nothing is seen during a saccade.

Optimal sampling problem. — We now discuss our method for for predicting human scanning behavior. We first assume, without loss of generality (see Ref. 18) that the scanning strategy is periodic with a fixed, but arbitrary, scan period T. Using the techniques of [18] it is possible to show that for a fixed scanning strategy, ω, the minimum value of the cost functional Eq. (4) (neglecting the white-noise component of $\dot{u}$) is given by

$$J^*(\omega) = \min_u J(\omega,u) \tag{50}$$

$$= \hat{\underline{L}}\, \underline{\Sigma}_{avg}(\omega)\hat{\underline{L}}' + \gamma(\omega) + \text{terms independent of } \omega$$

where

$$\left.\begin{aligned} \hat{\underline{L}} &= g^{\frac{1}{2}}\, \hat{\underline{\ell}}\, e^{\underline{A}_1 \tau} = \text{"equivalent" gains}^{\dagger} \\ \underline{\Sigma}_{avg}(\omega) &= \frac{1}{T}\int_0^T \underline{\Sigma}(\omega,t)dt \end{aligned}\right| \tag{51}$$

and $\underline{\Sigma}(\omega,t)$ is the (periodic) solution of the Variance Equation

$$\dot{\underline{\Sigma}}(\omega,t) = \underline{A}_1\underline{\Sigma}(\omega,t) + \underline{\Sigma}(\omega,t)\underline{A}_1' + \underline{W}_1 - \underline{\Sigma}(\omega,t)\underline{C}_1'\underline{V}_y^{-1}(\omega(t))\underline{C}_1\underline{\Sigma}(\omega,t) \tag{52}$$

with periodic boundary conditions

$$\underline{\Sigma}(t) = \underline{\Sigma}(t+T) > \underline{0} \tag{53}$$

† Recall that $\hat{\underline{\ell}} = (\underline{\ell}^*, 0)$.

The correction term $\gamma(\omega)$ arises because of the method we have chosen to represent motor noise.[†] It is given by

$$\gamma(\omega) = [\underline{\Sigma}_{avg}(\omega)]_{n+1,n+1} \cdot \left(\frac{e^{-\tau/\tau_N}}{\tau_N} \right)^2 \cdot g \qquad (54)$$

and will be small in cases when τ_N is small (i.e., when $1/\tau_N$ is sufficiently greater than the bandwidth of the overall closed-loop system). Fortunately, this is almost always the case so that we can approximate $J^*(\omega)$ by

$$J^*(\omega) \approx \hat{\underline{L}}\, \underline{\Sigma}_{avg}(\omega)\, \hat{\underline{L}}' + \ldots \qquad (55)$$

to correspond in form with the results reported in Refs. [17]-[18]. (In a later chapter we shall present a different characterization for motor noise that does not result in the introduction of a correction term $\gamma(\omega)$, and which is more appealing from a physical viewpoint.)

The determination of the human operator's sampling strategy rests on the assumption that the operator behaves in an approximately optimal fashion and samples his instruments accordingly. In other words, the human chooses a sampling strategy $\omega^*(t)$ that minimizes $J^*(\omega)$, or equivalently, he chooses the ω^* that minimizes

$$I(\omega) = \hat{\underline{L}}\, \underline{\Sigma}_{avg}(\omega)\, \hat{\underline{L}}' \qquad (56)$$

[†]Recall that in Ref. 18 , where motor noise is absent, so too is the additional term $\gamma(\omega)$. It is easy to see that $[\underline{\Sigma}_{avg}(\omega)]_{n+1,n+1} \to 0$ as $V_m \to 0$. Recall that this term is the error associated with estimating $u(t)$.

Note that since $\hat{\underline{L}}$ depends on the cost functional weightings, the time delay, and the system dynamics, the human's monitoring behavior depends upon the control requirements and the control actions in an explicit manner. This is intuitively appealing.

Problem solution. — In the above development we reduced the sampling problem to a deterministic nonlinear (matrix) optimization problem, the solution of which provides our predictions of human visual sampling. Solving this problem for ω^* is, in general, a difficult task. In some cases numerical search techniques can be used to predict average scanning behavior, especially when there are only two displays.

In the two display case, the scan sequences of interest have the form {1,0,2,0} and average scan behavior can be represented by the numbers t_1 and t_2 which are the durations of time spent fixating displays 1 and 2 respectively. Thus

$$T = t_1 + t_2 + 2t_o \ , \ t_o = \text{given}$$

and for a particular T, the value of t_1 that minimizes $I(\omega)$ may be found by a scalar search. We then vary T and for each T compute the optimal t_1. In this way we search for the optimal pair (t_1^*, T^*) or (t_1^*, t_2^*) corresponding to the optimal sampling strategy $\omega^*(t)$.

Once ω^* is computed, it then becomes possible to predict various measures of human response, as in the no-scan case. It is simple to show that all of the cost computations for the scanning case are equivalent to those of the no-scan case but with $\underline{\Sigma}_{avg}(\omega^*)$ replacing $\underline{\Sigma}$ in Eqs.(20)-(22).

When there is scanning, the notion of a frequency-domain representation of the human operator is somewhat tenuous from a theoretical standpoint, since one is now dealing with overt and purposeful nonstationary behavior. The equations (17)-(19) that define human strategy become time-varying with the replacements $\underline{\Sigma} \rightarrow \underline{\Sigma}(\omega,t)$ and $\underline{V}_y \rightarrow \underline{V}_y(\omega(t))$. However, the same experimental measures that are made in the no-scan case can be made when the human is scanning. These measurements may be thought of as representing "average" frequency-domain characteristics of the human. In order to predict these average characteristics with the model, we must replace the time varying quantities $\underline{\Sigma}(\omega,t)$ and $\underline{V}_y(\omega(t))$ with suitable "average" values. Such an average value for the error covariance matrix is already available from the solution of the "optimal sampling problem" namely $\underline{\Sigma}_{avg}(\omega^*)$. An average value for $\underline{V}_y(\omega^*)$ can be defined in a similar manner. Noting that $\underline{V}_y^{-1}(\omega)$, rather than $\underline{V}_y(\omega)$ itself appears in all calculations, we define

$$\underline{V}_{avg}^{-1} = \frac{1}{T}\int_0^T \underline{V}_y^{-1}(\omega^*(t))dt \tag{57}$$

where T is the scan period. But since $\underline{V}_y(\omega)$ is piecewise constant

$$\underline{V}_{avg}^{-1} = \sum_{i=1}^{k} \underline{V}_y^{-1}(i) \cdot f_i \; ; \; f_i = t_i/T \tag{58}$$

where f_i is the fractional time spent in fixating instrument i. Note that since the observation noise matrices are diagonal, the average noise covariance associated with the j-th displayed variable, $y_j(t)$ is simply

$$(V_{yj})_{avg} = \left(\sum_{i=1}^{k} V_{yj}^{-1}(i) f_i \right)^{-1} \tag{59}$$

The frequency domain expressions (24)-(26) can now be evaluated with $\underline{\Sigma}_{avg}$ and $\underline{V}_{avg}$ replacing $\underline{\Sigma}$ and $\underline{V}_y$ respectively.

A simplified approach for tasks involving scanning. — The major drawback with the above approach to scanning predictions is the need to solve a formidable optimization problem. Only in the simplest cases is it possible to minimize $I(\omega)$ to find ω^* (although it may be possible to find suitable approximations to ω^*, i.e., suboptimal scanning patterns).

Fortunately, there is a reasonable approximate method for predicting human response in cases for which there is sampling. The method involves finding an approximation to $\underline{\Sigma}_{avg}(\omega)$. Since $\underline{\Sigma}(\omega,t) = \underline{\Sigma}(\omega,t+T)$ we obtain, averaging Eq. (52) over one period T

$$\underline{Q} = \underline{A}_1 \underline{\Sigma}_{avg}(\omega) + \underline{\Sigma}_{avg}(\omega)\underline{A}_1' + \underline{W}_1 - \frac{1}{T}\int_0^T \underline{\Sigma}(\omega,t)\underline{C}_1' \underline{V}_y^{-1}(\omega)\underline{C}_1 \underline{\Sigma}(\omega,t)dt \tag{60}$$

Since $\underline{C}_1' \underline{V}_y^{-1} \underline{C}_1$ and $\underline{\Sigma}(\omega,t)$ are both positive definite for all t, a reasonable approximation to the integral average is merely the product of the averages†, viz,

$$\frac{1}{T}\int_0^T \underline{\Sigma}(\omega,t)\underline{C}_1' V_y^{-1}(\omega)\underline{C}_1 \underline{\Sigma}(\omega,t) \approx \underline{\Sigma}_{avg}(\omega)\underline{C}_1' \underline{V}_{avg}^{-1}(\omega)\underline{C}_1 \underline{\Sigma}_{avg}(\omega) \tag{61}$$

where $\underline{V}_{avg}^{-1}$ is given by Eq. (58).

†In addition, we have generally found $\underline{\Sigma}(\omega,t)$ to be slowly varying over a period, giving further cause to this approximation.

Thus, for a given strategy ω (described parametrically by the fractional allocations f_i), the solution $\hat{\underline{\Sigma}}(\omega)$ of

$$\underline{0} = \underline{A}_1\hat{\underline{\Sigma}} + \hat{\underline{\Sigma}}\,\underline{A}_1' + \underline{W}_1 - \hat{\underline{\Sigma}}\,\underline{C}_1'\underline{V}_{avg}^{-1}(\omega)\underline{C}_1\hat{\underline{\Sigma}} \tag{62}$$

will provide an approximation to $\underline{\Sigma}_{avg}$ that is very easy to compute. The minimization of

$$I(\omega) \approx \hat{\underline{L}}\,\hat{\underline{\Sigma}}(\omega)\hat{\underline{L}}' \tag{63}$$

will thus involve a minimization over the quantities f_i subject to the constraint

$$\sum_{i=1}^{k} f_i = 1 - f_o. \tag{64}$$

where f_o is the fractional time spent in switching foveal attention, and must be prespecified in the problem formulation. The solution of this problem for the optimal allocation of fixation time is much simpler than the optimal sampling problem posed earlier. It is a standard type of (algebraic) constrained minimization problem. Techniques for its solution are well-developed and include nonlinear programming, steepest descent, etc. The resultant $\hat{\underline{\Sigma}}(\omega^*)$ is then used in the expressions for scores, describing functions, spectra, etc.

Note that the sampling period T does not appear explicitly in in the reformulated sampling problem. However, as part of the problem specification we must choose a value of $f_o = t_o/T$ = fractional "dead-time". Choosing f_o is thus tantamount to picking a period T. For a given value of f_o (or T) the model optimally

adjusts the free parameters f_i to minimize Eq. (63).† We note that $I(\omega)$ is a monotonically decreasing function of f_o.

There is some evidence to show that the choice of f_o (or T) is not crucial in predicting human response characteristics. Results of some experiments [17] suggest that the human's choice of a scan period T may be governed by subjective considerations (or habit) rather than by strict optimality criteria. In addition, numerical experience in computing $I(\omega)$ as given in Eq. (56) has indicated that the minimum of $I(\omega)$ is fairly insensitive to variations in T, but is sensitive to variations in the fractional allocations t_i/T. Thus, relatively crude estimates of f_o may often suffice in practice.

Summary

In the foregoing we have shown how optimal control and estimation theory may be used to develop a model of human response in manual tracking tasks. The tasks we considered were those in which the controlled element was linear and the system was disturbed by a white noise input. The model included representations of human limitations and a cascade combination of a Kalman filter, a least-mean-squared predictor and a set of optimal feedback gains as compensating elements. An "optimal scanning mechanism" was also added to the model to account for situations where the human operator must visually scan several instruments in order to achieve his control objectives.

†For values of T much larger than the "time-constant" of Eq. (52), our assumptions leading to Eq. (63) become relatively poorer.

The use of the model in predicting task performance, controller describing functions and power spectra was demonstrated. The model was then validated by comparing model results with experimental data from three simple, but classical, manual control tasks.† The ability of the model to reproduce all the essential data in these experiments, using relatively few parameters, is most encouraging. Nevertheless, before the model can be truly useful as a design tool, greater insight into its detailed behavior, more systematic methods for picking its parameters, and techniques for extending its range of validity and applicability are all needed. These issues are addressed, in varying degrees of detail, in subsequent chapters.

†Data validating the scanning model were not presented. However, a recent report [17] suggests that good predictions of human scanning behavior should be possible with this model.

SENSITIVITY STUDIES

In this chapter we investigate the manner in which changes in model input parameters produce changes in model outputs. The cases to be analyzed include foveal tracking of K/s, K/s^2 and K/s(s-1) dynamics. We will study the effects of changes in "neuromotor time-constant" (τ_N), time-delay (τ), observation noise ratios[†] (ρ_i), motor noise ratio[†] (ρ_m), cost functional weightings (q_i,r) and input disturbance bandwidth. Parameters will be varied about those values that yielded a "best" match to data obtained from actual experiments.

The objective of this study is to learn which model outputs are most affected by a given model input, and to understand how and why changes in the model parameters shape predictions of human response. A desirable, if not necessary, goal of such a study is to obtain a method for choosing model parameters that will provide, in some definitive way, a "best" match to human response data. This is a necessary first step before one can use the model as an analysis tool or in a purely predictive manner in complex situations.

K/s Dynamics

The parameters that were found to give a good match to experimental data were $\tau_N = .08$, $\tau = .15$, $\rho_1 = \rho_2 = -20$ dB, $\rho_m = -25$ dB. The model predictions that result from this set of values were presented in the last chapter. Herein, these values will be varied (one at a time) and the resulting changes in model outputs shown.

[†]We choose to vary the noise ratios rather than the noises V_y,V_m themselves, since the ratios appear to be more intrinsic to the foveal tracking situations studied herein.

τ_N variations. — Changing τ_N is tantamount to changing the bandwidth and gain of the human operator model. Decreasing τ_N (i.e., decreasing g) places relatively more importance on keeping the error variance low in the cost functional J(u). Thus, error score will always decrease while control input power increases, especially at higher frequencies. With increasing τ_N the feedback system becomes more sluggish and performance at higher frequencies becomes relatively poorer.

Figure 8 shows the effect of variations in τ_N upon the equivalent describing function between displayed error and control. Note that for decreasing τ_N, the gain increases as expected, but with the greatest variation occurring beyond crossover. In general, this will always be true since the dominant effect of τ_N is felt in the rate of control (i.e., $\dot{u}$) which is manifested in the high frequency characteristics.

Note further that τ_N variations have only a small effect upon describing function phase in the range ω=4 to 30 rad/sec. The pole introduced by the first-order lag $(\tau_N s+1)^{-1}$ contributes up to 90° of phase lag in the feedback controller. Changing τ_N from .06-.14 moves this pole from 16 to 7 rad/sec. which accounts for the (approximately 45°) phase variations.

Normalized remnant, shown in Fig. 9 , is seen to be affected little by τ_N. The shape of the remnant spectrum is basically first-order. For low values of τ_N the remnant increases somewhat at high frequencies since the overall bandwidth of the feedback controller is increased and greater amounts of high-frequency

†Thus increasing crossover frequency.

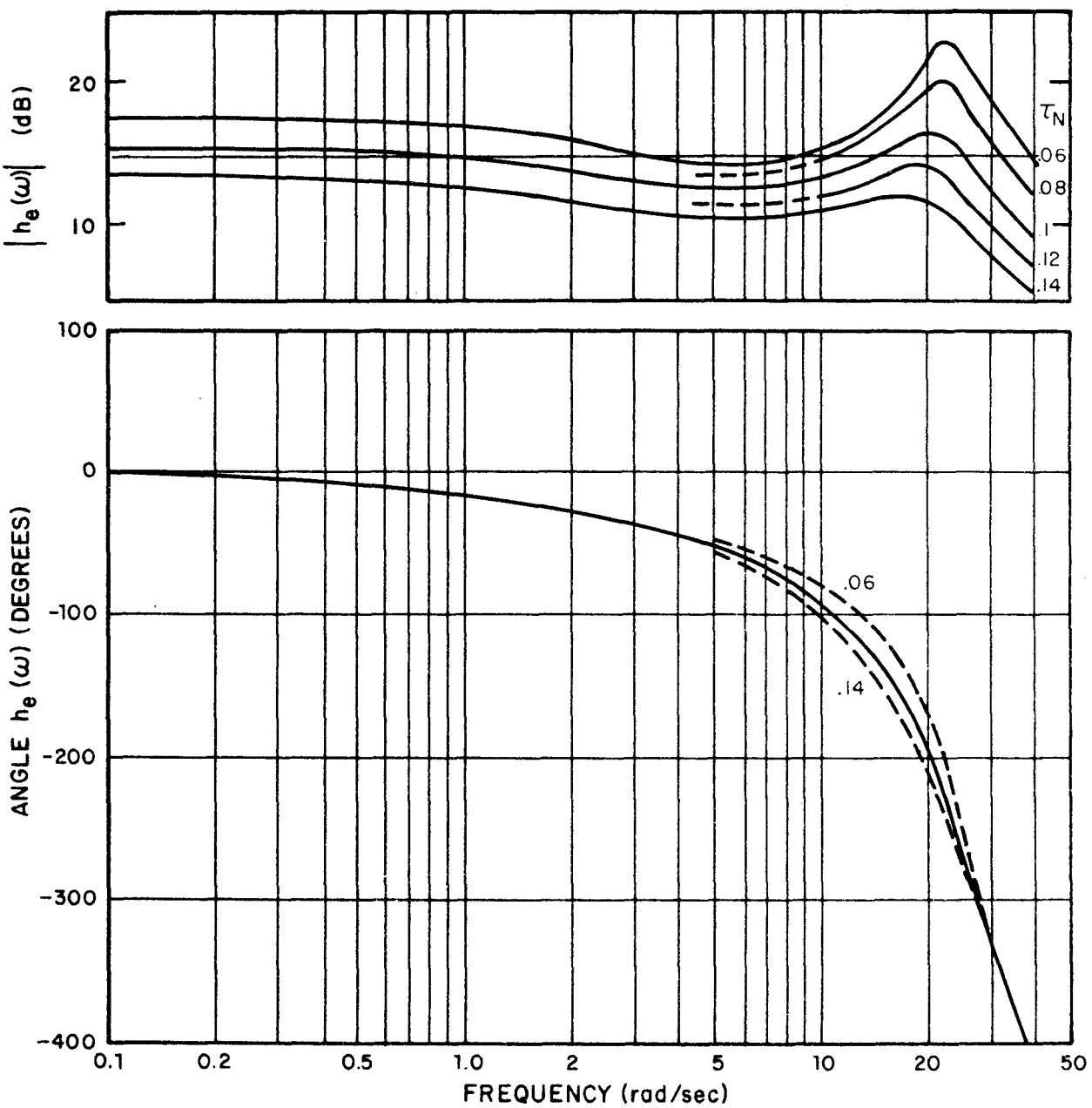

FIG.8 EFFECTS OF τ_N VARIATIONS ON MODEL DESCRIBING FUNCTION, k/s DYNAMICS

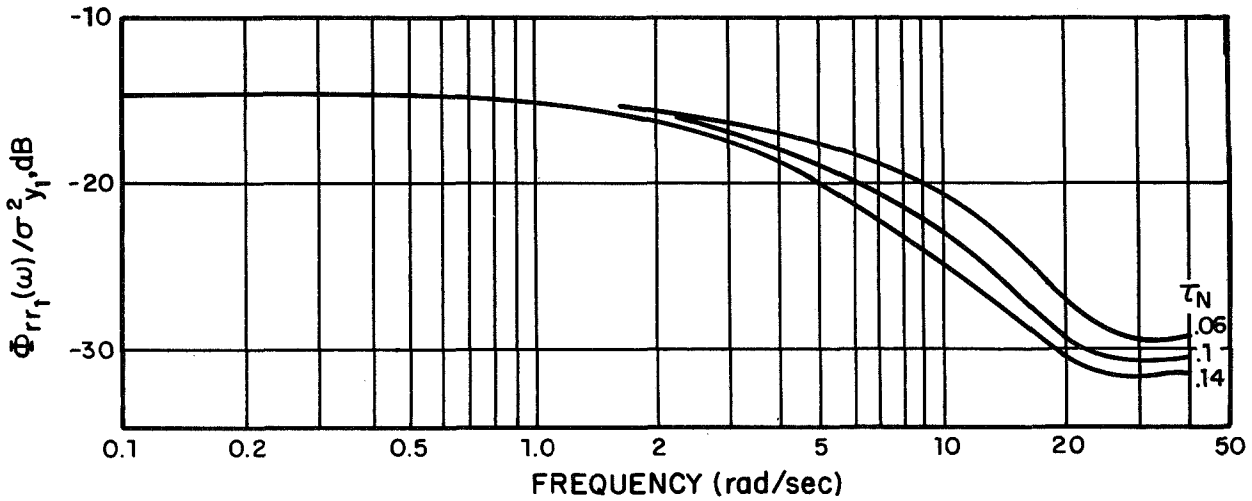

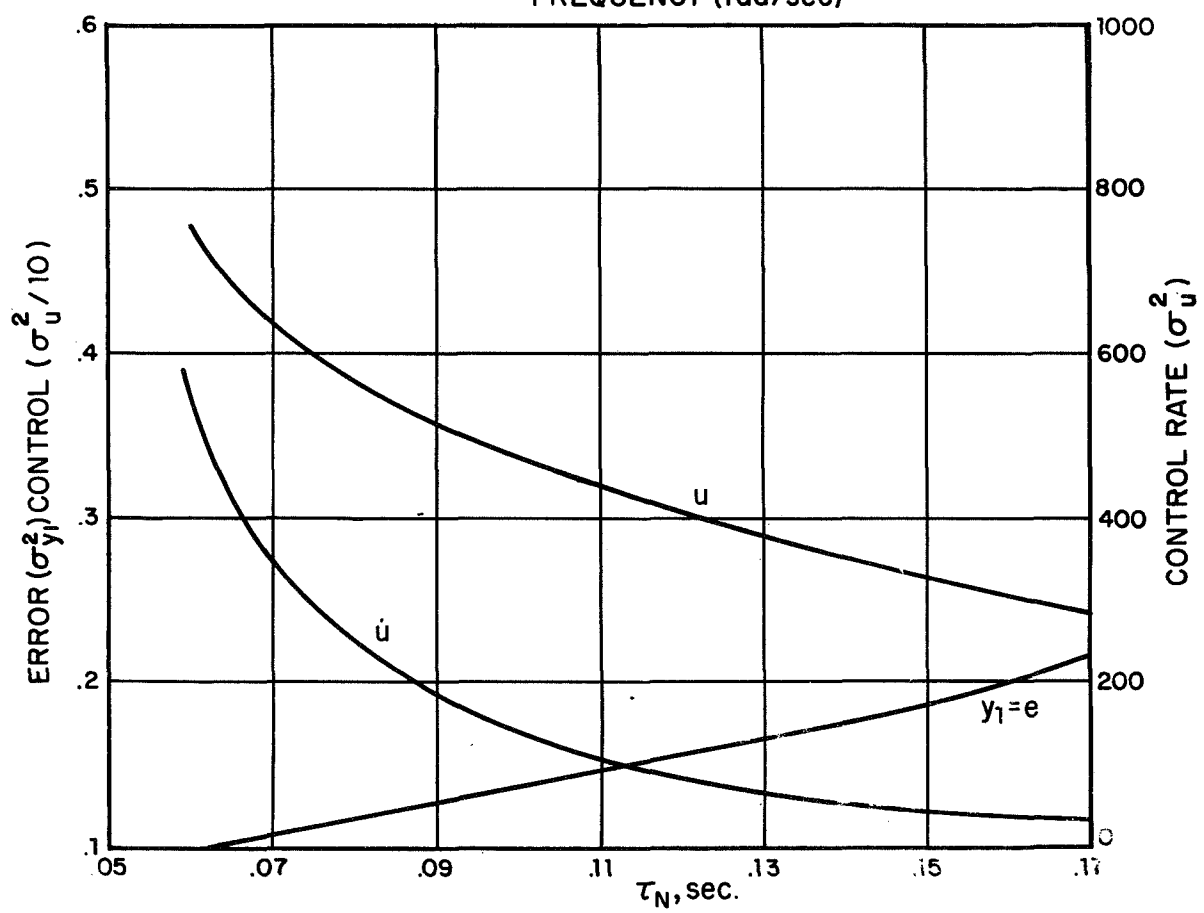

FIG.9 EFFECTS OF τ_N ON REMNANT AND SCORES, [illegible] AXIS

remnant (as well as correlated power) circle in the closed-loop system. However, the major contribution to these remnant variations occurs from changes in the characteristics of the motor noise (as it is currently being treated). The motor noise, because of its being filtered by $(\tau_N s+1)^{-1}$, appears at the system input as an injected first-order noise with break frequency at $1/\tau_N$. Changes in τ_N reshape this noise (for $\omega>1/\tau_N$) which causes the apparent break frequency of the remnant spectrum to vary from 3.5 to 6.0 rad/sec as τ_N is decreased from .14 to .06. If the motor noise were zero, or if it did not depend in such a direct manner on τ_N, the effects of changes in τ_N upon remnant would be negligible.

The sensitivity of scores (error, control, control-rate) are shown in Fig. 9. These curves show the trade-off between system error and input control signal as indicated earlier. For smaller τ_N the system expends more energy and achieves a lower error score.

An interesting sidelight of this study concerns the relationship between crossover frequency, ω_c, and the control rate weighting, g. Hofmann suggests that an approximate relationship between ω_c and g is[†]

$$\omega_c \doteq .707\ g^{-\frac{1}{4}} \tag{65}$$

This expression was derived under zero remnant conditions. In Fig.10 we compare ω_c as predicted by the model, with that given by Eq. (65). Note that Eq. (65) is a good approximation for higher values of g ($4\cdot10^4$ corresponds to τ_N=.1). For low values of g the differences between Eq. (65) and model predictions can be attributed to remnant effects. Decreasing the observation noises will increase gain and give higher crossover frequencies. (See Fig.13.)

[†]Private Communication, L.G. Hofmann.

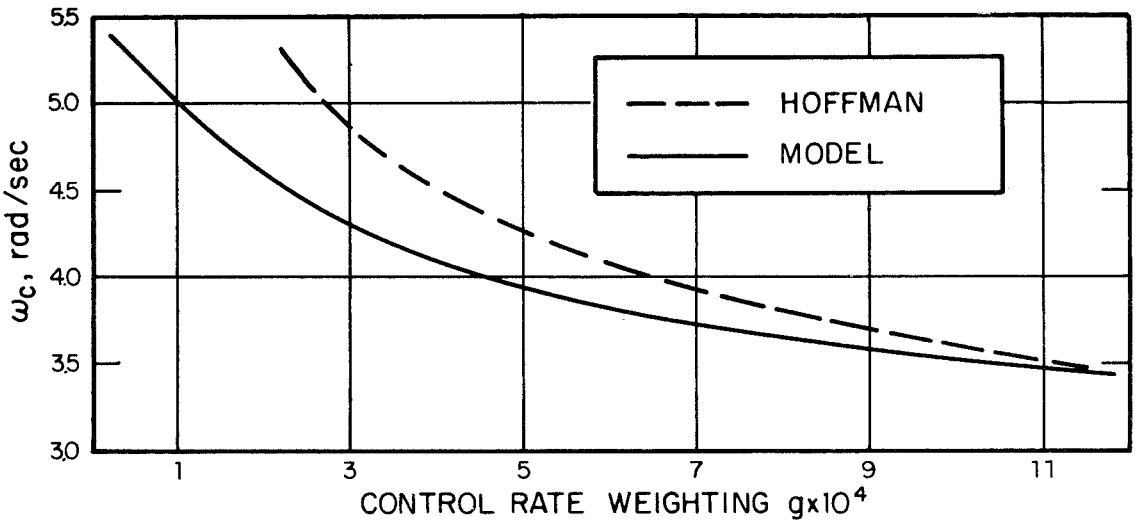

FIG.10 SYSTEM CROSSOVER VERSUS CONTROL RATE WEIGHTING

τ variations. – The effects of time-delay variations (from .1 - .2 sec.) upon the describing function are shown in Fig.11. The most noticeable effect is seen in the high frequency phase. Such is expected since this frequency range is well beyond crossover and the only model element still contributing to the phase lag is the time delay $e^{-s\tau}$. Thus, for high frequencies, the shape of the phase curve is almost entirely governed by the time-delay, and

$$\frac{\Delta\phi}{\Delta\omega} \simeq \frac{180^\circ}{\pi}\,\tau$$

The effects of time-delay upon the magnitude of $h_e(\omega)$ are clearly evident. Increasing time-delay decreases the gain, as might be expected, except about the high frequency resonant peak. Here, the resonance becomes more pronounced for increasing time-delay,

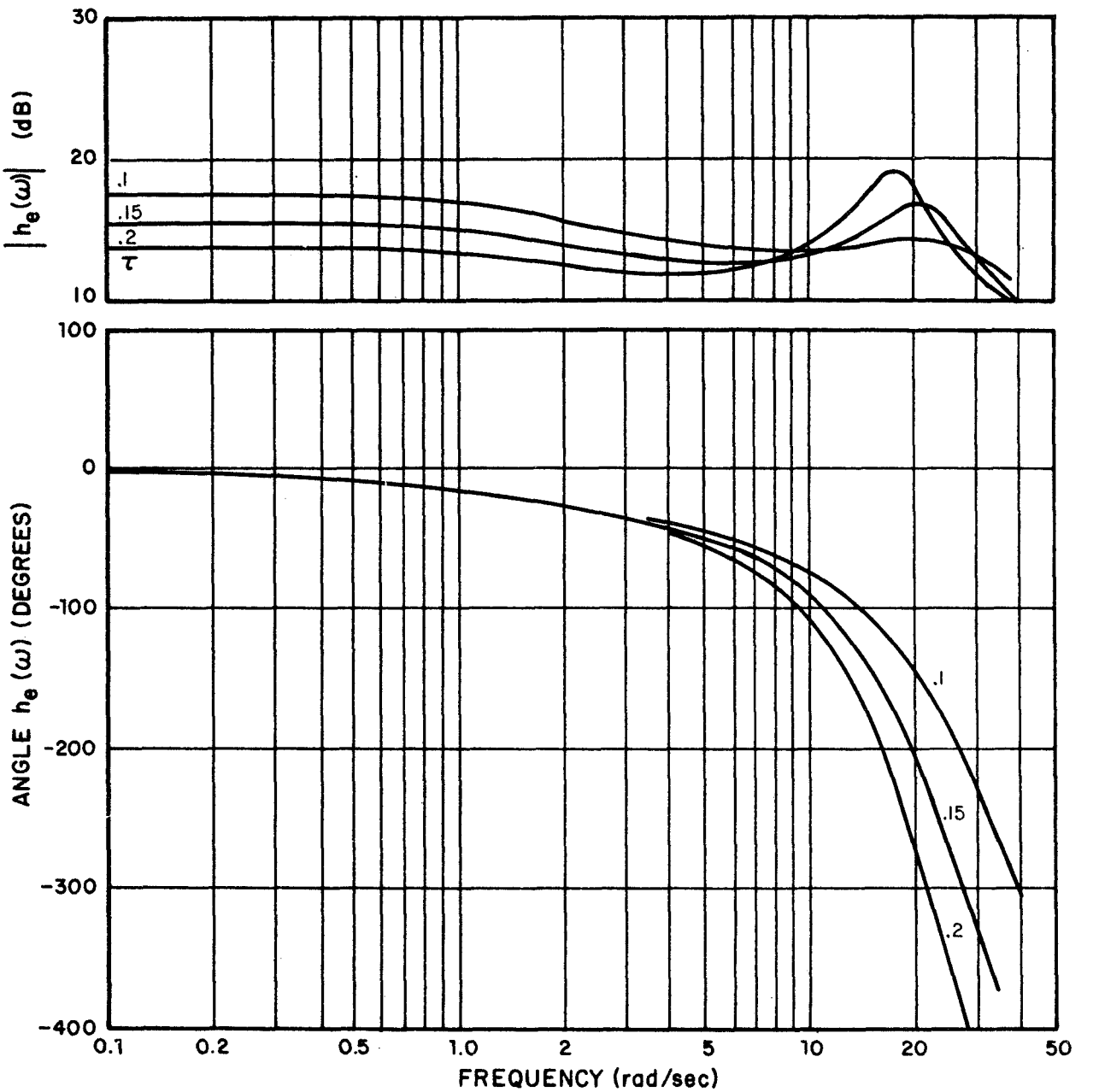

FIG.11 EFFECTS OF TIME DELAY ON MODEL DESCRIBING FUNCTION, k/s DYNAMICS

probably as a result of the predictor's need to extrapolate over a longer time interval. Also, from a classical servo-mechanism viewpoint, a greater time-delay moves the system closer to instability.† Thus, we see a more sharply defined resonance as τ increases.

The effects of time-delay variations upon remnant were found to be minimal and therefore are not shown. The effects were similar to those of Fig. 9 — the first-order break frequency of the remnant spectrum varied from only 4 to 5 rad/sec as τ decreased from .2 to .1 sec.

Increases in τ caused increases in all scores. The most notable increase was in the error score which doubled from .093 to .184 as τ increased from .1 to .2. Other scores, however, were far less sensitive. Control and control rate scores increased by less than 20% over this same range.

Observation noise variations. — To study the effects of changes in ρ_i we first vary ρ_1 and ρ_2 separately and then together. Variations in describing function and remnant caused by changing ρ_1 are shown in Figs. 12 and 14, while ρ_2 variations are given in Figs. 13 and 14. Note that the effects of ρ_1 upon controller describing function are negligible. However, the value of ρ_1 does influence greatly the low frequency normalized remnant.

Variations in ρ_2 have a very pronounced effect on the describing function. Gain increases over the entire frequency range as

†Decreasing phase margins, etc.

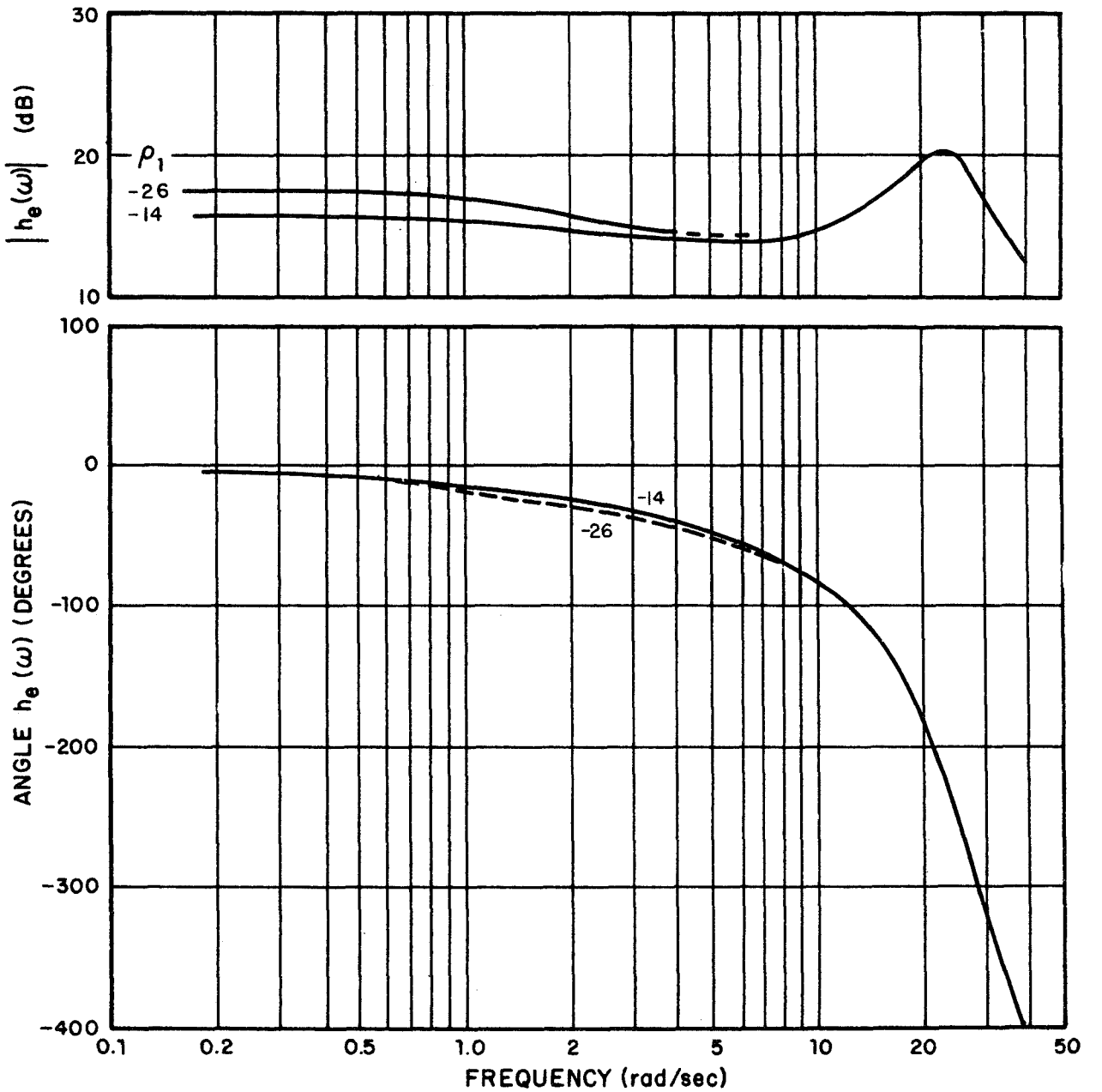

FIG.12 EFFECTS OF POSITION NOISE ON MODEL DESCRIBING FUNCTION, k/s DYNAMICS

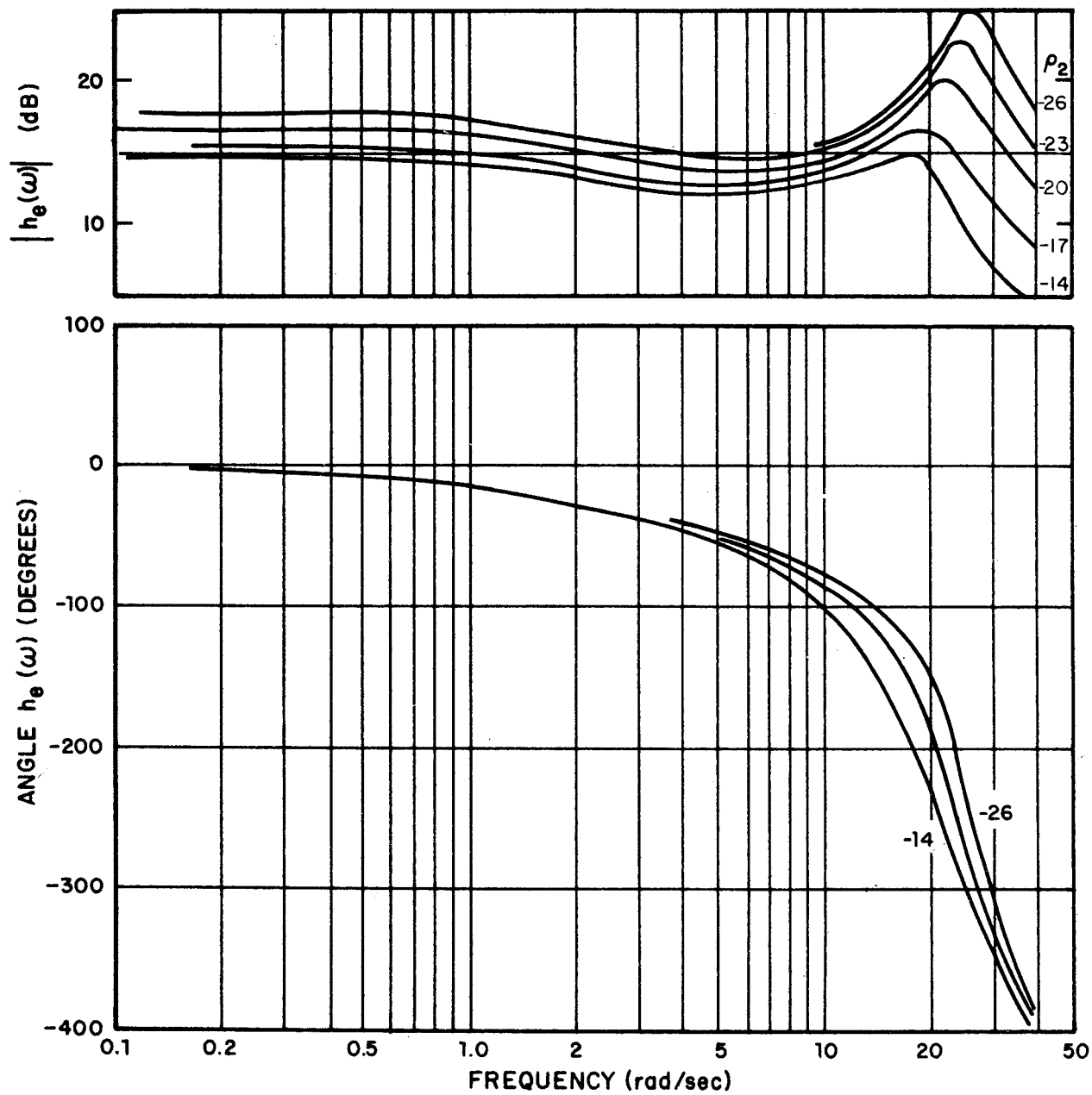

FIG.13 EFFECTS OF RATE NOISE ON MODEL DESCRIBING FUNCTION, k/s DYNAMICS

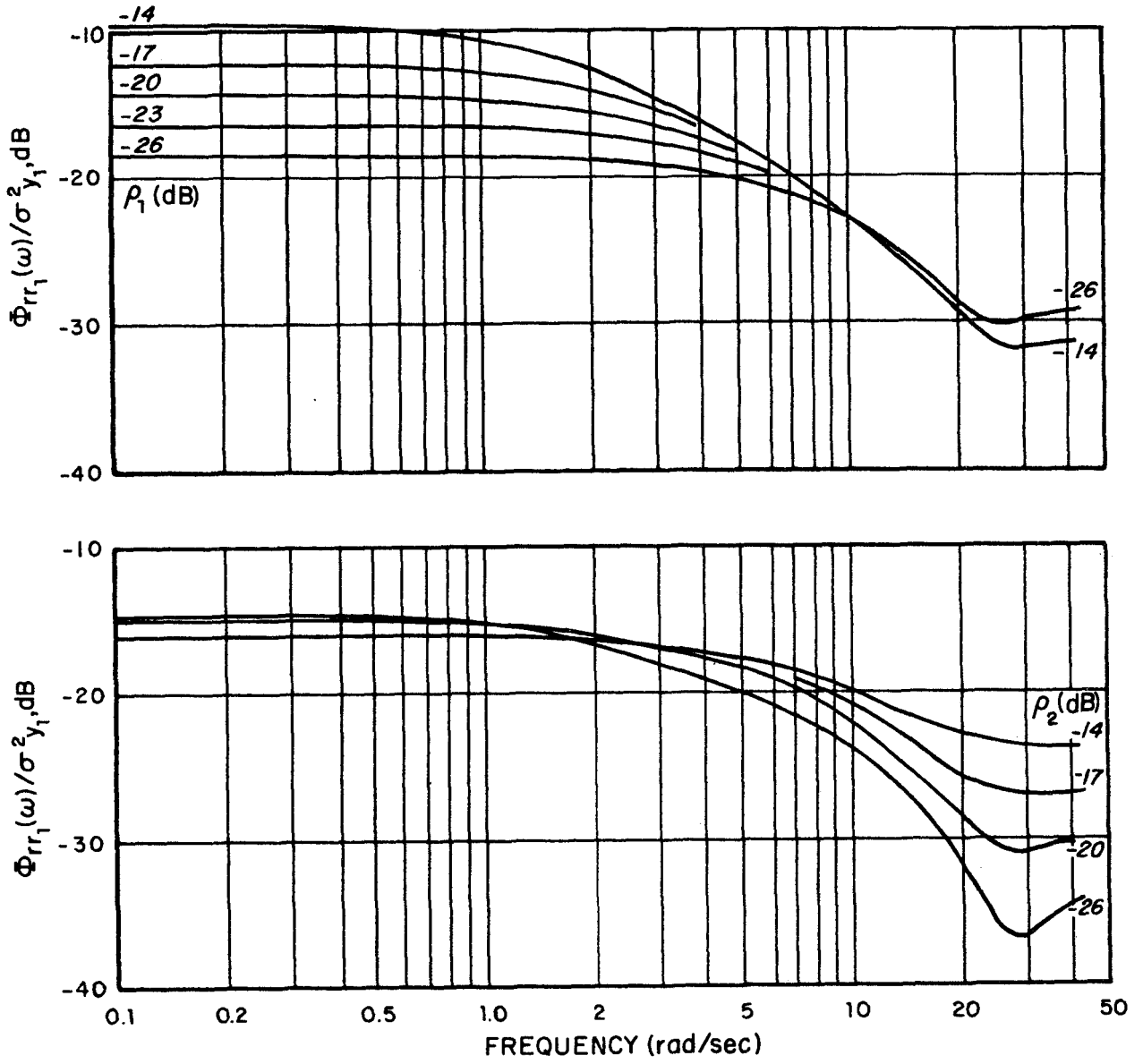

FIG.14 EFFECTS OF OBSERVATION NOISE ON NORMALIZED REMNANT SPECTRUM, k/s DYNAMICS

observation noise decreases. This result, coupled with the insensitivity with respect to ρ_1 indicates that, for K/s dynamics, the controller responds more to error rate than to error information. Better estimation of $y_2(t)$ permits more accurate control inputs to be generated while allowing for a higher gain on $y_2(t)$. Note that in this respect decreasing ρ_2 or decreasing τ_N have the same effect on the describing function - both, either directly or indirectly, increase the controller gain.

Lower velocity noise will necessarily result in lower remnant at high frequencies. Figure 14 shows this trend. Note that low frequency remnant, resulting primarily from position noise V_{y1}, is virtually unaffected by changes in ρ_2 (or V_{y2}).

The influence of observation noise ratio on scores is shown in Fig. 15. A lowering of any observation noise must necessarily result in lower scores, however, the sensitivities will vary, depending on the importance of the various displayed outputs to the overall control task. We thus find the scores to be more sensitive to ρ_2 than to ρ_1 in the range -14 to -26 dB, since velocity information is more useful for control purposes.

We have seen that the dominant effects of position noise are at low frequencies while those of velocity noise are at high frequencies. Thus, simultaneous variations in both ρ_1 and ρ_2 should affect system response in an additive way. Accordingly, Fig. 16 is the result of varying ρ_1 and ρ_2 simultaneously. Note that describing function† and remnant variations are essentially the superposition of the variations seen in Figs. 12-14.

†We show only $|h_e(\omega)|$. The phase is virtually indistinguishable from that of Fig.13.

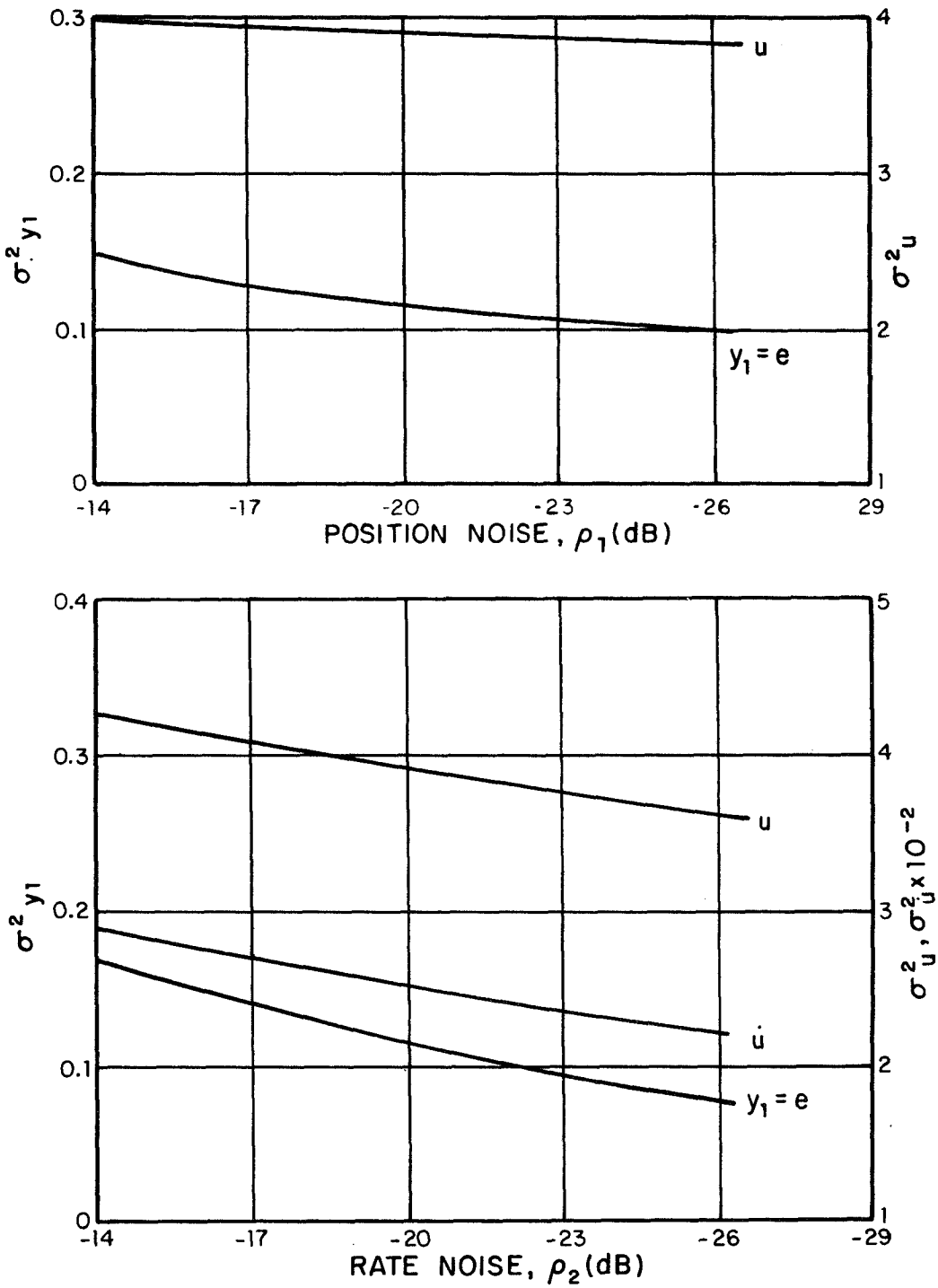

FIG.15 EFFECTS OF OBSERVATION NOISE ON SYSTEM VARIANCES, k/s DYNAMICS

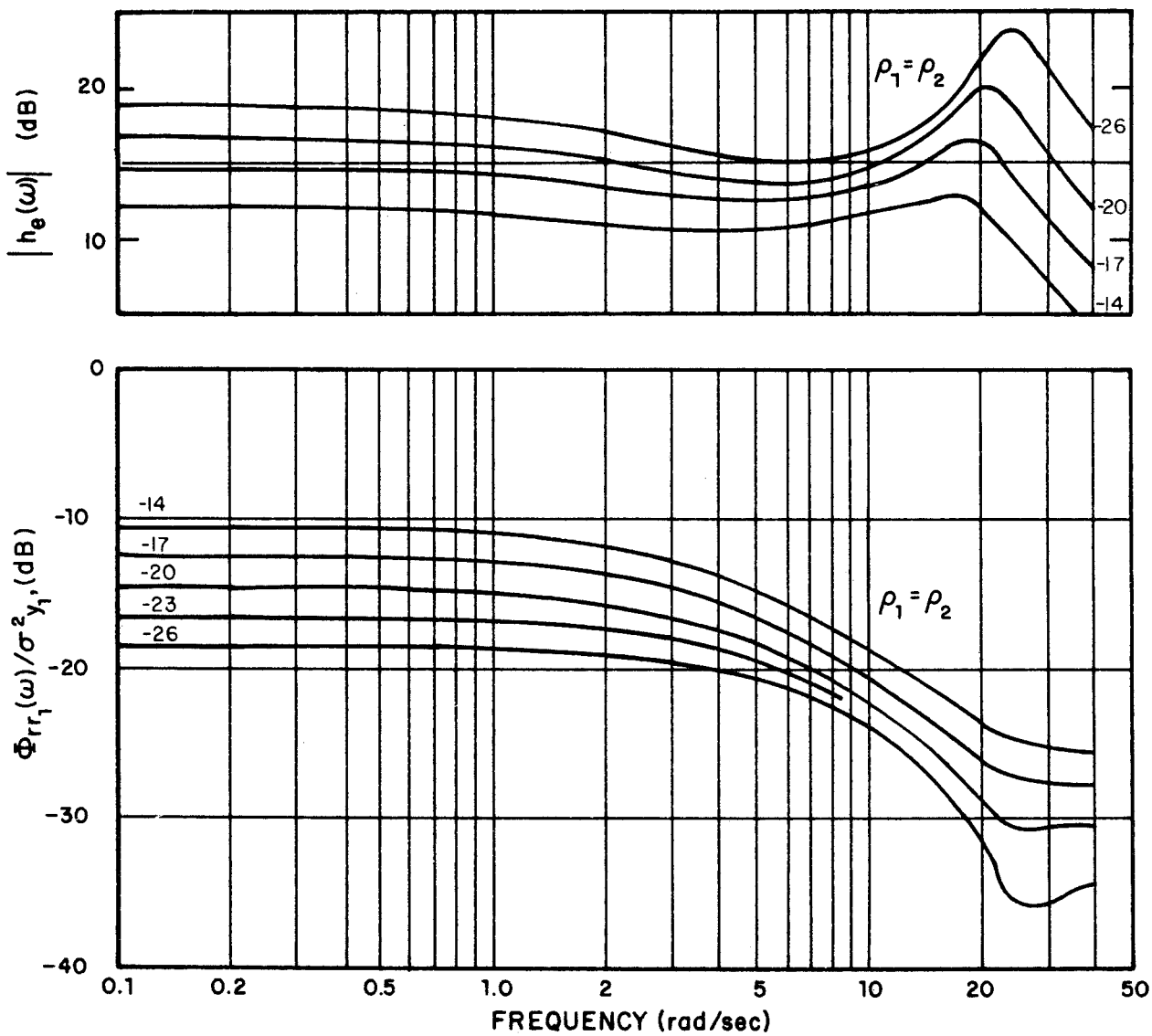

FIG.16 EFFECT OF SIMULTANEOUS VARIATIONS IN OBSERVATION NOISE RATIOS, k/s DYNAMICS

ρ_m variations. — Motor noise was introduced as an additional (uncorrelated) system input to account for the fact that the human can not estimate perfectly the control input, u(t), or signals linearly related to u(t). In cases where the input noise disturbance enters the system in parallel with u(t) (such as prevails here), the need for such a construct is obviated. In such cases, therefore, motor-noise should not appreciably affect the Kalman estimator or, in turn, the feedback strategy, $\underline{h}(\omega)$. On the other hand, increasing the motor noise introduces more remnant in the closed-loop system. This increases all variances, especially that of u and $\dot{u}$, since the motor noise is injected in parallel with the control signal.

Figure 17 shows the dominant effects of motor-noise variations. As expected, $h_e(\omega)$ is affected little by ρ_m. With increasing ρ_m, the magnitude of $h_e(\omega)$ does decrease slightly due to a slight lowering of estimator gains — estimation of all system states becomes more difficult. The scores and normalized remnant have a more pronounced response to motor noise changes. Note that the dominant effect on remnant is at high frequencies. This is because motor noise, in being treated like an additional (wideband) system input, finds its low-frequency components being more easily "tracked-out" by the feedback system than are its high-frequency signals.†

Input bandwidth variations. — In the cases studied thus far, the input forcing function was first-order noise with a pole at ω_1 = 2 rad/sec. We now study the effects of pole location on system performance. We keep τ_N = .08, τ = .15, $\rho_1 = \rho_2$ = -20 dB, ρ_m = -25 dB.

†Recall the manual control experiments in which a low bandwidth driving signal had a small high-frequency "shelf" added. It was often found that most of the error power was due directly to this high-frequency component.

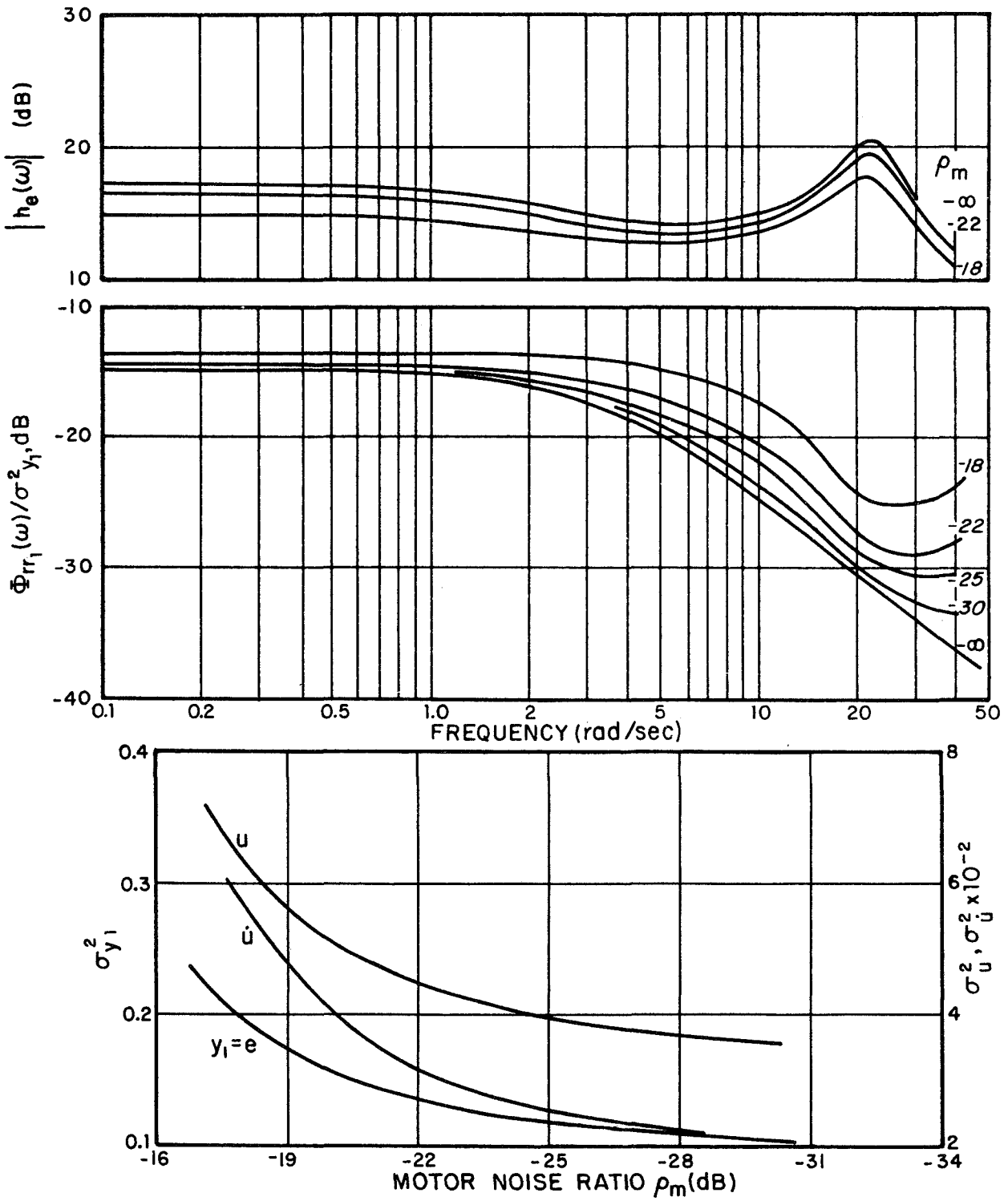

FIG.17 EFFECTS OF MOTOR NOISE, k/s DYNAMICS

Figure 18 shows the dominant effect of input bandwidth, ω_i. As ω_i decreases, $h_e(\omega)$ increases (along with some phase variation), especially at low frequencies, since it is relatively easy to track a low-frequency signal. Of special interest in this case is the crossover frequency, ω_c. It is stated in Ref. 4 that as input bandwidth increases beyond crossover, the system crossover will "regress" to lower frequencies. Accordingly, Fig.18 shows system crossover (the intersection of the line AA' = ω^2 with $h_e(\omega)$) as a function of ω_i. For low bandwidth, crossover is relatively invariant at ω_c = 4.8 rad/sec. However, as ω_i nears this value, the crossover frequency is predicted to indeed "regress" towards lower values.

Bandwidth variations were found to have a negligible effect on system remnant. This is in accord with the experimental results reported in Ref. 14 where it was found that bandwidth did not seem to affect normalized remnant.

K/s^2 Dynamics

The same type of sensitivity study as performed for K/s dynamics was done for the K/s^2 dynamics of Eq. (47). The nominal parameters taken for this case were τ_N = .1, τ = .2, $\rho_1 = \rho_2$ = -20 dB, ρ_m = -25 dB. The resultant nominal describing function and remnant spectrum appear in Fig. 5..

τ_N variations. — As in the K/s dynamics case studied before, variations in τ_N (or equivalently g) scale the optimal gains $\underline{\ell}^*$ and also allow for more rapid control movements.† Thus, Fig. 19 shows

†If there were a weighting r on control, then variations in g would have a reduced effect on $\underline{\ell}^*$. However, the 1:1 correspondence between g and τ_N would still remain.

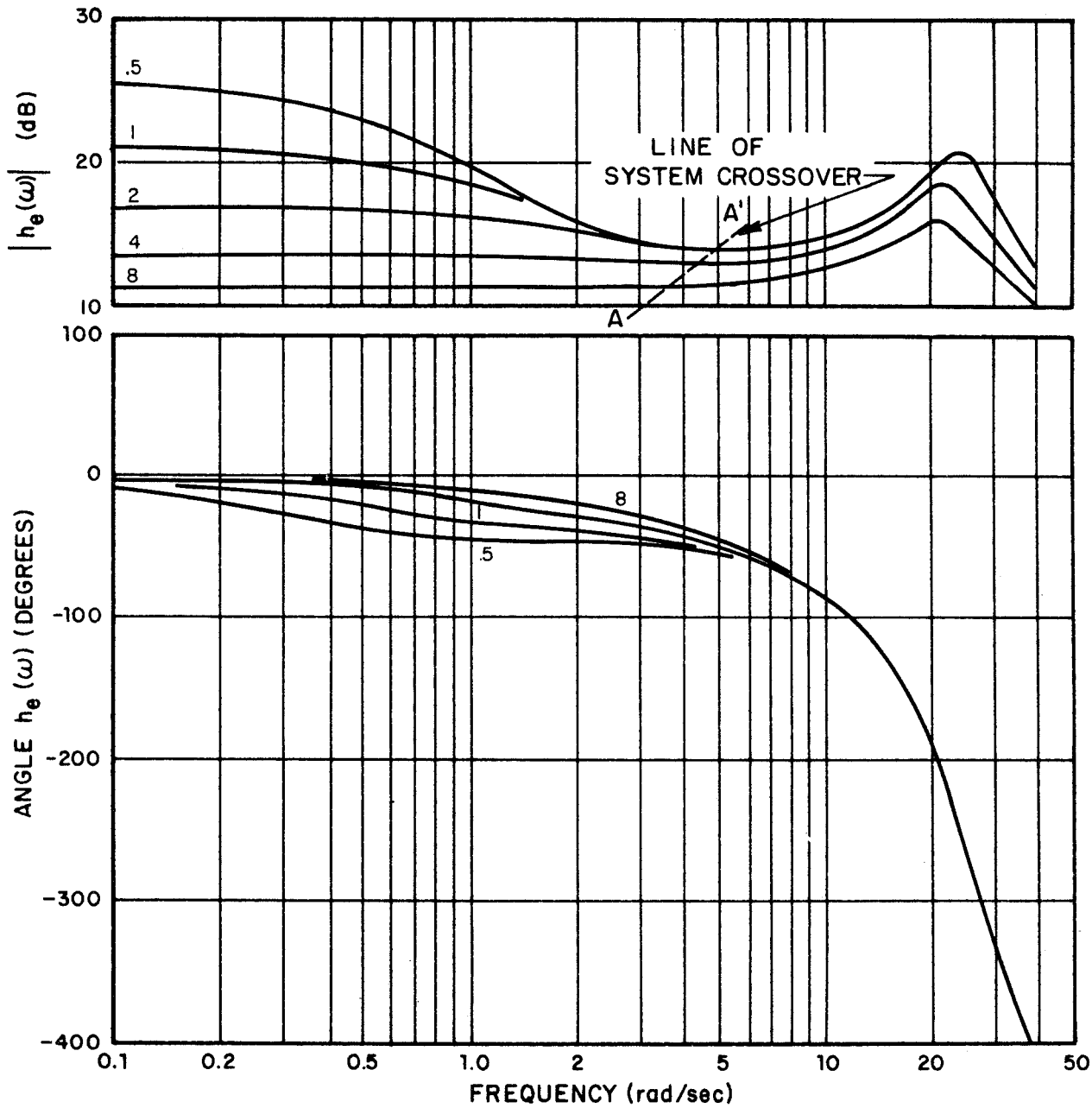

FIG.18 EFFECTS OF INPUT FORCING FUNCTION BANDWIDTH ON MODEL DESCRIBING FUNCTION, k/s DYNAMICS

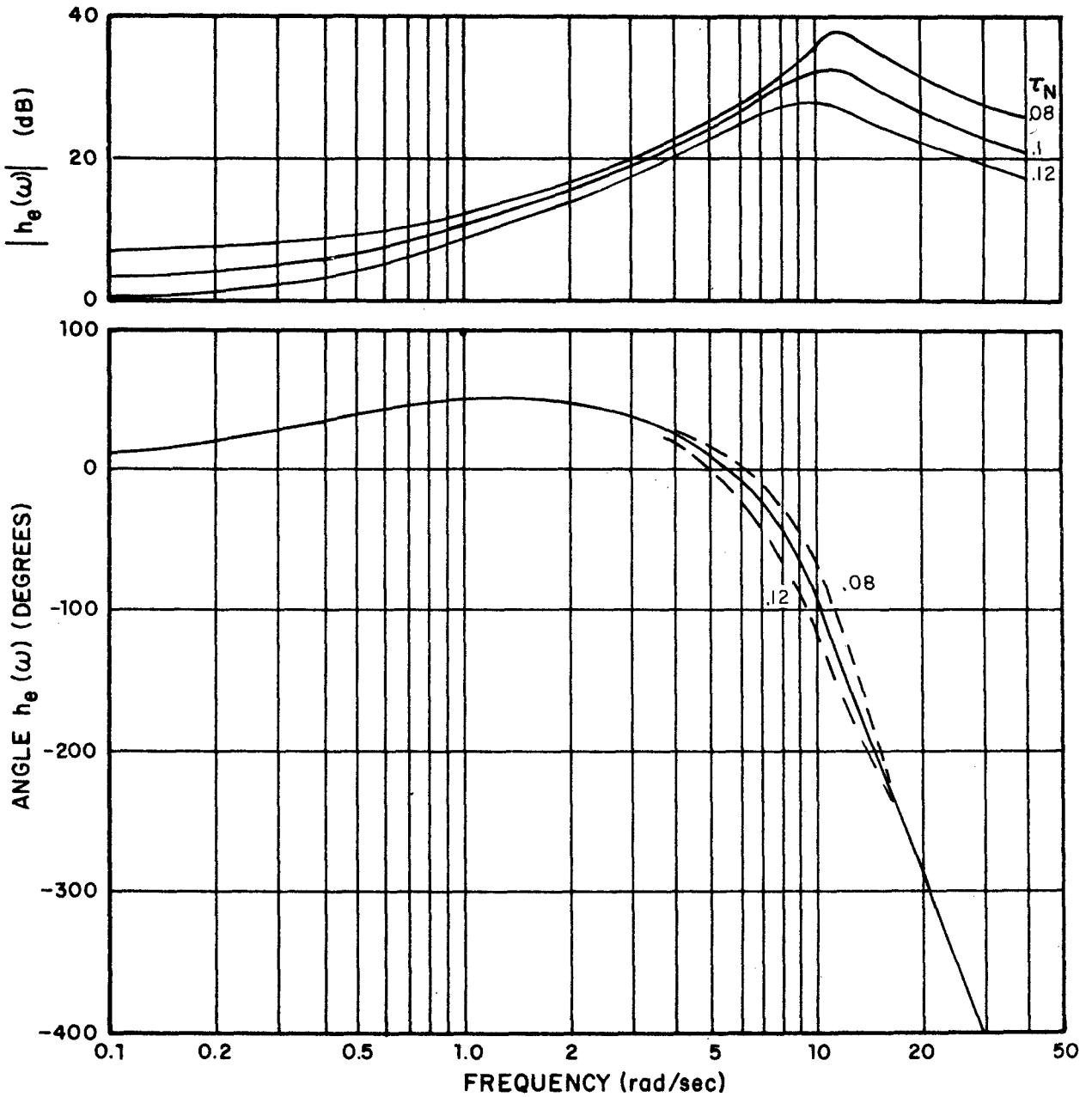

FIG.19 EFFECTS OF τ_N VARIATIONS ON MODEL DESCRIBING FUNCTION, k/s^2 DYNAMICS

that as τ_N decreases the feedback gain increases, with the greatest increase being for $\omega>10$ rad/sec. Effects of τ_N upon the phase are small and are much the same as for K/s dynamics.

Decreasing τ_N introduces a trade-off in the cost functional $J(u)$. Error score decreases at the expense of increased control rate and more control effort. Figure 20 clearly shows this trade-off. Note that large increases in control effort result in relatively small decreases in error score. This is because of the second-order filtering of the plant. In general, the more filtering between control and error, the less sensitive will be σ_e^2 to changes in control power resulting from τ_N variations. (Compare with Fig. 9, for example, where the plant introduces only a first-order filter.)

The effects of τ_N upon normalized remnant spectrum (reflected on error-rate) were found to be minimal and are not shown. As τ_N was varied over a range .07 to .12 the normalized remnant changed by only 1-2 dB at high and low frequencies. In the mid-frequency range $1.0<\omega<10$. remnant varied less than 1 dB about the nominal of Fig. 6.

<u>τ variations.</u> – Time-delay variations have the same effect on describing function (Fig. 21) as was observed for K/s dynamics. Increasing τ decreases $|h_e(\omega)|$ slightly at lower frequencies while at the same time it sharpens the high-frequency resonant peak. However, the most noticeable effect of time-delay variations is seen in the high-frequency phase lag. It is apparently true that the high-frequency phase characteristics are almost entirely the result of time-delay.

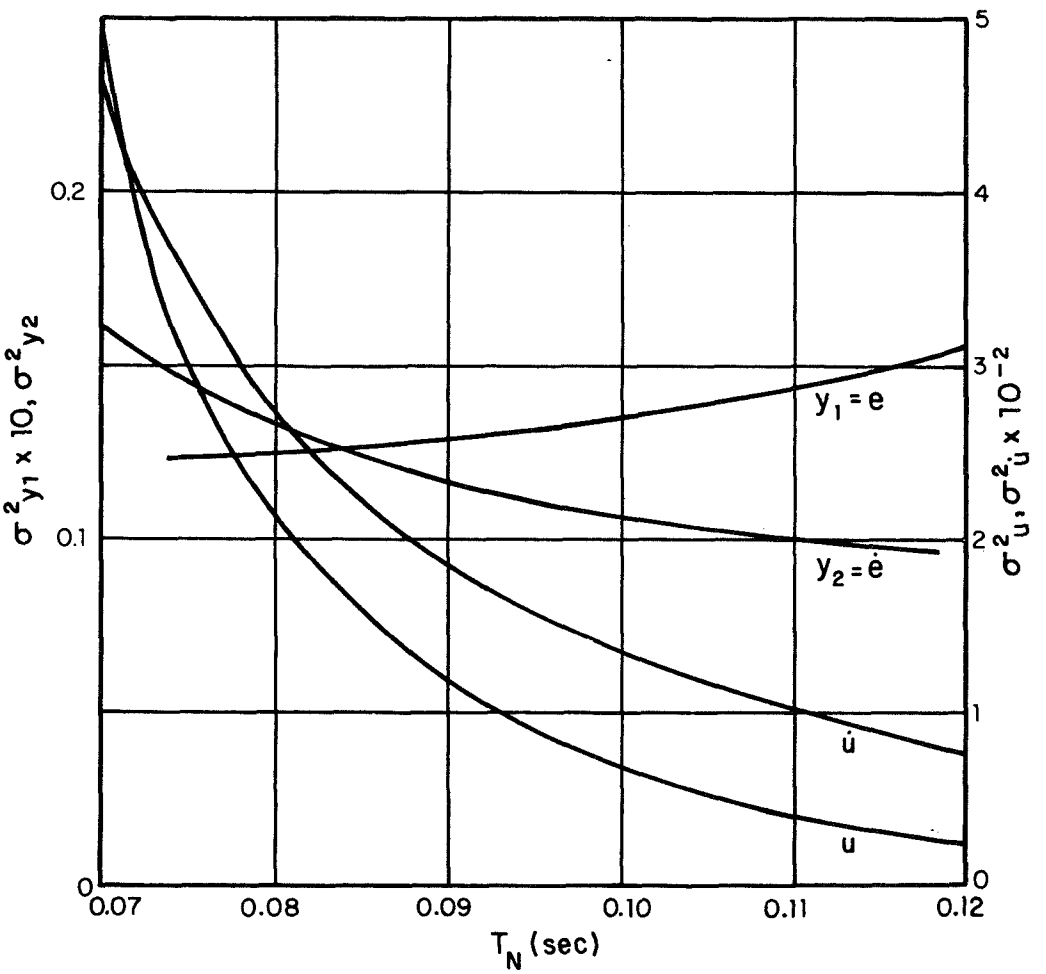

FIG.20 EFFECT OF τ_N VARIATIONS ON SYSTEM VARIANCES, k/s^2 DYNAMICS

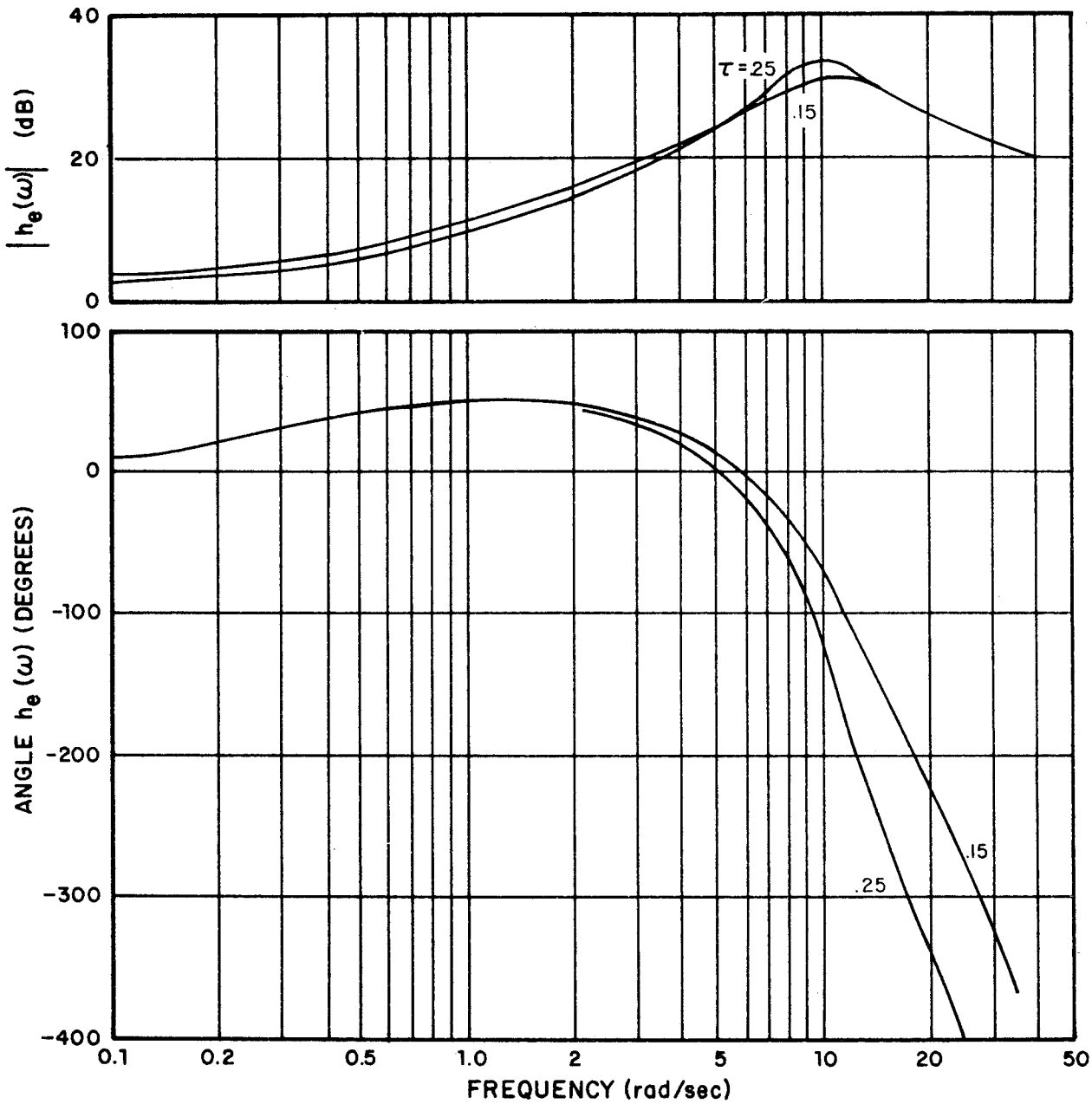

FIG.21 EFFECTS OF TIME-DELAY ON MODEL DESCRIBING FUNCTION, k/s^2 DYNAMICS

Once again, normalized remnant is virtually unaffected by changes in τ. However, system variances all scale monotonically with τ. Table 2 gives system scores for three different values of τ. Note the (almost) linear increase in scores as τ varies from .15 to .25.

Table 2

System Variances as a Function of Delay

τ_N=.1, V_{y1}=V_{y2}=-20 dB, V_m=-25 dB

Variance	τ=.15	τ=.2	τ=.25
e	.011	.014	.017
$\dot{e}$	.093	.108	.125
u	1.16	1.33	1.53
$\dot{u}$	57.7	67.3	77.8

Observation noise variations. — The effects of observation noise ratio upon system performance was studied by varying both ρ_1 and ρ_2 about their nominal -20 dB values.

Variations with respect to ρ_1 were studied first. It was found that changing ρ_1 over the range -10 to -30 dB resulted in little, if any, change in the describing function, scores or remnant. This gross insensitivity to ρ_1 is understandable since the feedback system is acting essentially like a differentiator (i.e., u(t) is proportional to $\dot{e}(t)$). Therefore, $\dot{e}(t) = y_2(t)$ is the key quantity to be estimated by the model. Changes in ρ_1 have little effect on this estimation, since the Kalman filter makes little use of $y_1(t)$ in estimating $y_2(t)$, except possibly when $y_2(t)$ is small or when ρ_2 is large.

On the other hand, it is expected that ρ_2 would have a more pronounced effect on system performance. This is indeed true and Figs. (22)-(23) show the effects of ρ_2 variations. The basic effects are as found for K/s dynamics: Better estimation of $y_2(t)$ allows for higher controller gains and more precise input generation. This is especially true at higher frequencies where $h_e(s) \approx sh_2(s)$. Decreasing ρ_2 results in a universal lowering of scores (Fig. 23) as well as a decrease in remnant. The major changes in remnant spectrum occur beyond crossover, i.e., in the frequency range where the feedback control system responds almost entirely to $y_2(t)$. Thus, velocity noise variations find their dominant effect at higher frequencies, as expected.

Because of the gross insensitivity with respect to ρ_1, the results corresponding to simultaneous variation of ρ_1 and ρ_2 are almost identical to those corresponding to variations in ρ_2 alone. We therefore do not show the effects of varying both noises together.

Motor noise variations. – Unlike the case for K/s dynamics, the input noise disturbance in the K/s^2 system being studied does not enter the system in parallel with the control signal u(t). (See Eq. (47).) It enters in parallel with $x_3 = \int u(t)dt$, i.e., as a velocity rather than as an acceleration disturbance. Therefore, recalling the discussion on motor-noise in the last chapter, one would expect motor-noise to have a noticeable effect on system response. Such is indeed the case as seen in Figs. (24)-(25). The reasons for the observed variations are discussed below.

In the absence of motor-noise, $\dot{x}_3 = u$ and the Kalman estimator obtains a perfect estimate of $x_3(t)$ simply by integrating u(t). Since $\dot{x}_2 = y_2 = x_3 + x_1$ (where x_1 is the first-order noise disturbance), estimation of y_2, coupled with knowledge of x_3, provides a

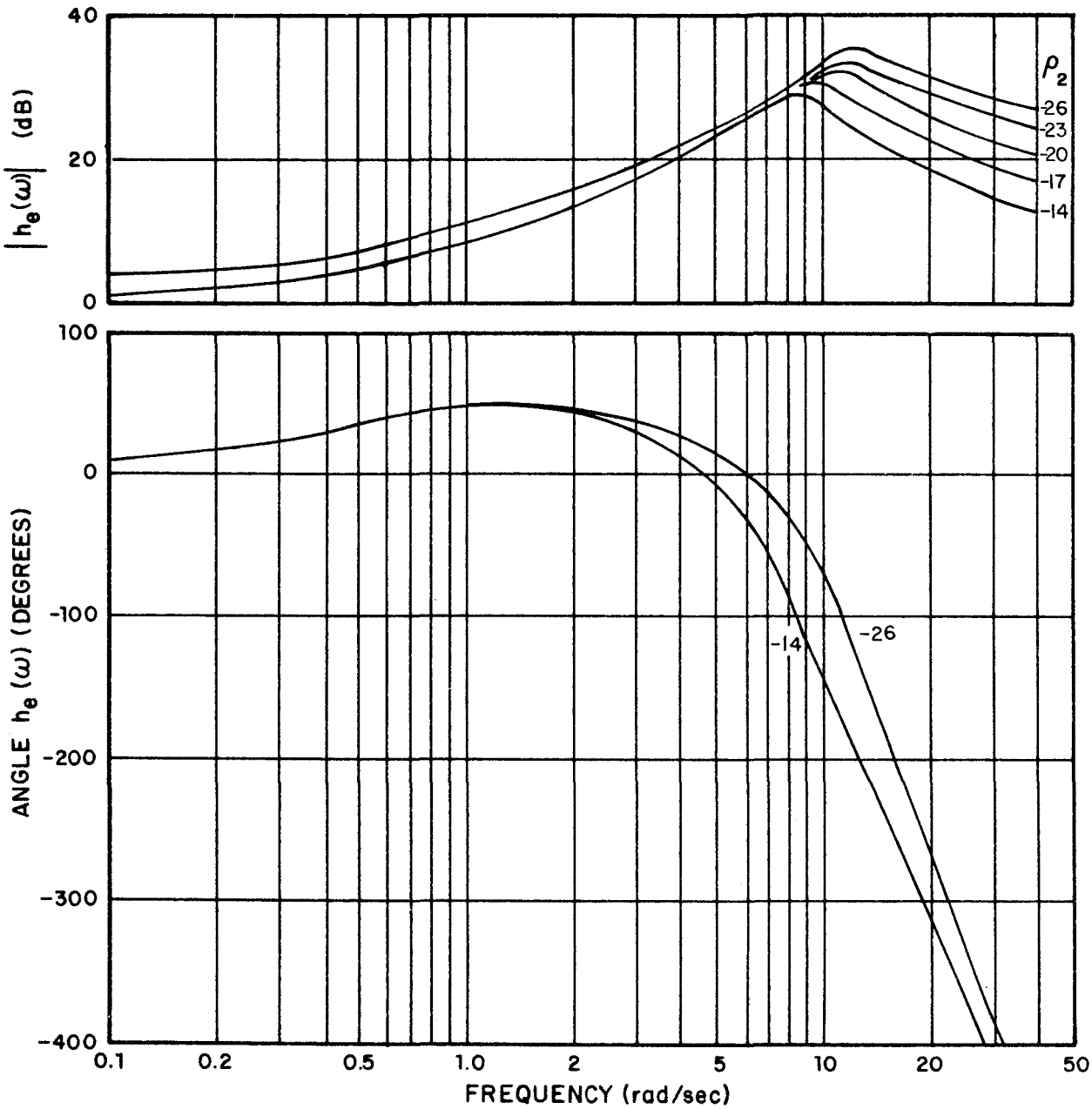

FIG.22 EFFECT OF OBSERVATION NOISE ON MODEL DESCRIBING FUNCTION, k/s^2 DYNAMICS

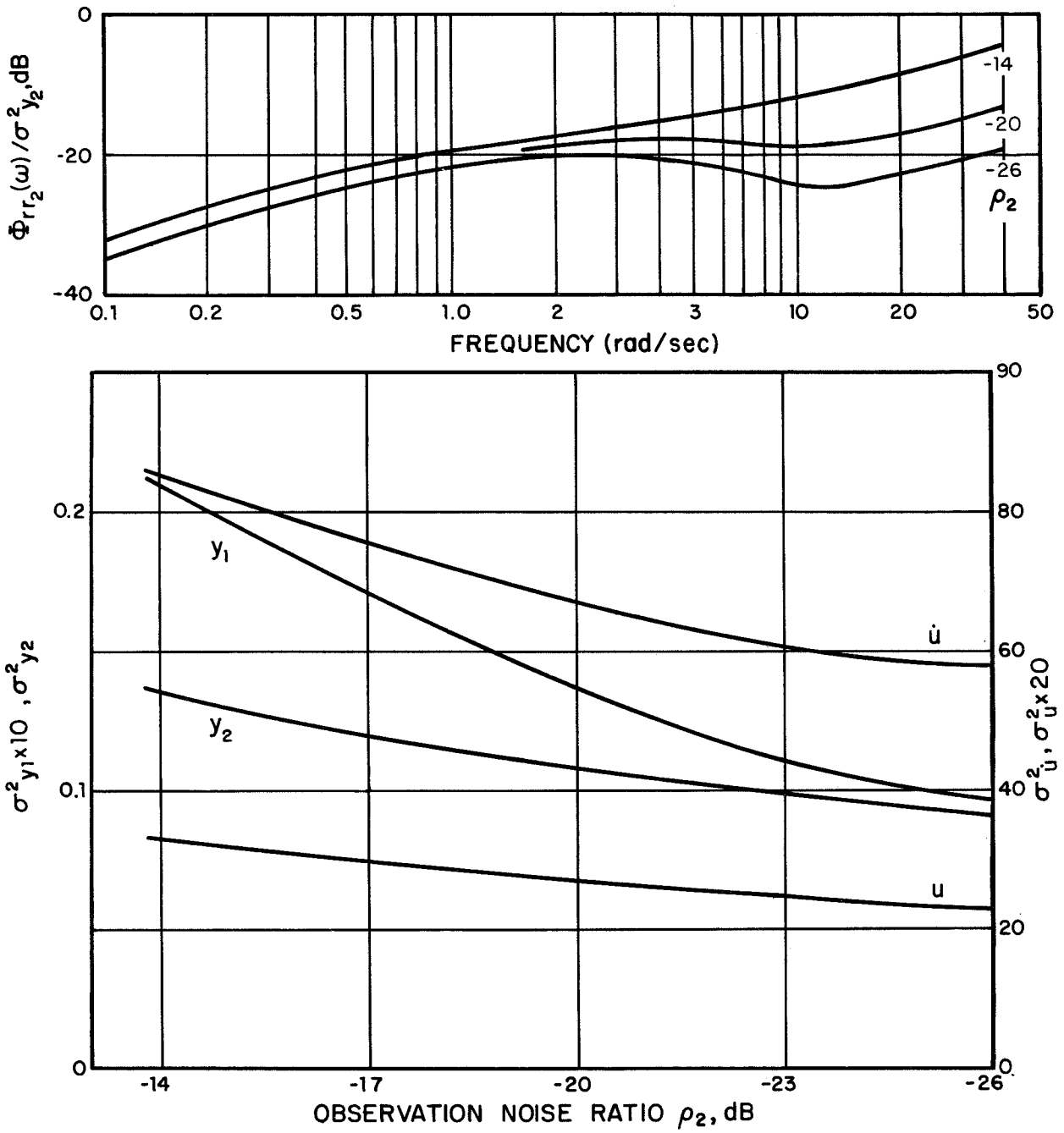

FIG.23 EFFECTS OF OBSERVATION NOISE ON REMNANT AND SCORES, k/s^2 DYNAMICS

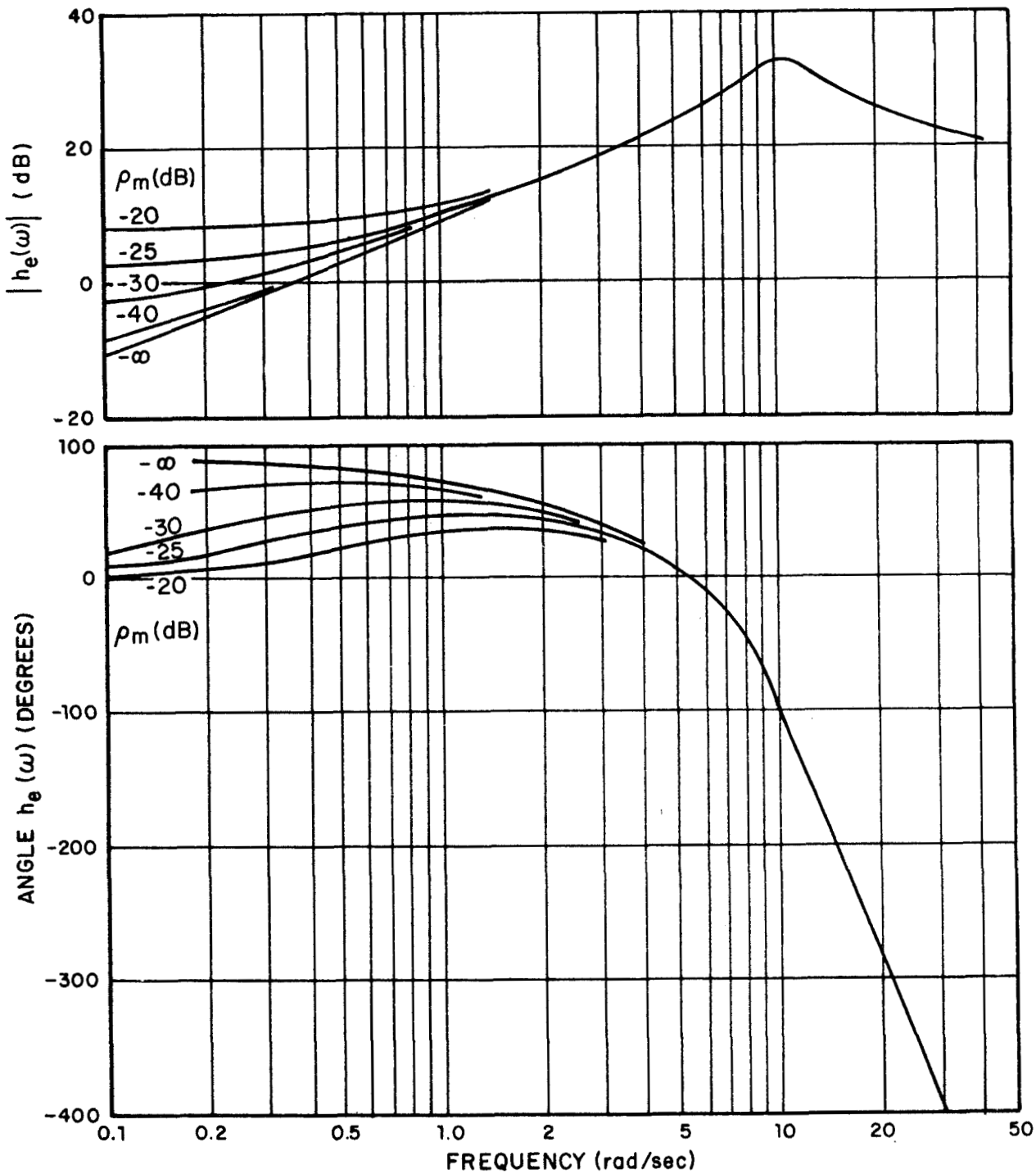

FIG.24 EFFECTS OF MOTOR NOISE ON MODEL DESCRIBING FUNCTION, k/s^2 DYNAMICS

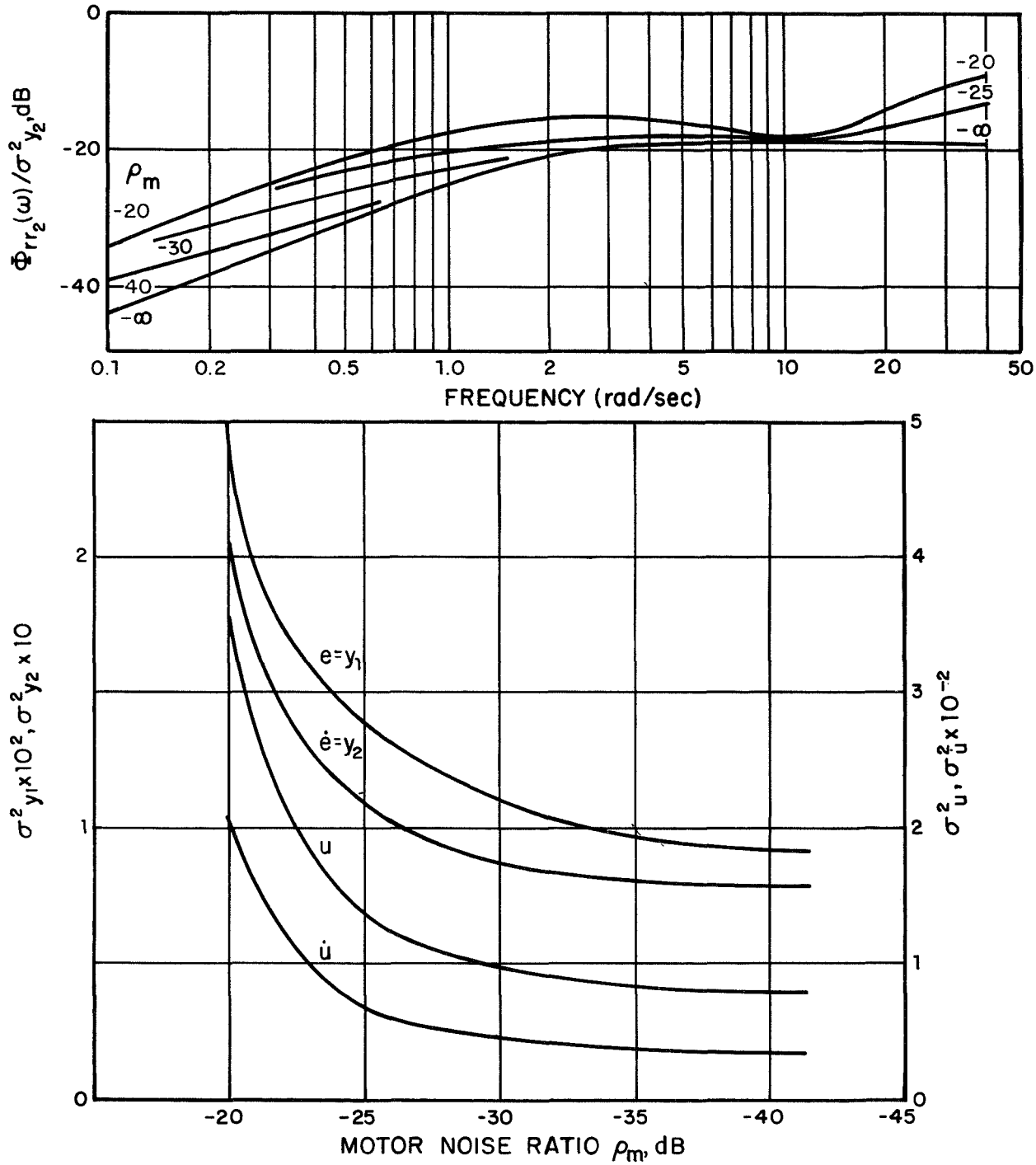

FIG.25 EFFECTS OF MOTOR NOISE ON REMNANT AND SCORES, k/s^2 DYNAMICS

direct estimate of x_1. Thus, setting $u(t) \approx -\dot{x}_1$ will result in low values of $\dot{x}_2$ and in turn of x_2.

In general, when both position and velocity information are available, the position information (i.e., $y_{1p}(t)$) is of limited use in estimating velocity [19]. Velocity is estimated almost directly from the observation $y_{2p} = y_2 + v_{y2}$. Therefore, in the absence of motor-noise, position information is virtually unneeded ($h_1(s) \to 0$) and $h_e(s) \approx sh_2(s)$ as seen in Fig. 24.

On the other hand, when motor-noise is present, $x_3(t)$ can no longer be estimated from u(t) by integration and position information is useful. Therefore, a good estimate of x_1 depends indirectly on proper use of $y_{1p}(t)$. Clearly, the importance of position information will depend monotonically on the level of motor-noise: the greater V_m, the more the use of $y_{1p}(t)$. The trends of Figs. (24)-(25) clearly show this phenomena. The increase in remnant results from both increased motor-noise as well as from the higher gains placed on $y_1(t)$ and its associated noise $v_{y1}(t)$. Note the extreme sensitivity in scores for $\rho_m > -25$ dB. This is primarily a result of the input disturbance effects associated with treating $v_m(t)$ as a driving noise.

From the above results it is clear that motor-noise will have a major effect on system behavior (especially at low frequencies) when the input disturbance does not enter with u(t). To understand the cause and effect relationship requires an analytic study of motor-noise, and the phenomena that it attempts to represent. In a later chapter we investigate this point in more detail.

Bandwidth variations. – The effects of input forcing function bandwidth upon human controller describing function is investigated. The results are shown in Fig. 26. It is seen that increased bandwidth results in lower describing function gains (phase remains essentially unaltered). System crossover frequency (where $|h_e(\omega)|$ intersects the line AA' = ω^4 in Fig. 26) decreases almost linearly from 3.2 to 2.2 as input break frequency increases from .5 to 8 rad/sec. Therefore, we again see a "crossover regression" phenomena.

Velocity weighting, q_3. – Until now, the effects on system performance of changing the cost functional weightings have not been studied. Herein we investigate the results of adding a velocity weighting, q_3, where q_3 may be regarded either as a subjective or as an objective weighting.†

Since the cost functional weightings are paramount in the determination of the feedback gains $\underline{\ell}^*$ (see Eq. 10), changing J(u) will have noticeable effect on system response. Furthermore, introducing a weighting on, say x_3, will necessarily effect a tradeoff: $\sigma^2_{x_3}$ will decrease at the expense of increases in other system variances.

The effects of varying q_3 from 0 to .5 are shown in Figs. (27)-(28). In this study the control rate weighting g was adjusted each time to give τ_N = .1. Note that increasing q_3 results in a universal decrease in $|h_e(\omega)|$. This decrease is somewhat more pronounced at low frequencies. Since more importance is being attached to $y_2(t)$, the position $y_1(t)$ becomes less important for control and $h_e(s)$ more closely resembles $sh_2(s)$, owing to the decrease in $h_1(s)$. (Note that since τ_N = .1 in all cases, the position of the resonant peak does not change.)

†x_3 is one component of the velocity signal. The noise x_1 is the other.

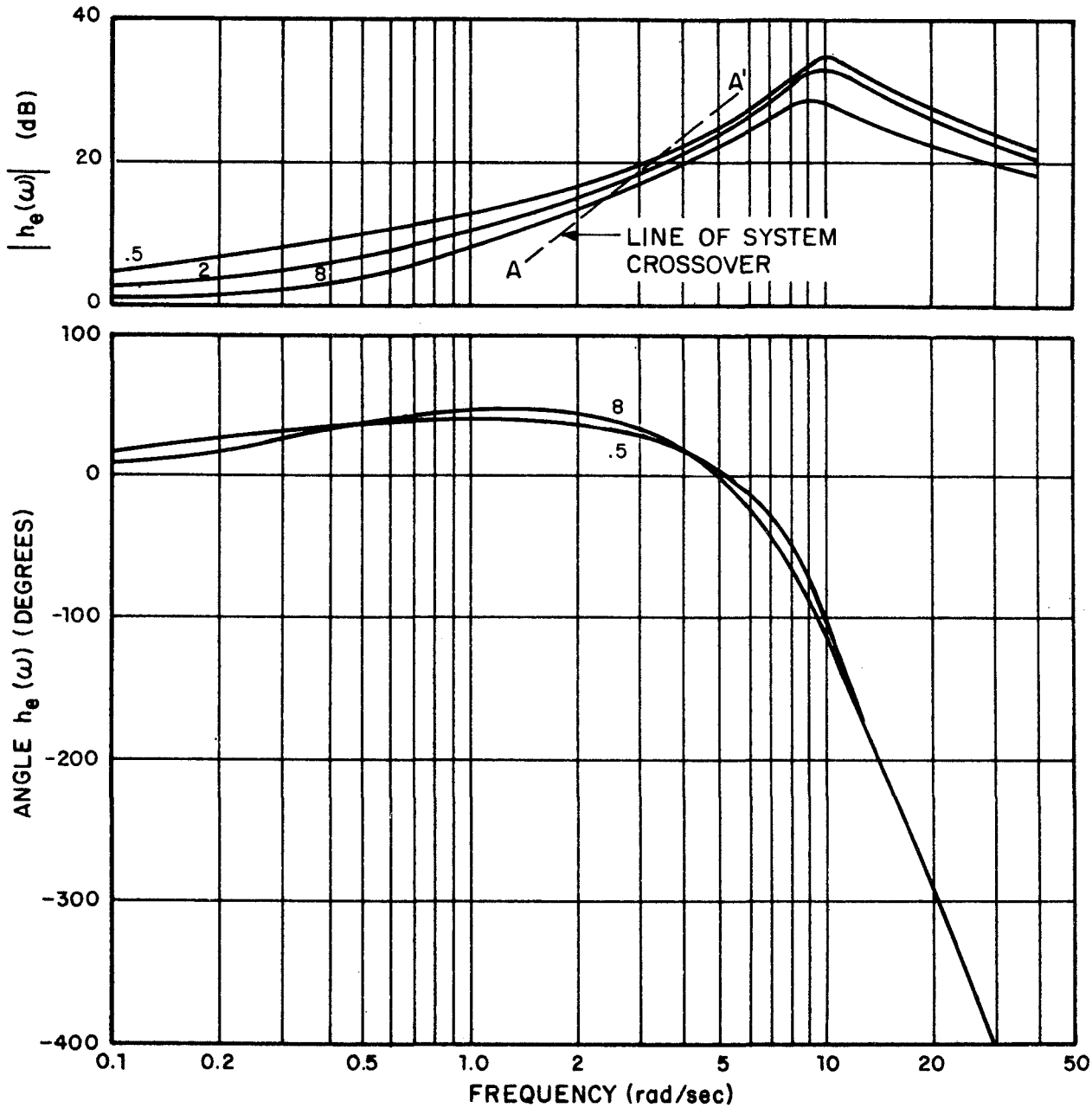

FIG.26 EFFECTS OF INPUT FORCING FUNCTION BANDWIDTH ON MODEL DESCRIBING FUNCTION, k/s^2 DYNAMICS

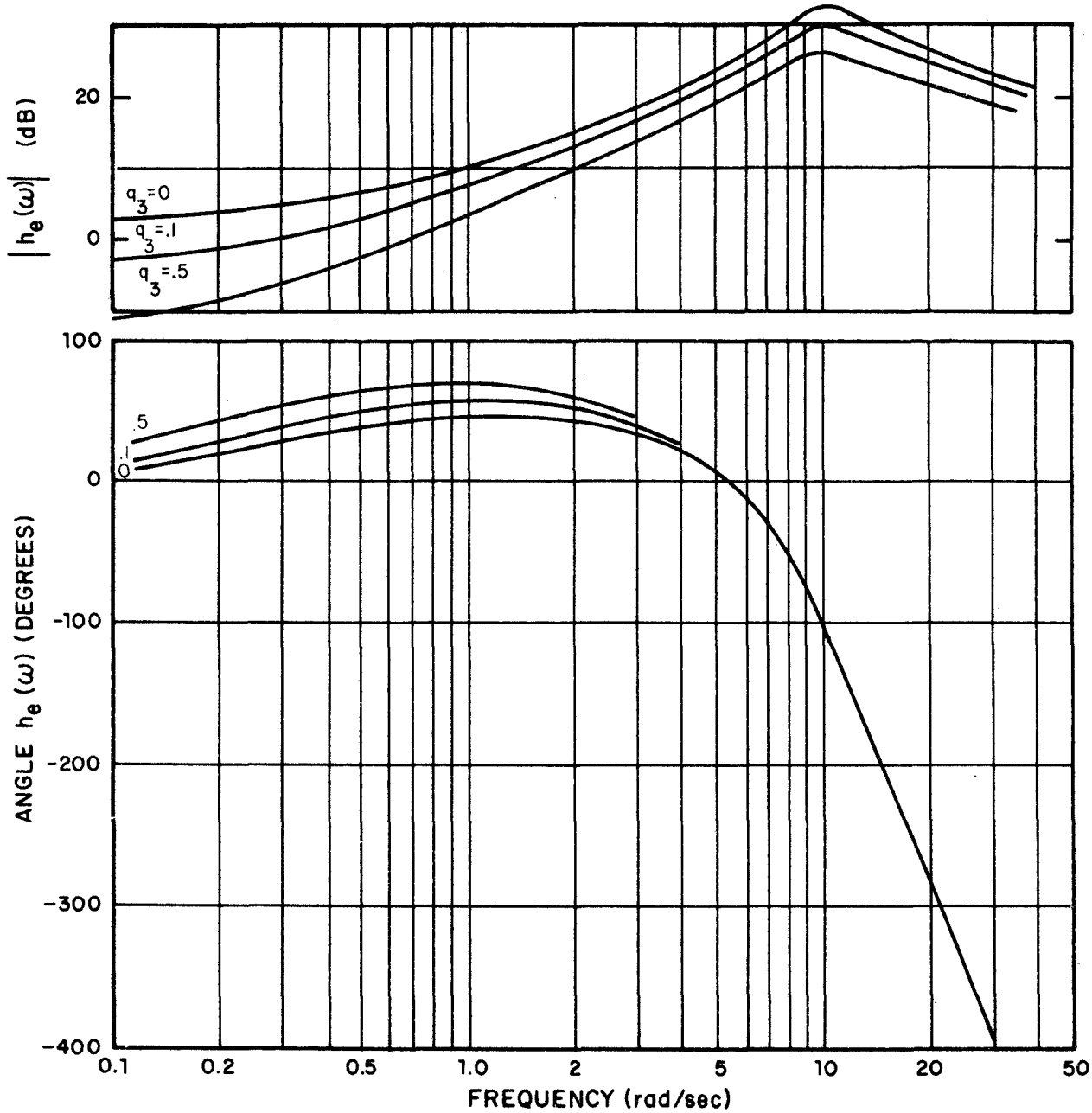

FIG.27 EFFECTS OF WEIGHTING ERROR RATE ON MODEL DESCRIBING FUNCTION, k/s^2 DYNAMICS

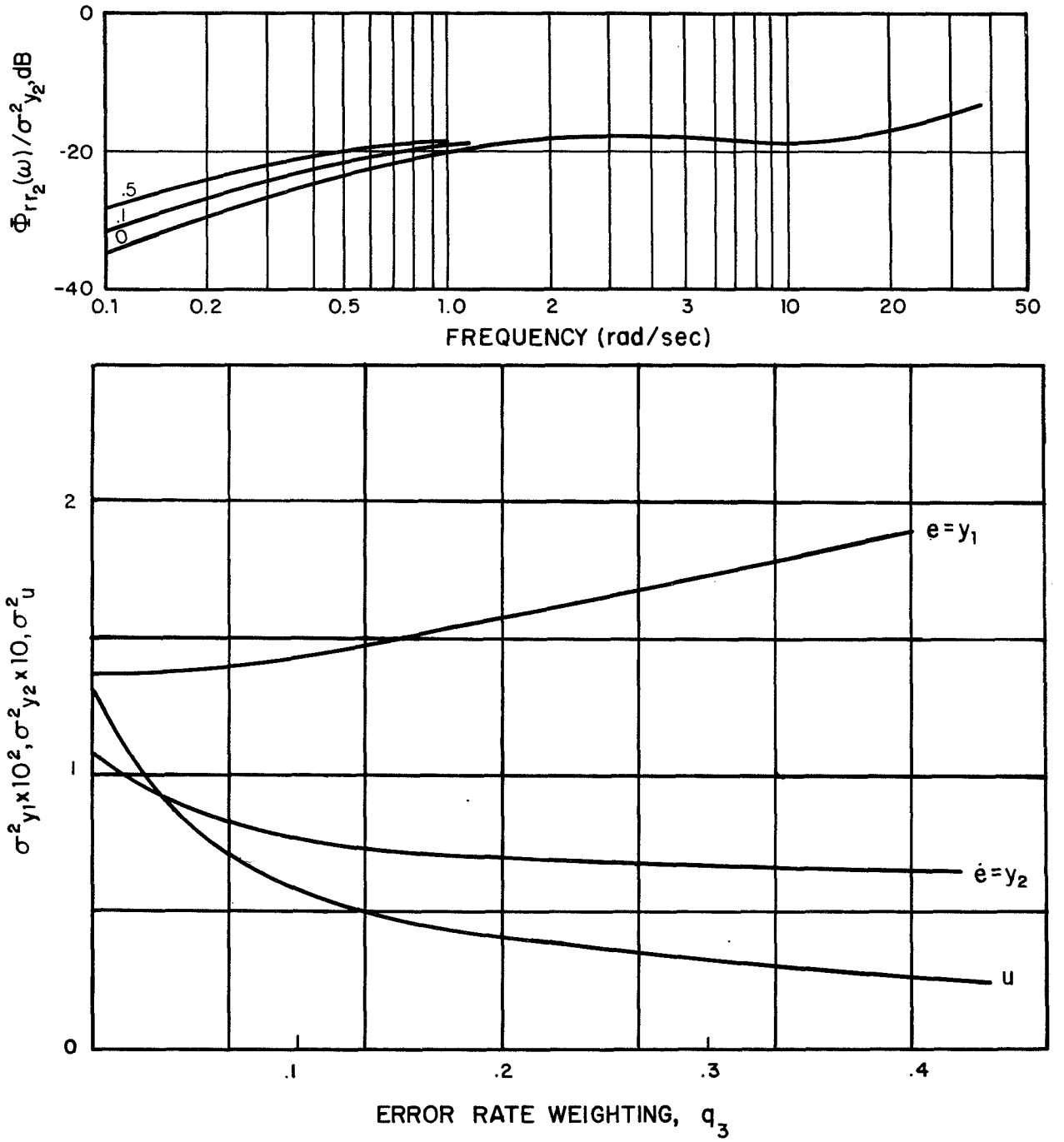

FIG.28 EFFECTS OF WEIGHTING ERROR RATE ON REMNANT AND SCORES, k/s^2 DYNAMICS

The trade-off in system scores is shown in Fig. 28. (Control rate score is not shown since $\sigma_{\dot{u}}^2 \approx 50\ \sigma_u^2$ here.) Note that the introduction of a small (.05) velocity weighting results in a substantial decrease in σ_u^2 (and $\sigma_{\dot{u}}^2$) accompanying the decrease in error rate score. However, note that error score is not very sensitive to q_3. By readjusting the optimal gains $\underline{\ell}^*$, the system reduces control and error rate variances at the expense of only small increases in error score.

In general, the introduction of additional weightings into the cost functional J(u) will result in new control gains and a trade-off in variances. The nature and sensitivity of the trade-off will depend strongly on the resulting gains and the system parameters $\underline{A}$,$\underline{b}$. There does not appear to be any general rules as regards describing functions, spectra, etc. However, by studying the consequences of introducing additional weightings, it may be possible to determine the existence of subjective weightings in actual situations by "matching" the human response data.

K/s(s-1) Dynamics

As a further study of the model, we decided to investigate the manual tracking of an <u>unstable</u> system. The dynamics considered were those studied in Ref. 12 . The pertinent equations are (x_1 = first-order noise disturbance, x_3 = error, x_2 = error rate).

$$\dot{x}_1(t) = -2\ x_1(t) + w(t)\ ;\ w_{11} = 20.94$$

$$\dot{x}_2(t) = x_2(t) + x_1(t) + u(t) \qquad (65)$$

$$\dot{x}_3(t) = x_2(t)$$

The displayed quantities are $y_1 = x_3$, $y_2 = x_2$. Note that the input disturbance x_1 enters the system in parallel with u(t) for this case.

The model parameters that provided a best match to experimental data were found to be $\tau_N = .09$, $\tau = .2$, $\rho_1 = \rho_2 = -26$ dB, $\rho_m = -30$ dB. The large deviation in observation noise ratios (-26 dB) from the -20 dB values found typically in most other situations was a most unexpected result reported in Ref. 12 . In our sensitivity studies we shall suggest a reason as to why the observation noise was so low.

A comparison of model "predictions" with experimental data is shown in Fig. 29. The results appear very similar to those of K/s^2 Dynamics (Fig. 5). This is expected. However, in this system the high-frequency resonant peak is much more pronounced than it was for K/s^2 due to the inherent instability introduced by the plant. Because of this instability it is expected that input parameter variations will have notable effects on model outputs. We shall see that such is indeed the case.

τ_N variations. — The effects of τ_N variations are shown in Figs. (30)-(31). Note that describing function variations have much the same character as for K/s^2 dynamics. Gains increase as τ_N is lowered. The greatest increase is at frequencies beyond the resonant peak. Here, slight changes in τ_N cause large changes in the apparent resonance, due in great measure to the plant instability. Describing function phase lag varies slightly in the region $5<\omega<15$ as the pole associated with τ_N varies from 9 to 14 rad/sec. These same phase effects were noted in all the systems previously studied.

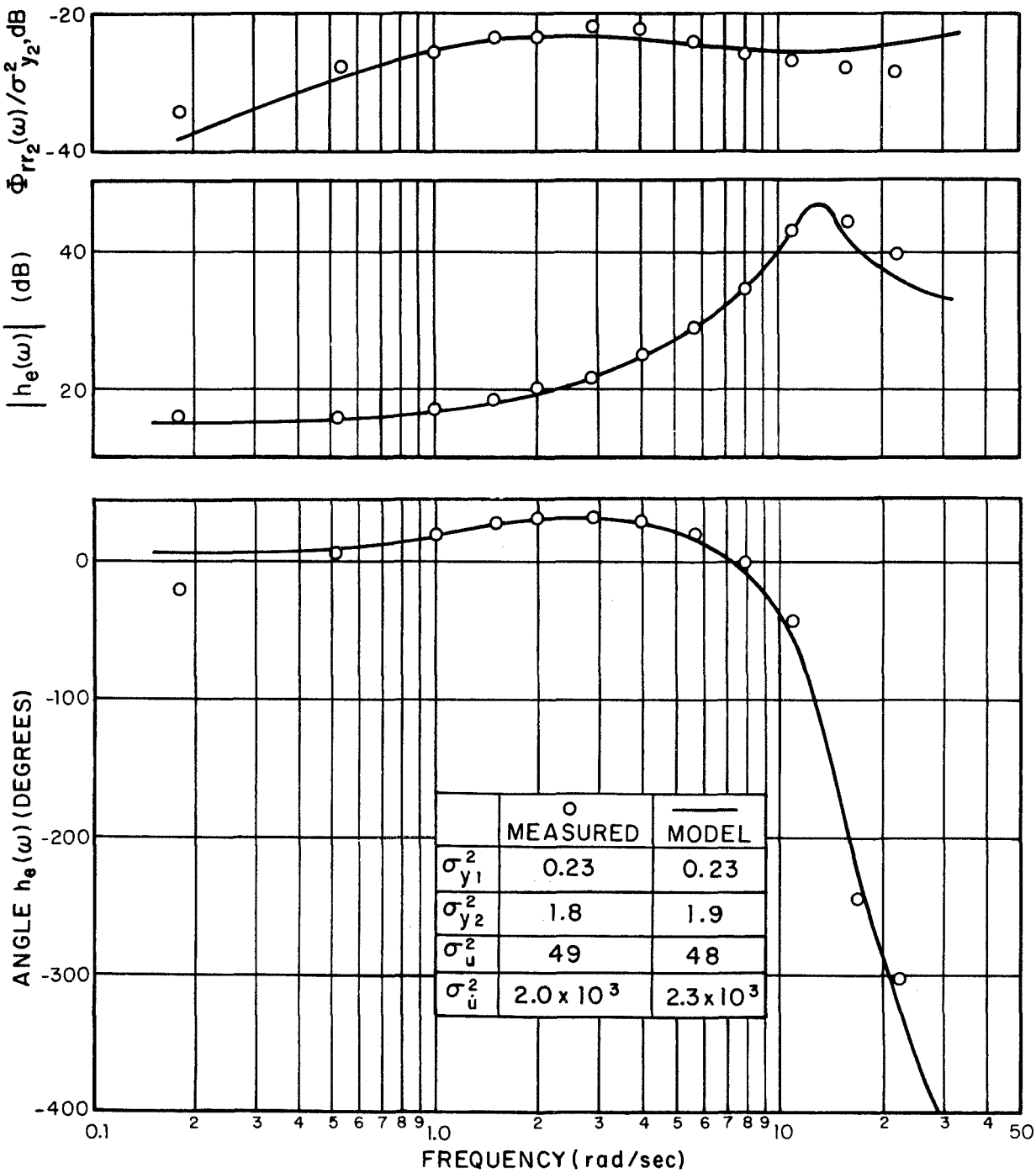

FIG.29 MEASURED AND PREDICTED PERFORMANCE MEASURES, k/s(s-1) DYNAMICS (Average of four subjects)

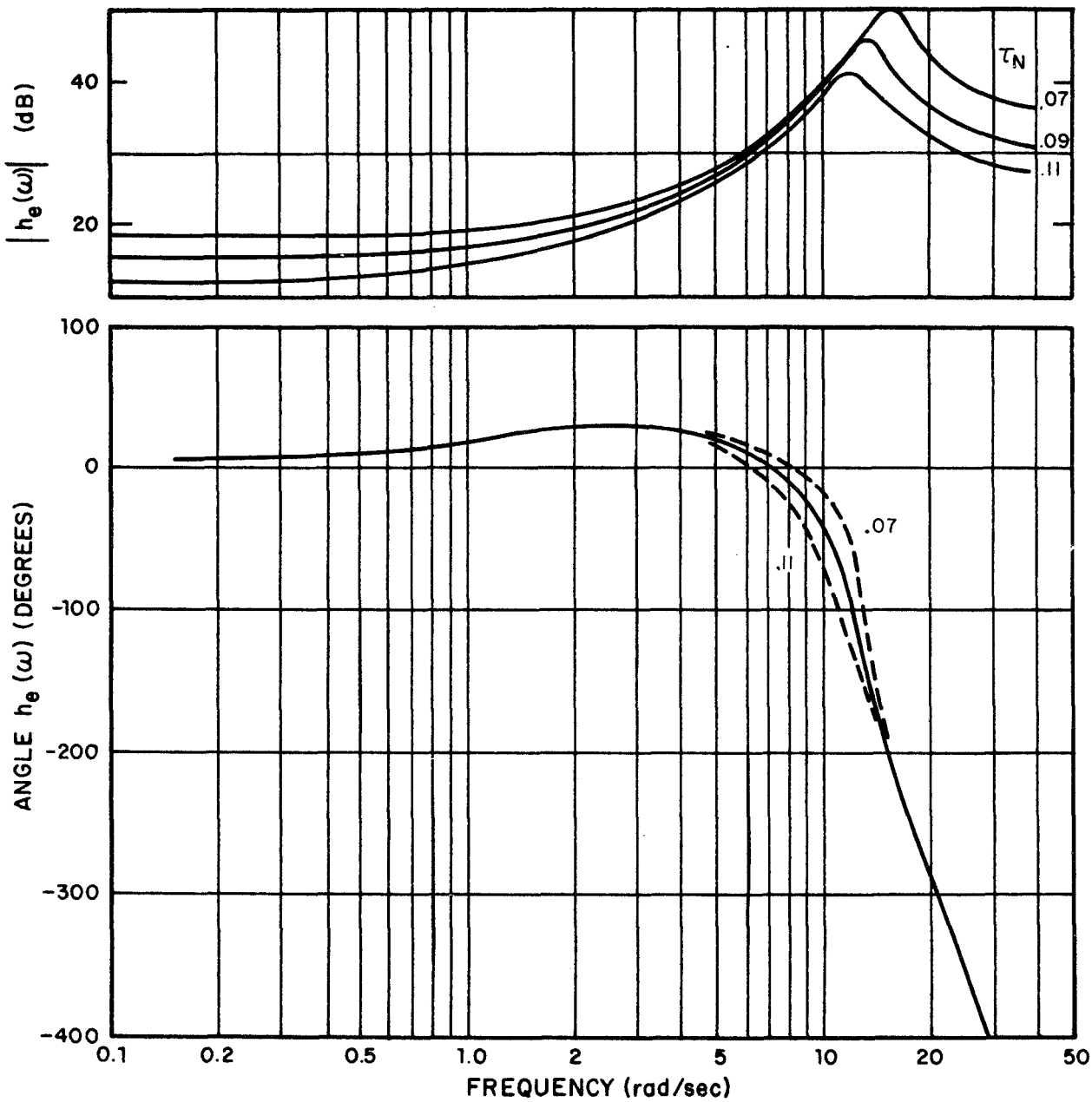

FIG.30 EFFECTS OF τ_N VARIATIONS ON MODEL DESCRIBING FUNCTION, k/s(s-1) DYNAMICS

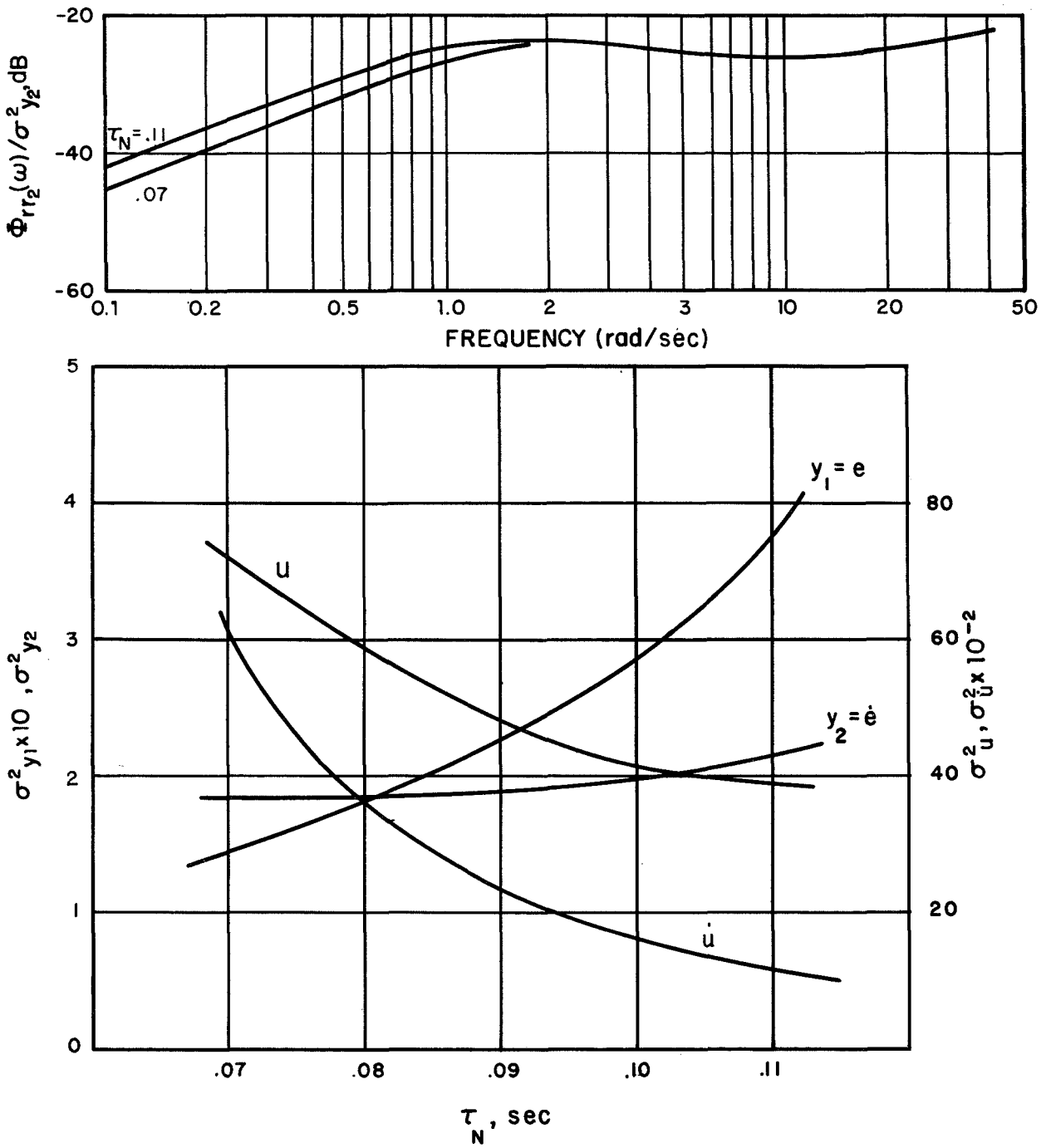

FIG.31 EFFECTS OF τ_N VARIATIONS ON REMNANT AND SCORES, k/s(s-1) DYNAMICS

The effects of τ_N upon normalized remnant are minimal, especially for $\omega>1.0$ rad/sec. Thus, as observed in all previous cases, remnant spectrum is, for the most part, not a function of τ_N. In retrospect, the insensitivity of normalized remnant with respect to τ_N is expected. Varying g (hence τ_N) results in uniform increases or decreases in all of the optimal gains $\underline{\ell}^*$. This in turn uniformly increases or decreases the control power $\Phi_{uu}(\omega)$, without changing its spectral "shape". Since remnant depends only on the ratio $\Phi_{uu_r}(\omega)/\Phi_{uu_i}(\omega)$, as in Eq. (39), τ_N will not appreciably influence this ratio or the remnant.

The scores that result from τ_N variations show the trends expected: Error decreases as control power increases. Of particular interest is the high sensitivity of error and control scores to τ_N, due to the plant instability. Note, however, the relative insensitivity of error-rate. This probably arises since increases in u (which tend to increase $\dot{e}$) and decreases in e (which tend to decrease $\dot{e}$) have counterbalancing effects.

τ variations. – The effects of time-delay changes upon human controller describing function are shown in Fig. 32. The trends are much the same as those of Figs. (11) and (21), although somewhat more pronounced. Gain decreases as τ increases, except about the high frequency resonance. Since the introduction of additional time-delay can only have more of a destabilizing effect on the overall system, the resonant peak sharpens.

The phase variations at high frequency are, of course, a direct result of the delay $e^{-s\tau}$, and

$$\Delta\phi \simeq \frac{180^\circ}{\pi} \tau\Delta\omega \text{ for } \omega>10 \text{ rad/sec}$$

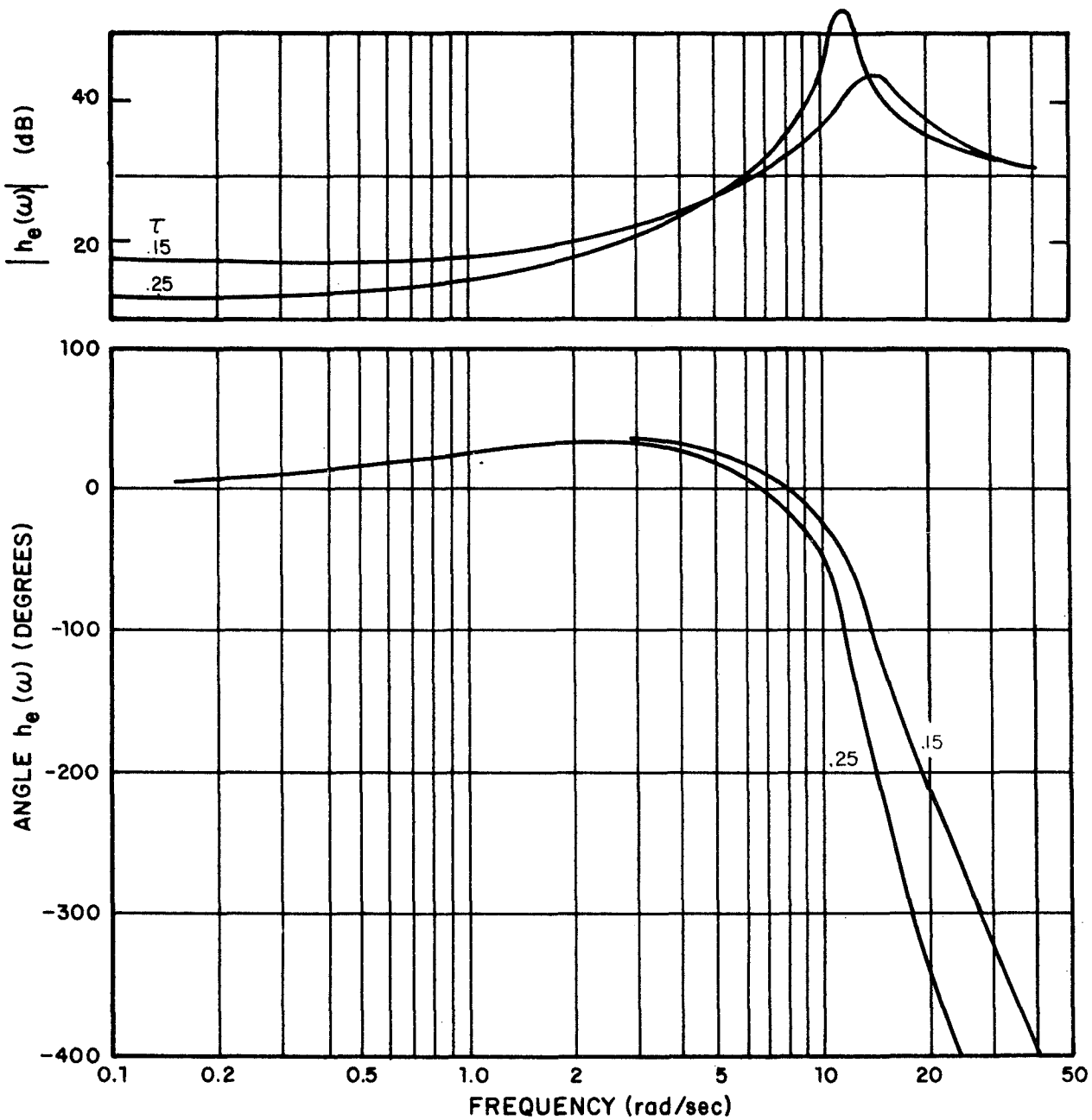

FIG.32 EFFECTS OF TIME-DELAY VARIATIONS ON MODEL DESCRIBING FUNCTION, k/s(s-1) DYNAMICS

The changes in scores listed in Table 3 reflect the system's instability. All scores are highly sensitive to τ and increase sharply (but linearly) as τ is increased. Error and error rate almost triple and control quantities double as τ increases from .15 to .25 sec.

Table 3

System Variances as a Function of Delay

τ_N=.09, V_{y1}=V_{y2}=-26 dB, V_m=-30 dB

Variance	τ=.15	τ=.2	τ=.25
e	.137	.230	.379
$\dot{e}$	1.23	1.91	2.95
u	34.8	48.4	68.5
$\dot{u} \times 10^{-3}$	1.6	2.3	3.3

As was found in the cases considered earlier, normalized remnant showed no appreciable change with respect to changes in τ. Over the frequency range ω>1.0 remnant varied by less than 1 dB as τ varied from .15 to .25 sec.

ρ_1 and ρ_2 variations. — As was found to be the case for K/s^2 dynamics, variations in position noise, V_{y1}, had little effect upon system performance. As ρ_1 was increased from -20 to -30 dB there was no perceptible change in $h_e(\omega)$. Scores increased by less than 10% and normalized remnant increased by about 2-3 dB only at frequencies below 1.5 rad/sec. The reasons for this insensitivity are much the same as for K/s^2: position information is relatively

unimportant for control, i.e., $h_e(s) \approx sh_2(s)$, and the estimation of velocity is not very dependent upon having a good estimate of position.

On the other hand, a good estimate of velocity is most important for control purposes and system performance is indeed sensitive to changes in ρ_2 as shown in Figs. (33)-(34). The variations in describing function are very much similar to those due to τ_N (see Fig. 30). As ρ_2 decreases, $|h_e(\omega)|$ increases somewhat at low frequencies and shows a marked increase beyond the resonant peak.

The similarity between τ_N and ρ_2 variations, as regards their effect on $h_e(\omega)$, has been noticed before. These similarities are not surprising since decreases in either parameter allow the feedback controller to respond more positively to velocity information,† thereby increasing $|h_e(\omega)|$ at high frequencies.

As ρ_2 increases, so does the normalized remnant. This increase is particularly notable at high frequencies where velocity information is most pertinent for control purposes.

System variances (Fig. 34) are very sensitive to ρ_2 as is expected. Note that there is almost a 2:1 correspondence between observation-noise-ratio and scores. Decreasing ρ_2 by 6 dB (i.e., a factor of 4) reduces scores by almost a factor of 2. This is a much greater sensitivity than has been observed in other cases, and is a result of the system's unstable mode. In this situation, then, a substantial decrease in error score can be achieved by a

†Decreases in τ_N allow a higher frequency content in u(t), while decreases in ρ_2 allow for a more accurate estimation of velocity.

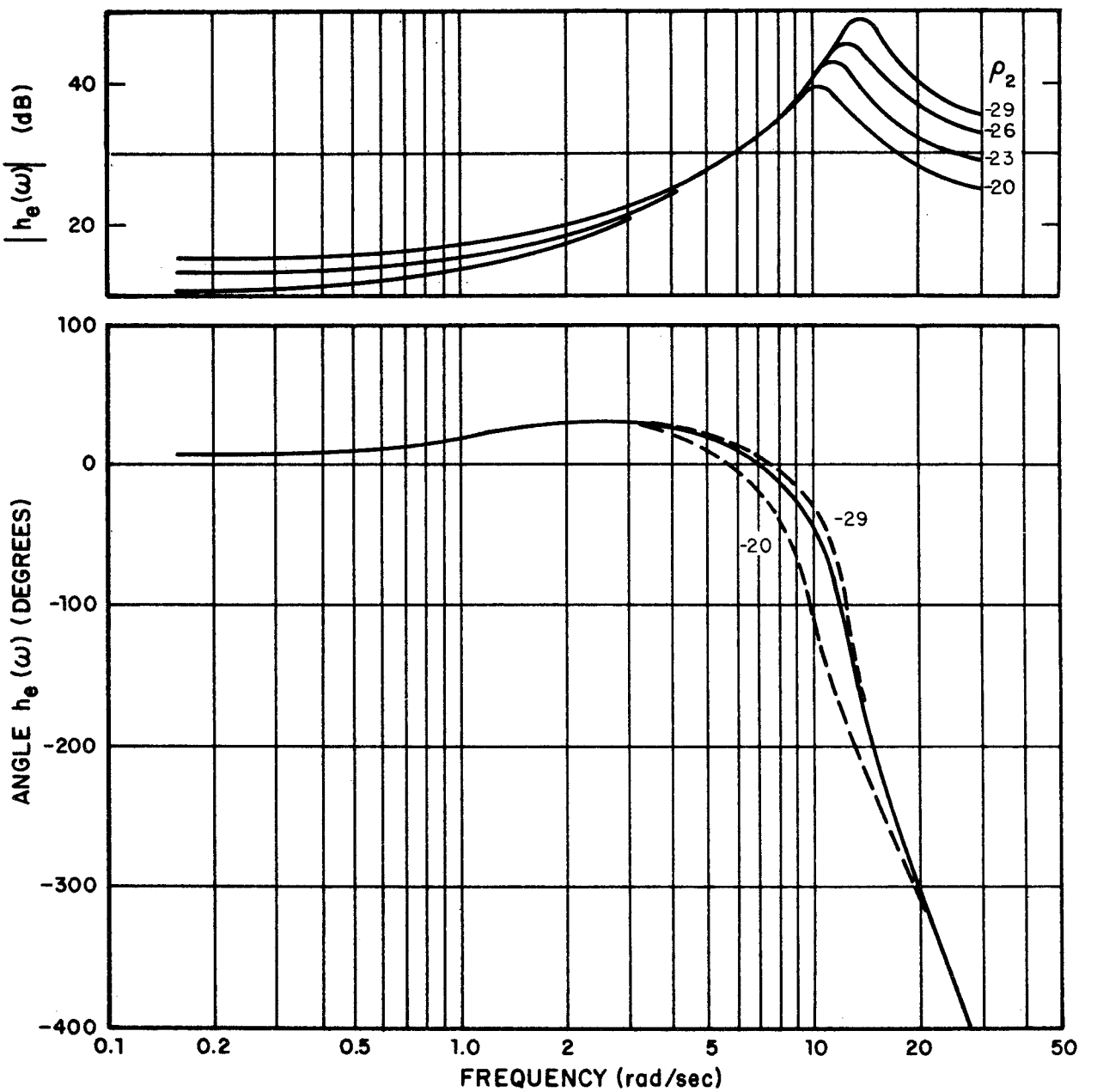

FIG.33 EFFECTS OF OBSERVATION NOISE ON MODEL DESCRIBING FUNCTION, k/s(s-1) DYNAMICS

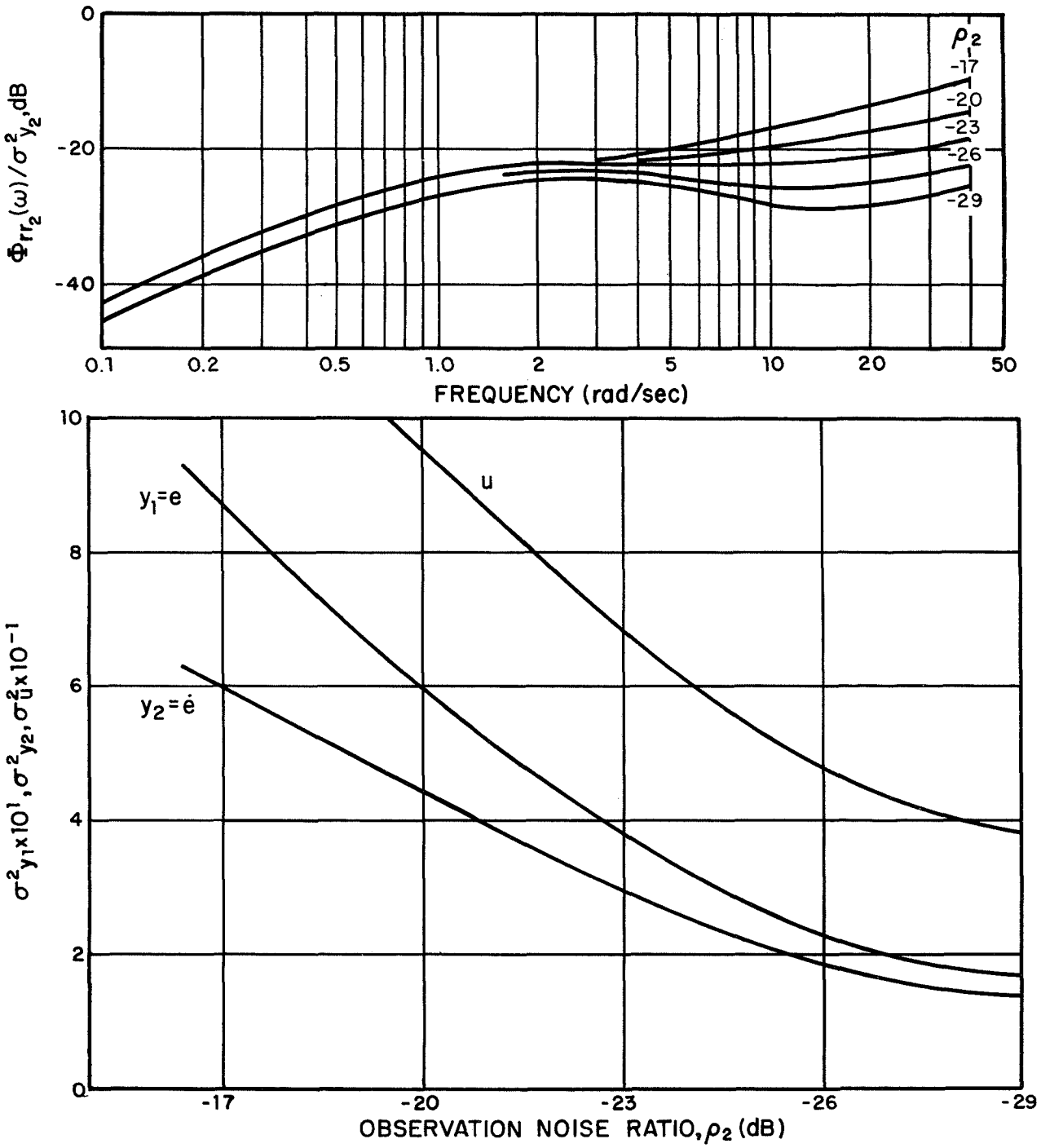

FIG.34 EFFECTS OF OBSERVATION NOISE ON REMNANT AND SCORES, k/s(s-1) DYNAMICS

moderate lowering of observation noise. It appears that the human operator in performing this task was capable of lowering his associated observation noise (e.g., by "concentrating" harder) to take advantage of the large decrease in scores that result. This lowering of noise ratio coupled with the score sensitivities is discussed further in Ref. 12 .

Motor noise variations. — Inasmuch as the input disturbance to the system enters in parallel with the control signal, it is expected that variations in V_m about the nominal of -30 dB would result in only slight effects upon system describing function. Indeed this was found to be the case. Since the motor noise is treated as an additional (uncorrelated) input disturbance, increasing ρ_m results in increased normalized remnant and in increased system variances. For motor noise levels above -20 dB the model predicts the closed-loop system to be essentially uncontrollable. This is a direct result of our driving an unstable system with wideband noise. (See Fig. 35)

Summary

In this section we summarize the results of our sensitivity studies of simple manual control tasks (i.e., single input, single display indicator). To avoid repetition we summarize only the salient effects of variations in each of the human response parameters τ_N, τ, ρ_i, ρ_m.

τ_N variations. — Decreasing τ_N increases the optimal feedback gains. Describing function magnitude increases over the entire frequency range with a proportionately greater increase in the high frequency range ω>10. rad/sec. Phase and normalized remnant

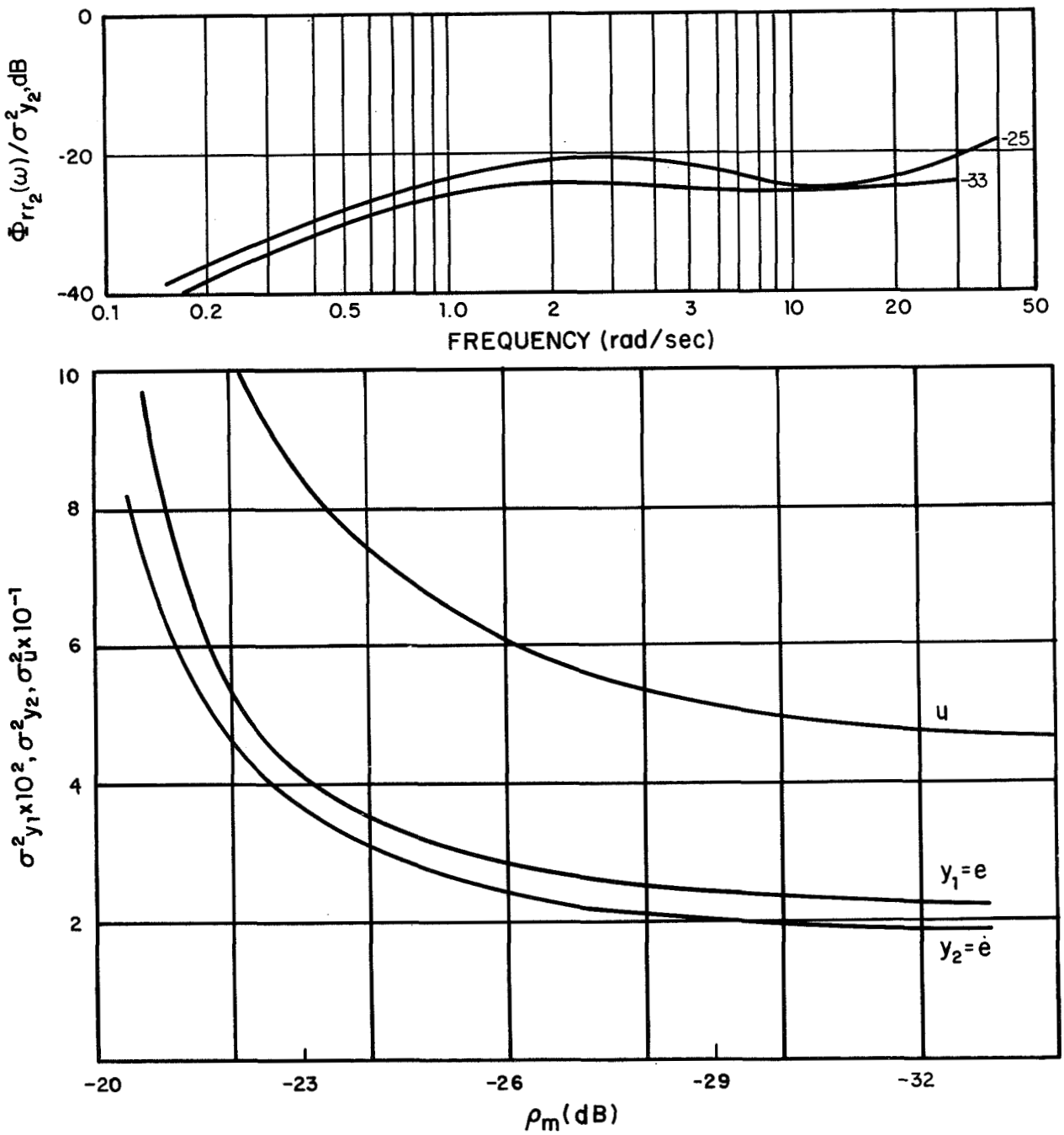

FIG.35 EFFECTS OF MOTOR NOISE ON REMNANT AND SCORES, k/s(s-1) DYNAMICS

are affected little by τ_N.[†] Decreasing τ_N (i.e., decreasing g) lowers the error score at the expense of increases in control rate and control power.

τ variations. — Increases in time-delay are reflected by increases in high frequency phase lag. Describing function gain decreases, except about the resonant peak where increases in τ result in a sharper resonance. This seems to indicate that the high frequency peaking can be associated in large measure with the time-delay and compensating optimal predictor. Finally, all scores increase monotonically with τ, in an almost linear manner.

Observation noise variations. — The noise ratios ρ_i and the Kalman filter play the major role in shaping the normalized remnant spectrum. High frequency remnant is primarily influenced by ρ_2, whereas the effects of ρ_1 are seen at low frequencies. ρ_2 variations have the same general effect on describing function as have τ_N variations. Variations in ρ_1 have little effect on $h_e(\omega)$. All system scores increase with increases in either ρ_1 or ρ_2 because of the higher remnant introduced.

We found that model predictions are far less sensitive to ρ_1 (or V_{y1}) than to ρ_2 (or V_{y2}). This is because position (e) may be estimated from rate ($\dot{e}$) observation even when ρ_1 is relatively large. On the other hand, position information is almost useless in estimating rate. Thus, increasing ρ_1 (for fixed ρ_2) has limited effect, but increasing ρ_2 (for fixed ρ_1) prevents the model from accurately estimating error rate.

[†]In our studies the noise ratios ρ_i, ρ_m were kept constant. Thus, normalized remnant was the system quantity to be examined. However, one may wish to keep V_{yi} and V_m constant, in which case the unnormalized remnant is the pertinent model output. Either approach is valid provided that one stays consistent.

Motor noise variations. – When the input noise disturbance enters the system in parallel with the human's control input, small amounts of motor noise have only minor effect upon model outputs. However, as ρ_m is increased, the normalized remnant and system scores (especially control related scores) increase. These increases are a result of our treating the motor noise as an additional input disturbance to the system.

When the input disturbance does not enter in parallel with u(t), motor noise prevents the Kalman estimator from integrating the control signal to obtain perfect state estimates. In this case, small amounts of motor noise have a dominant effect on low frequency remnant and describing function characteristics.

A Technique for Model-Matching

It is most important to be able to use the model to match experimental data in a systematic fashion. This model-matching is necessary to determine reasonable estimates for intrinsic pilot parameters to be used in predicting performance in a new situation. In addition, the model parameters themselves may be useful as derived measures of performance. Thus, for example, measuring observation noises by matching data from simple tracking experiments may prove to be a useful way of evaluating certain displays. Under certain circumstances the derived measures can be a good deal more sensitive than direct measures of performance.

One plausible technique for choosing parameters that match model outputs with experimental measurements of scores, describing function gain and phase, and remnant is the following:

1. Choose a "reasonable" set of values for the human response parameters τ_N, τ, ρ_i (or V_{yi}) and ρ_m (or V_m)†.

2. Pick values of ρ_1 and ρ_2 (or V_{y1} and V_{y2}) that result in good approximations to the measured remnant spectrum.

3. Adjust τ such that model predictions match observed high frequency phase measurements.

4. Adjust τ_N until predicted gain ($1.0<\omega<10.$) matches describing function data.

5. Choose a value of ρ_m (or V_m) that gives a match to control score.

6. Compare all model predictions with the data. If results are unsatisfactory,†† return to step 2.

7. "Fine tune" τ_N, τ, ρ_i, ρ_m. The resulting values are the human response parameters that best match the data.

The above model-matching scheme is not meant to establish universal guidelines. However, it is a reasonable way for one to proceed, based on the results of our sensitivity studies of simple manual control systems. Since τ and τ_N do not affect remnant, the observation noises can be chosen primarily on the basis of matching remnant spectrum. τ and τ_N may then be chosen to match describing function data.

A mathematical criteria function that can be used to "grade" the closeness of model predictions with data is needed in any matching scheme. The precise form of this function would depend on the specific

---

†e.g., $\tau_N \approx .1$, $\tau = .2$, $\rho_i = -20$ dB, $\rho_m = -25$ dB for foveal viewing conditions.

††An adjustment of cost functional weightings q_i, r may be called for if results are continually poor.

application. For example, it may be of greater importance to match remnant spectrum than, say, scores in obtaining estimates of observation noise ratios. The criterion function would thus place relatively more weight on those manual control characteristics that are required to be more closely matched.

The determination of suitable matching criteria and matching tolerances is a difficult, and important, problem. Its solution would go a long way towards defining a standardized and systematic set of procedures for extracting model parameters from data.†

†A preliminary technique for extracting estimates of observation noise associated with different viewing conditions is reported in Levison [33].

PREDICTION OF PILOT PERFORMANCE IN A HOVERING TASK

In the first three chapters of this report we developed an optimal control model of the human operator and examined in detail its application to the prediction of human response in some basic, single-axis control tasks. In this chapter, we use the model to analyze a more complex control situation, namely the manual control of the longitudinal position of a hovering VTOL-type aircraft.

This is not the first time that the model will be employed in such a task. In a previous study (Ref. 17) we analyzed longitudinal hovering control for a particular VTOL configuration (XV-5A). In that study semi-empirical techniques, involving a fairly extensive preliminary experimental program, were used to determine most of the parameters of the optimal control model. Then, using these parameters, human performance in the hover task was predicted and compared with data obtained from simulation experiments in which skilled pilots executed the task. The results showed that the model could indeed reproduce most of the essential control characteristics of the pilots as well as closed-loop system performance. Good predictions of visual scanning behavior were also obtained, using the optimal sampling model described earlier in this report. Finally, a simplified technique for estimating average control behavior and performance was suggested and partially validated. This technique had the advantage that extensive pre-experimentation was not required for the analysis.

Here, we will show that the model may be used to predict the effects on performance of changes in aircraft stability parameters.[†]

[†]In Ref. 17 the only configurational change investigated involved the presence or absence of an explicit display of longitudinal velocity.

The results that we obtain will provide further validation of the model and greater insight into its use. More importantly, they will demonstrate the real potential of the optimization approach to manned-vehicle systems analysis.

The Hovering Task

Vinje and Miller [20, 21] have conducted and analyzed a series of simulator experiments involving precision hovering control of a VTOL-type vehicle. As part of their investigation, they measured the effects of variations in aircraft stability parameters on rms hovering performance. As a further test of our model, we shall attempt to predict these effects and correlate our results with the experimental data.

Briefly, the pilot's task was to minimize longitudinal position errors while hovering in turbulent air.† Only longitudinal motions were considered and the pilot was not required to control the height of the aircraft. With these assumptions, the following linearized equations of motion were used to simulate the hover task

$$\begin{aligned} M_u\, u + M_q\, q - \dot{q} &= -M_\delta\, \delta - M_u\, u_g \\ X_u\, u - g\theta - \dot{u} &= -X_u\, u_g \end{aligned} \tag{66}$$

where

u_g	longitudinal component of gust velocity, ft/sec
$u=\dot{x}$	velocity perturbations along the x-axis, ft/sec
θ	pitch attitude, rad

†The VTOL hovering experiments are described in detail in Ref. 20.

$q=\dot{\theta}$	pitch rate, rad/sec
δ	control stick input, in
M_u	speed stability parameter, rad/ft-sec
M_q	pitch rate damping, 1/sec
M_δ	control sensitivity, $(rad/sec^2)/in$
X_u	longitudinal drag parameter, 1/sec
g	gravitational constant, 32.2 ft/sec^2

The simulated gust u_g was equivalent to first-order filtered white noise with filter pole at .314 rad/sec. The rms level of the gust, σ_{u_g}, was set at 5.14 ft/sec.

Thus, the equations of state for the task could be written in the following form:

$$\begin{bmatrix} \dot{u}_g \\ \dot{u} \\ \dot{x} \\ \dot{q} \\ \dot{\theta} \end{bmatrix} = \begin{bmatrix} -.314 & 0 & 0 & 0 & 0 \\ X_u & X_u & 0 & 0 & -g \\ 0 & 1 & 0 & 0 & 0 \\ M_u & M_u & 0 & M_q & 0 \\ 0 & 0 & 0 & 1 & 0 \end{bmatrix} \begin{bmatrix} u_g \\ u \\ x \\ q \\ \theta \end{bmatrix} + \begin{bmatrix} 0 \\ 0 \\ 0 \\ M_\delta \\ 0 \end{bmatrix} \delta + \begin{bmatrix} w_1 \\ 0 \\ 0 \\ 0 \\ 0 \end{bmatrix} \tag{67}$$

The pilots were provided with a Norden contact analog display on which both aircraft attitude (θ) and position (x) were indicated explicitly. (The display is described in Ref. 20.) Hence, in accordance with our usual assumptions, the displayed outputs were

$$\begin{bmatrix} u \\ x \\ q \\ \theta \end{bmatrix} = \begin{bmatrix} 0 & 1 & 0 & 0 & 0 \\ 0 & 0 & 1 & 0 & 0 \\ 0 & 0 & 0 & 1 & 0 \\ 0 & 0 & 0 & 0 & 1 \end{bmatrix} \begin{bmatrix} u_g \\ u \\ x \\ q \\ \theta \end{bmatrix} \tag{68}$$

i.e., x,θ and their first derivatives u and q respectively.

The experiments that we will consider involve changes in X_u, M_u and M_q about a common or "nominal" operating point corresponding to values of -.1, .0207, and -3.0, respectively. For each configuration, the subject pilot was instructed to select a control sensitivity M_δ that he considered "optimum" for performance with that particular configuration. The parameter values corresponding to the cases investigated here are listed in Table 4. The case numbers identifying the various configurations are those assigned in Ref. 21.†

Table 4

Variations in VTOL Stability Derivatives

Case	X_u	M_u	M_q	M_δ
Nominal (PH8)	-.1	.0207	-3.0	.431
PH1	0	↓	↓	.287
PH2	-.05	↓	↓	.420
PH5	-.3	↓	↓	.516
PH6	-.1	0	↓	.300
PH7	-.1	.0104	↓	.360
PH9	↓	.0312	↓	.481
PH10	↓	.0207	-1.0	.369
PH12	↓	.0207	-5.0	.493

†We restrict attention to results for a single pilot (pilot B).

Multiloop-Model Analysis

A closed-loop pilot-vehicle analysis of the above hover task, using quasi-linear, multiloop pilot models (Refs. 5,6) was used by Vinje and Miller in analyzing their data. We present the highlights of their approach in an attempt to provide further context for the results we have obtained with our model.†

In applying the multiloop-model approach, one must assume an a priori closed-loop system structure. In other words, an assumption must be made concerning those loops "closed" by the pilot. Vinje and Miller assumed the "series loop" model illustrated in Fig. 36. (A parallel loop model for this task is also a possibility (Ref. 8).) Once the loop topology has been decided upon, it is then necessary to assume specific forms for the individual transfers comprising the pilot model. For the structure of Fig. 36 this means choosing fixed forms for Y_{p_x} and Y_{p_θ}. The forms chosen by Vinje and Miller were

$$Y_{p_x} = K_{p_x}(T_{L_x}s+1)e^{-\tau_x s} \tag{69}$$

$$Y_{p_\theta} = K_{p_\theta}(T_{L_\theta}s+1)e^{-\tau_\theta s}/(\tau_N s+1) \tag{70}$$

In Eqns. (69-70), the "neuromuscular lag" (T_N), the θ-loop transport lag (τ_θ), and the x-loop transport lag (τ_x) were considered to be fixed parameters with values of .35 sec, .09 sec and .08 sec, respectively; the gains (K_{p_θ}, K_{p_x}) and the lead time constants (T_{L_θ}, T_{L_x}) were assumed to be "adaptable" parameters, chosen by

†Again, details may be found in Reference 21.

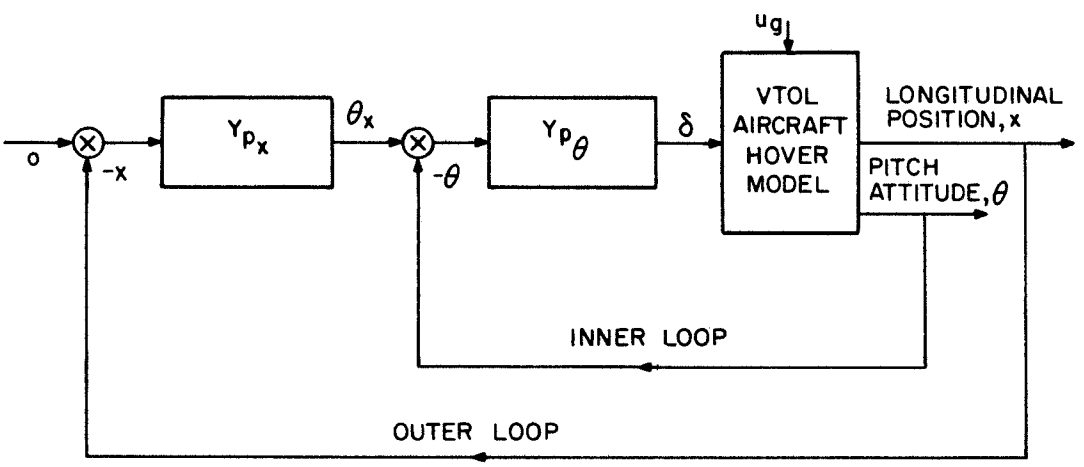

FIG.36 SERIES LOOP MODEL FOR PILOT LONGITUDINAL CONTROL IN HOVER

the pilot to achieve certain desired closed-loop characteristics.

Inasmuch as Y_{p_x} and Y_{p_θ} cannot be measured directly in this task, Vinje and Miller devised a technique for "identifying" the adaptable parameters. In particular, they iterated on K_{p_θ}, K_{p_x}, T_{L_θ} and T_{L_x} until the rms values σ_u, σ_x, σ_θ and σ_q computed by using the closed-loop model of Fig.36 "matched" the corresponding rms hover performance (as measured in the simulator experiments) to within 0.5%. Vinje and Miller did not use rms control activity (σ_δ) in their matching procedure in an attempt to minimize the effects of ignoring pilot remnant in the computation of the pilot-model adapted parameters. However, they compared measured values of σ_δ with those obtained from calculations based on the computed pilot-model parameters and found that these values of σ_δ differed, on the average, by about 17%.

Once values for the parameters of Y_{p_x} and Y_{p_θ} are given, it is possible to compute various loop closure characteristics, e.g. inner- and outer-loop crossover frequencies and phase margins. The inner-loop characteristics are obtained from Bode plots of $Y_{p_\theta} \cdot [\theta/\delta]$. The outer-loop characteristics are calculated by assuming the inner- (pitch) loop is closed; Bode plots of

$$Y_{p_x} \cdot \left[\frac{x}{\theta_x}\right]_{\theta \to \delta} = \frac{Y_{p_x} Y_{p_\theta} [x/\delta]}{1 + Y_{p_\theta} \cdot [\theta/\delta]} \tag{71}$$

yield the desired results.

Before leaving this discussion of the multiloop analysis, it is worth repeating and re-emphasizing that the pilot-model adapted parameters and the computed loop closure characteristics are derived measures of human performance that are designed to provide additional understanding of the pilot's behavior. The only direct measures made by Vinje and Miller in their experimental study were the measures of closed-loop rms hovering performance (σ_x, σ_u, σ_θ, σ_q, σ_δ).†

Predictions with the Optimal Control Model

In this section we present the results of applying the optimal control model of the human operator to the analysis of the hover task described earlier. We begin with a brief discussion of the choice of parameters for the optimal control model. Then we present and discuss model predictions for the various configurations listed in Table 4. We end with a brief summary and discussion of the results.

Model parameters. — In order to apply our model to this task, values for τ_N, τ, the ρ_i's, and ρ_m as well as cost functional weightings had to be chosen. We felt that, with respect to those parameters related primarily to intrinsic human limitations, values representative of those used in the single-axis studies constituted a good a priori choice. Thus, we let $\tau_N = .1$ sec, $\tau = .15$ sec, $\rho_1 = \rho_2 = \rho_3 = \rho_4 = -20$ dB and $\rho_m = -25$ dB.†† Note that all the observation noises were set equal and at their

†Another (subjective) measure, namely, pilot opinion rating was also taken but we will not discuss this measure at length here.

††Noise ratios were chosen within $\pm$ .5 dB and τ_N was within 10% of .1 sec for all cases.

"single-axis" values.† It is significant that we were able to keep this (initial) set of model input parameters fixed throughout the entire subsequent study.

The choice of a "subjective" cost functional is a bit more subtle. Recall that the pilots were instructed to minimize position error (σ_x). However, in order to accomplish this the pilot must suppress pitch errors inasmuch as such errors introduce disturbing longitudinal forces. In addition, one may expect that pilots try to avoid excessive attitude changes during the process of minimizing hovering errors. Accordingly, it seems reasonable to include a pitch or pitch-rate term in the cost functional; we chose to add a term proportional to mean-squared pitch rate, σ_q^2. Given this choice, a subjective weighting for pitch-rate must be selected. In the absence of any data, one might choose this weighting by asking pilots how much position error they would trade for maintaining low attitude rates. If, for example, they were willing to accept a mean-squared hovering error of 1 ft^2 in order to avoid mean-squared attitude rates in excess of 0.5 deg^2/sec^2 ($\approx .01$ rad^2/sec^2) then one might select a pitch-rate weighting that was 100 times greater than the position weighting. For this study, such a questioning of pilots was not possible. We, therefore, picked the pitch-rate weighting on the basis of the measured scores for the "nominal" configuration. In that case, values of σ_x^2 and σ_q^2 of approximately 1.2 ft^2 and .0024 rad^2/sec^2 were found. On this basis, we selected a pitch-rate weighting of 400 and we used this value in all subsequent calculations. Thus, the cost functional for this analysis was

$$J = \sigma_x^2 + 400\ \sigma_q^2 + g\ \sigma_\delta^2 \tag{72}$$

†This is a reflection of the fact that an integrated display was used so that visual scanning did not appear to be necessary.

where g was chosen so that $\tau_N \approx .1$ sec.[†]

Nominal case. – We now compare model predictions with measured and derived data for the nominal case (PH8 in Table 4). Measured and predicted scores are compared below in Table 5. The measured values are averages of ten runs and the quantities in parenthesis indicate the corresponding standard deviations. It can be seen that the agreement between predicted and measured scores is excellent.

Table 5

Comparison of Measured and Predicted Scores

Nominal Configuration (X_u=-.1, $M_u g$=.667, M_q=-3, M_δ=.431)

	σ_u	σ_x	σ_q	σ_θ	σ_δ
Measured	.79(.09)	1.16(.10)	.050(.003)	.032(.002)	.59(.03)
Predicted	.82	1.08	.055	.036	.63

It would be desirable to obtain comparisons of measured and predicted frequency domain data for this study that might provide a more complete validation of the model. Unfortunately, the data of Reference 21 does not include frequency domain measurements. Instead, the fixed-form expressions for Y_{p_x} and Y_{p_θ} were assumed

[†]In a recent study aimed at developing a scheme for predicting pilot ratings for VTOL vehicles, Anderson [22] suggested that pilots might attempt to minimize a performance measure of $\sigma_x + 10\sigma_q$. This suggestion was based on ad hoc considerations, and a rough correlation with data (including that of Ref. 21). In terms of a quadratic performance index, Anderson's criterion becomes $\sigma_x^2 + 20\sigma_x\sigma_q + 100\sigma_q^2$. Noting that in the nominal case $\sigma_x \approx 20\sigma_q$, we see that the pitch-rate weighting of 400 is not significantly different from Anderson's weighting.

and the parameter values (K_{p_θ}, K_{p_x}, T_{L_θ}, T_{L_x}) were adjusted to match scores.

In an attempt to correlate the multi-loop structure of our optimal-control-model with that of Vinje and Miller's model, we simply computed the equivalent transfers, Y_{p_θ} and Y_{p_x} in the following manner. From Fig. 36, we see that the control input

$$\delta = -Y_{p_x} Y_{p_\theta} x - Y_{p_\theta} \theta \tag{73}$$

On the other hand, the optimal control model of the human operator yields (see Eq. (23)).

$$\delta(s) = \underline{h}\,\underline{y} = h_1(s)u(s) + h_2(s)x(s) + h_3(s)q(s) + h_4(s)\theta(s)$$

$$= (sh_1+h_2)x(s) + (sh_3+h_4)\theta(s) \tag{74}$$

Comparing equations (73) and (74) gives

$$sh_3 + h_4 = -Y_{p_\theta} \tag{75}$$

$$\frac{sh_1+h_2}{sh_3+h_4} = Y_{p_x} \tag{76}$$

Consequently, with these expressions for Y_{p_θ} and Y_{p_x}, it is possible to use the optimal control model to compute equivalent "inner" and "outer" loop characteristics, just as is done in the fixed-form multiloop analysis.

Figures 37-40 show the results of performing some of the frequency domain calculations for the "nominal" configuration. (As a matter of interest, correlated and uncorrelated control spectra are shown in Fig. 37.) Bode plots of Y_{p_θ} and Y_{p_x}, as computed from Eqs. (75) and (76), are presented in Figs. 38 and 39. Also shown in these figures are the fixed-form Y_{p_θ} and Y_{p_x} corresponding to the parameter values (K_{p_θ}, T_{L_θ}, K_{p_x}, etc.) determined by Vinje and Miller. As can be seen, the corresponding Y_{p_θ}-transfers are in excellent agreement up to about 4 rad/sec; correspondingly good agreement between the Y_{p_x}-transfers is evident up to about 1.5 rad/sec.

In Fig. 40, the Bode plots for the transfer $\left\{Y_{p_\theta} \cdot \frac{\theta}{\delta}\right\}$, necessary to determine "inner"-loop closure characteristics, is presented.† We find that the optimal control model yields, for the pitch loop, "crossover" frequency and phase margin of approximately 3.2 rad/sec and 30 degrees, respectively. Vinje and Miller obtain a pitch loop crossover frequency and phase margin of 3.1 rad/sec and 8 degrees. Similar computations for the "outer" or position loop result in model crossover and phase margin of 1.1 rad/sec and 21 degrees as compared to values of 1.0 rad/sec and 15 degrees derived by Vinje and Miller. Thus, the agreement in these characteristics is good, with the optimal control model providing slightly greater stability margins.

†The dashed portions of these curves correspond to what we believe are reasonable trends in the data. Unfortunately, our programs were designed to compute quantities at discrete frequencies (corresponding to values at which we normally measure). Time did not permit the recomputations necessary to define these frequency plots in more detail.

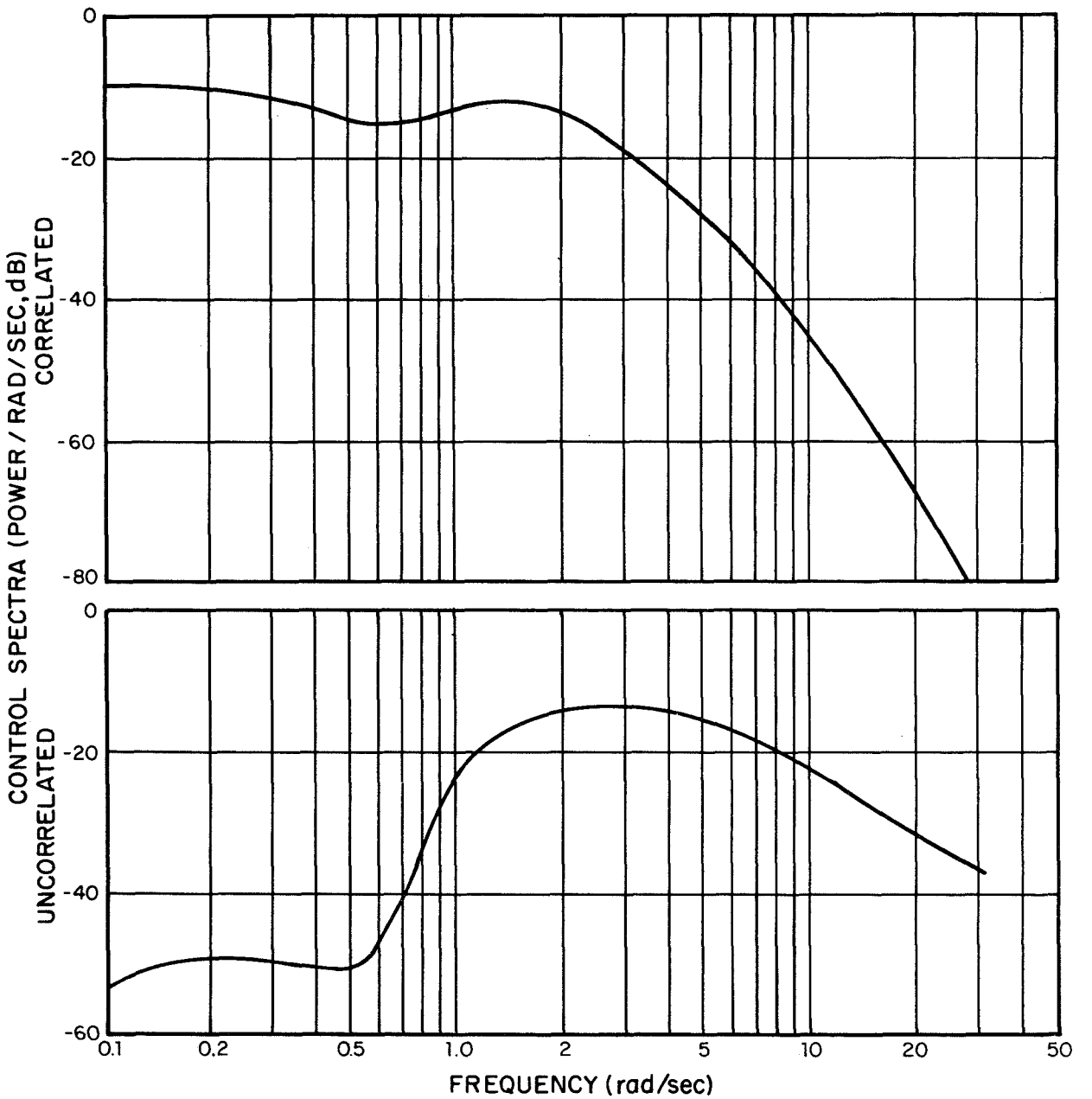

FIG.37 PREDICTED PILOT CONTROL SPECTRA FOR NOMINAL CONFIGURATION

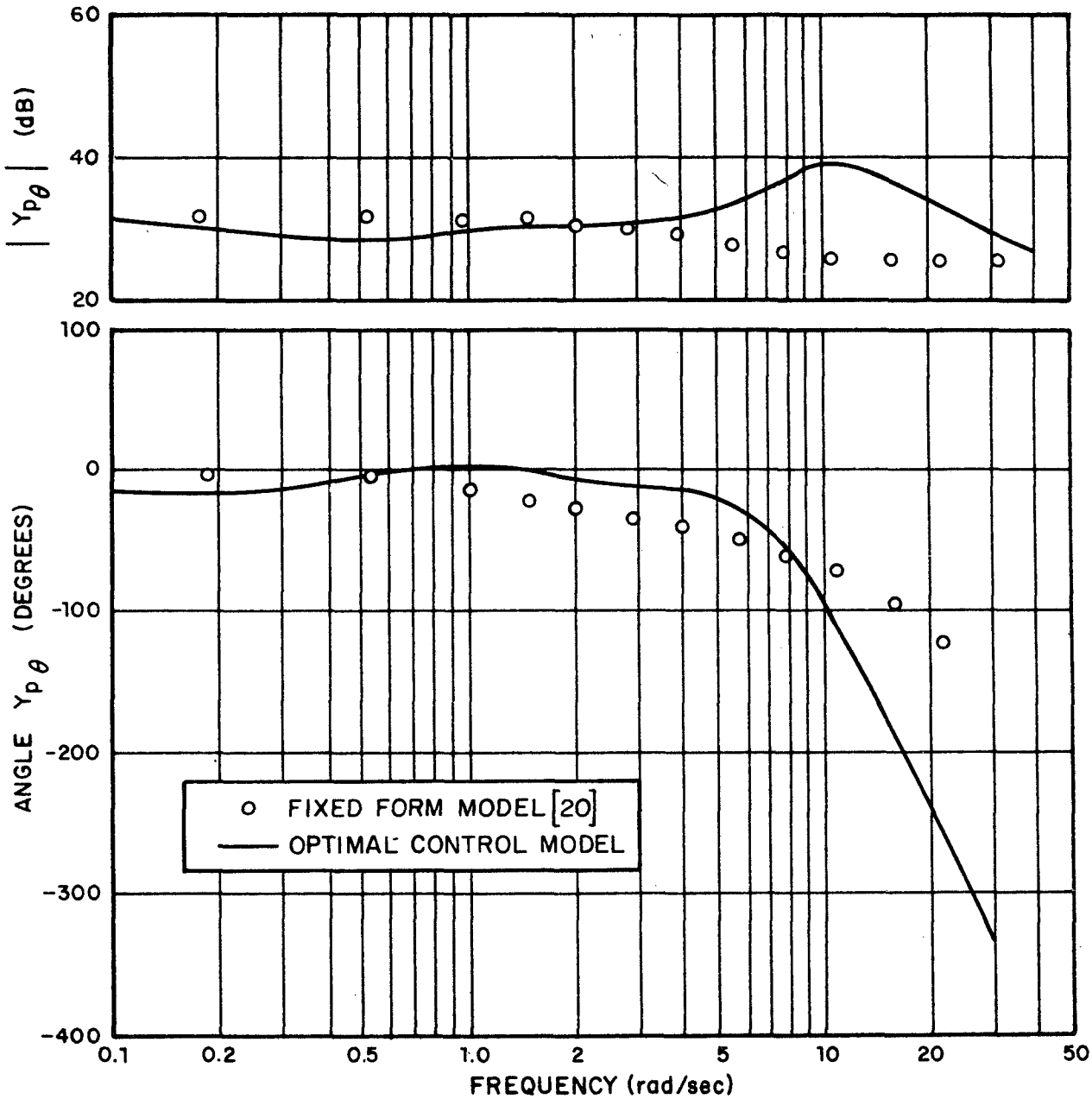

FIG.38 PITCH-LOOP PILOT DESCRIBING FUNCTIONS (Y_{p_θ}) FOR NOMINAL CONFIGURATION

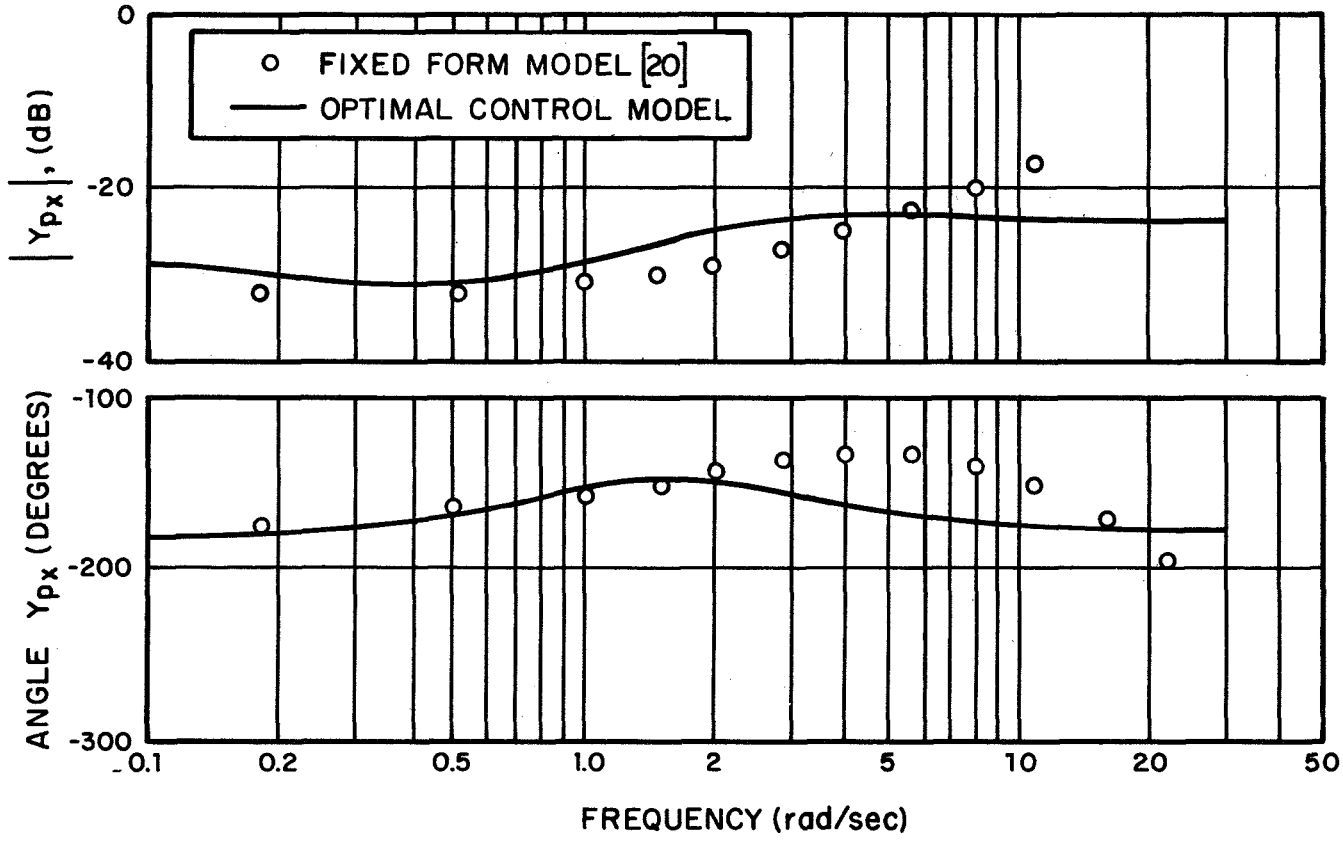

FIG.39 POSITION-LOOP PILOT DESCRIBING FUNCTIONS FOR NOMINAL CONFIGURATION

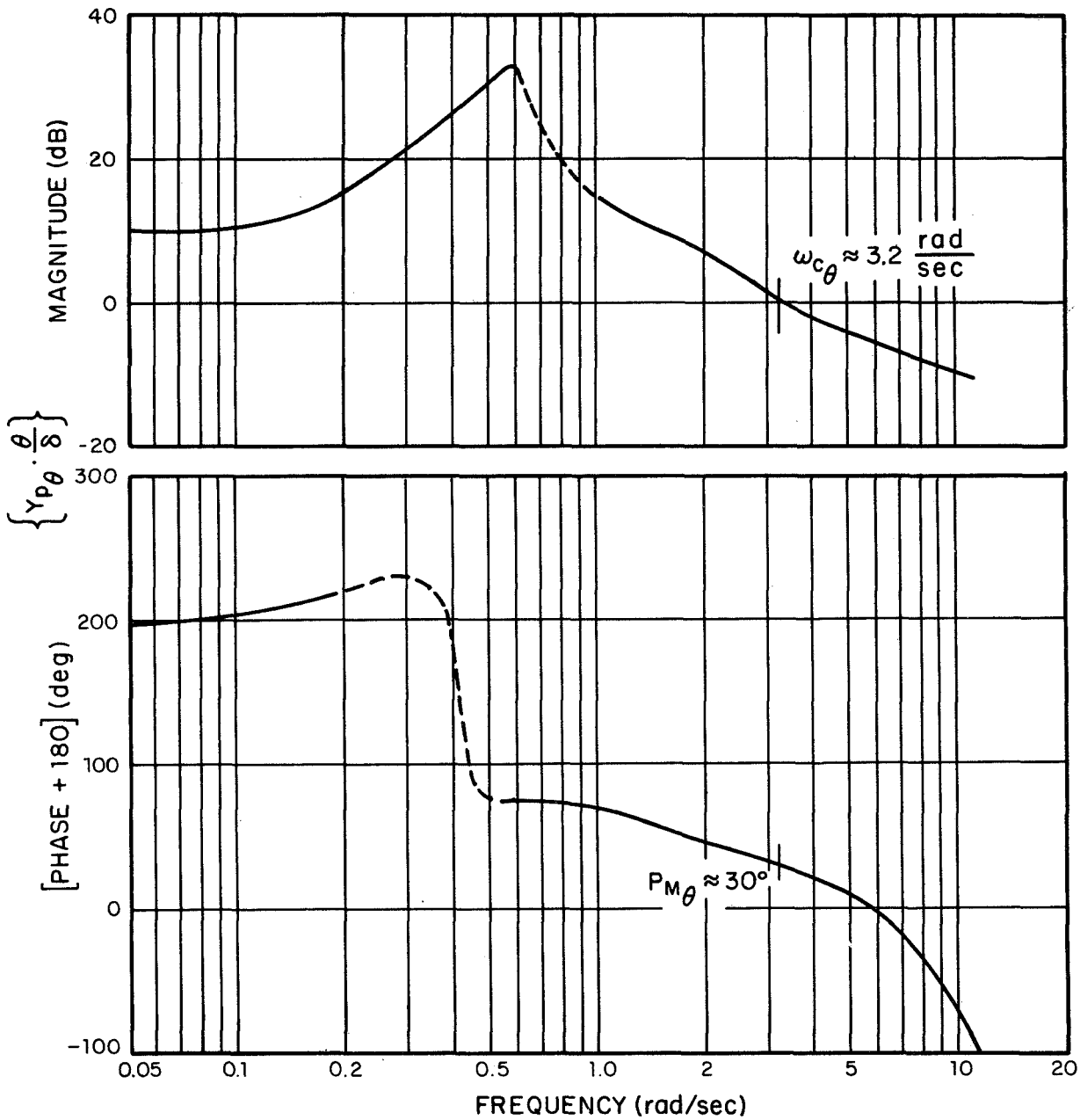

FIG.40 OPEN LOOP DESCRIBING FUNCTION FOR PITCH LOOP, $\{Y_{p_\theta} \cdot \theta/\delta\}$

Thus, the loop closure characteristics reveal that the Y_{p_θ} and Y_{p_x} predicted by the optimal control model agree closely with the derived values of Vinje and Miller up to frequencies slightly greater than the respective loop crossovers. The disagreements at higher frequencies cannot be resolved on the basis of the available data and they do not appear to be significant from the standpoint of system performance. We can be reasonably certain, however, that the high frequency deviations of the Y_p's result from the longer time delay and the inclusion of the predictor in the optimal-control model.

Effects of pitch rate damping, M_q[†]. — Predicted and measured rms-scores as a function of changes in pitch rate damping (with other derivatives held at "nominal" values) are plotted in Fig.41. It should be re-emphasized that no changes in the parameters of the pilot model are made in computing the effects of changing aircraft parameters. Again, agreement is quite good, especially for the cases with higher damping. For $M_q = -5.0$, all the predicted scores are within the standard deviations of the data and we have already seen similar agreement for the $M_q = -3.0$ case. Model predictions are poorest for the configuration with the least damping ($M_q = -1.0$), although the maximum deviation between predicted and measured scores does not exceed 25%. Unfortunately, it is difficult to assess the true mismatch between model scores and data for this case because standard deviations of the measured averages were not available.[††]

[†]The physical significance of the changes in various stability derivatives and the effects on aircraft response to control or gust inputs will not be discussed here. A detailed and illuminating discussion may be found in Reference 21.

[††]Standard deviations were published for the results of a second, different, subject. As might be expected, standard deviations increased as damping decreased.

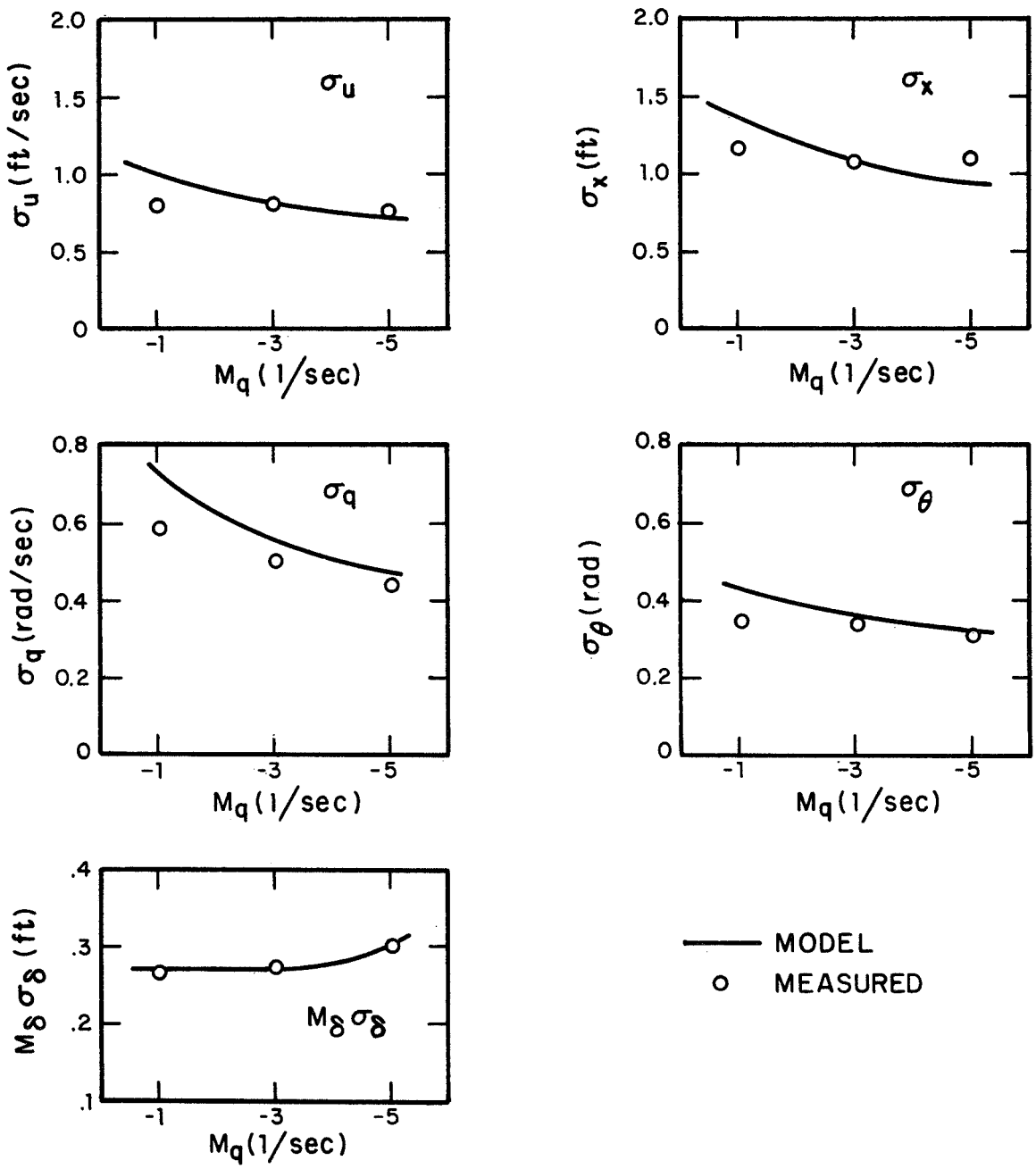

FIG.41 EFFECT OF PITCH-RATE DAMPING ON HOVERING PERFORMANCE, ($M_u g$ = .667, X_u = -.1)

What is perhaps most surprising about the score data for the low damping case is that all the scores predicted by the optimal-control model of the human operator exceed those achieved by the pilot. This suggests that the observation noise-ratios in the model may have been too high. We decreased these noise-ratios to approximately -23 dB and found that all predicted scores were then within 10% of measured values. This is an interesting result because it implies that the pilots became less "random", in an attempt to maintain the lower scores. Or, in Levison's terms [23] the pilots worked harder to achieve a criterion level. This correlates with the fact that the $M_q = -1.0$ case was rated unsatisfactory by the pilots [21] whereas the cases with higher damping were rated satisfactory.

The equivalent Y_{p_θ} and Y_{p_x} obtained from the optimal control model are plotted in Figs. 42-43. Naturally, the simplified fixed-form expressions of Reference 21 will not duplicate the low-frequency variations seen in the Y_{p_θ} transfer with $M_q = -1.0$. Nor will the high frequency behavior of corresponding transfers be duplicated for the reason mentioned earlier. However, it can be verified that in the neighborhood of crossover, both models yield pitch and position loop gains that agree quite well. Thus, we found inner and outer loop crossover frequencies that agreed with those of Reference 21 to within plotting accuracies.

Effects of speed stability parameter, M_u. – The effects on predicted and measured scores of changing the speed stability parameter M_u are shown in Fig. 44. The agreement is again very good except for the smallest value of $M_u=0$. The less precise agreement for the $M_u=0$ case is probably attributable to a value of motor noise that is too small. In this case there is no gust

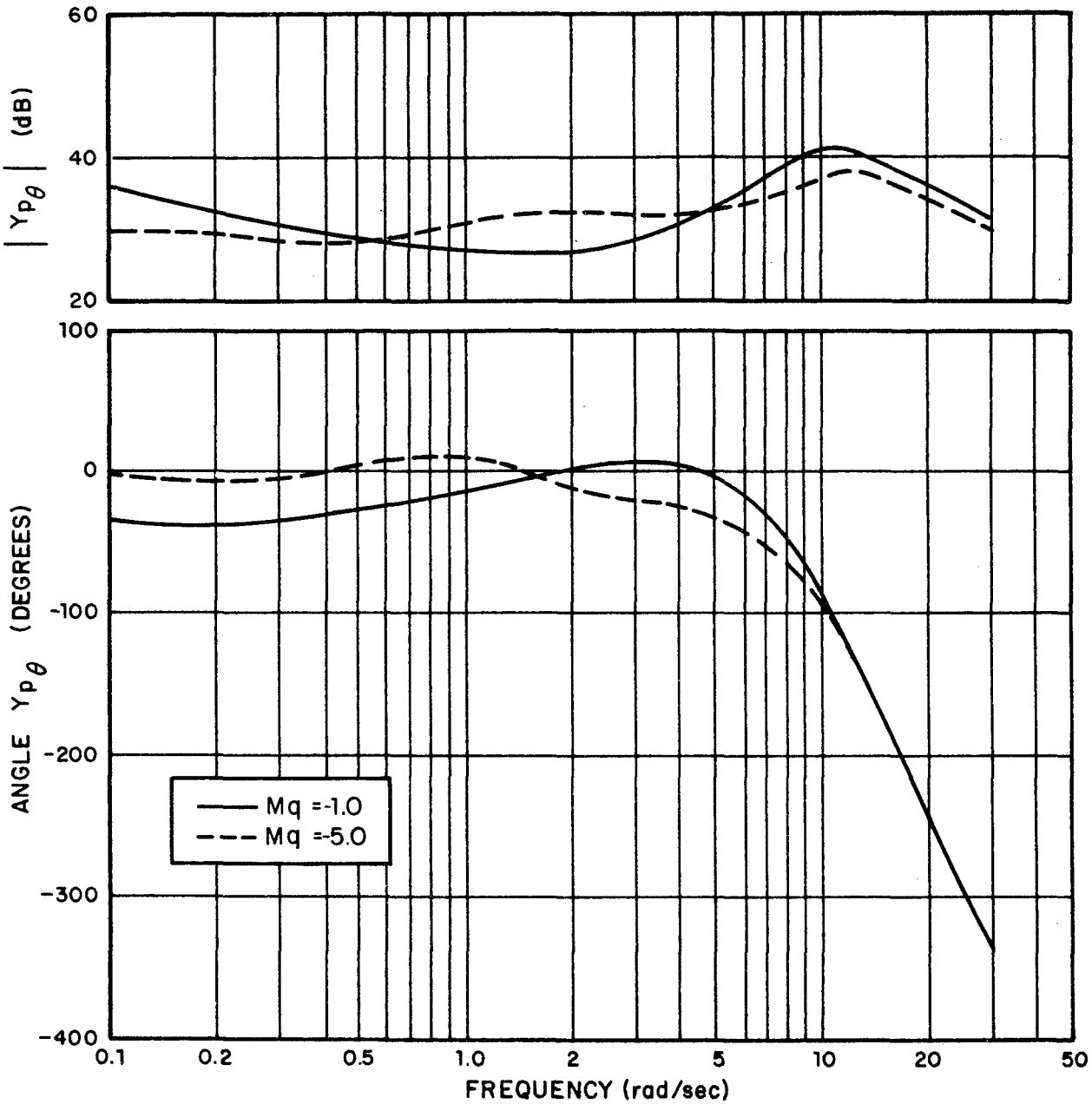

FIG.42 EFFECT OF PITCH RATE DAMPING ON PREDICTED PILOT DESCRIBING FUNCTION FOR PITCH LOOP, ($M_u g$ = .667, X_u = -.1)

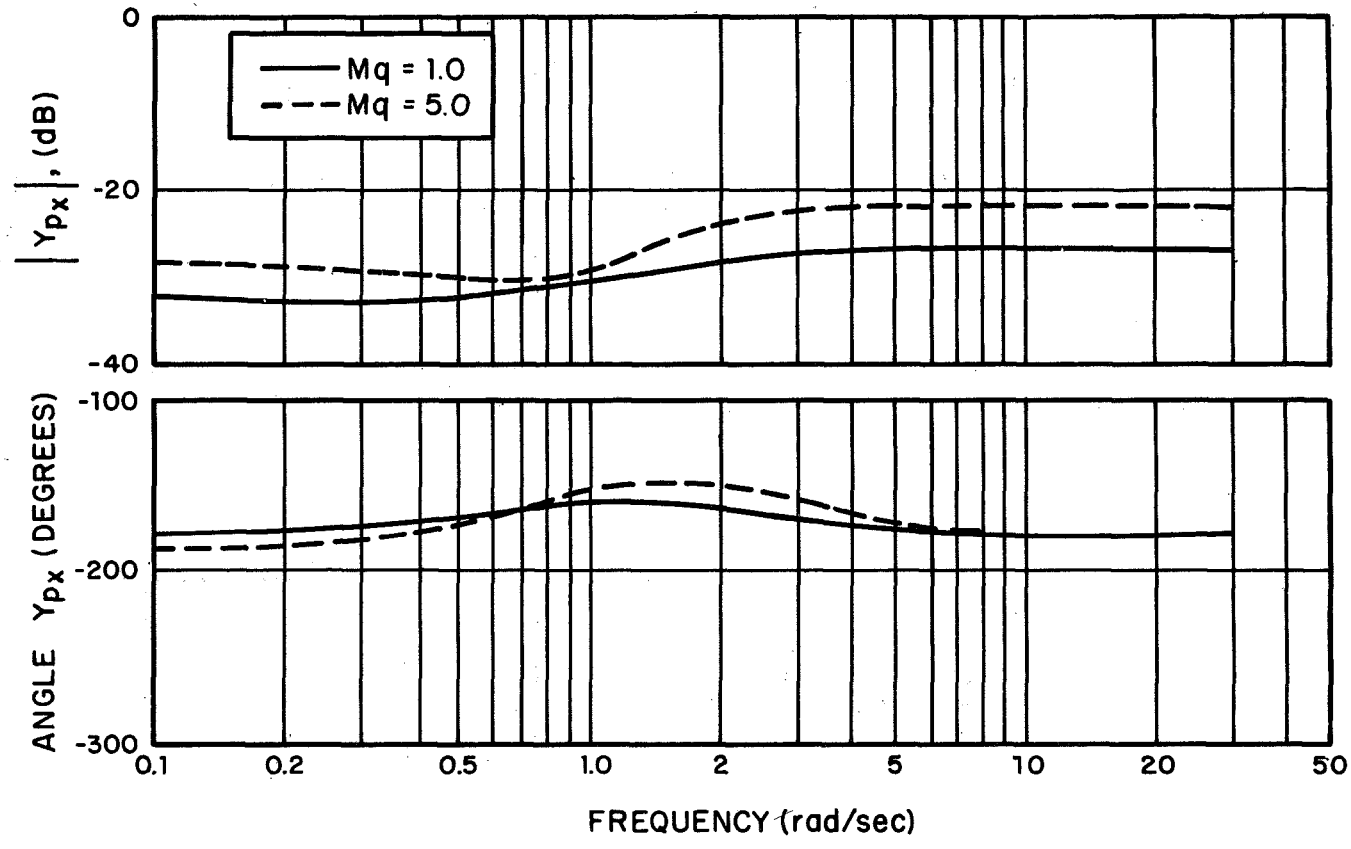

FIG.43 EFFECT OF PITCH RATE DAMPING ON PREDICTED PILOT DESCRIBING FUNCTION FOR POSITION LOOP, ($M_u g$ = .667, X_u = -.1)

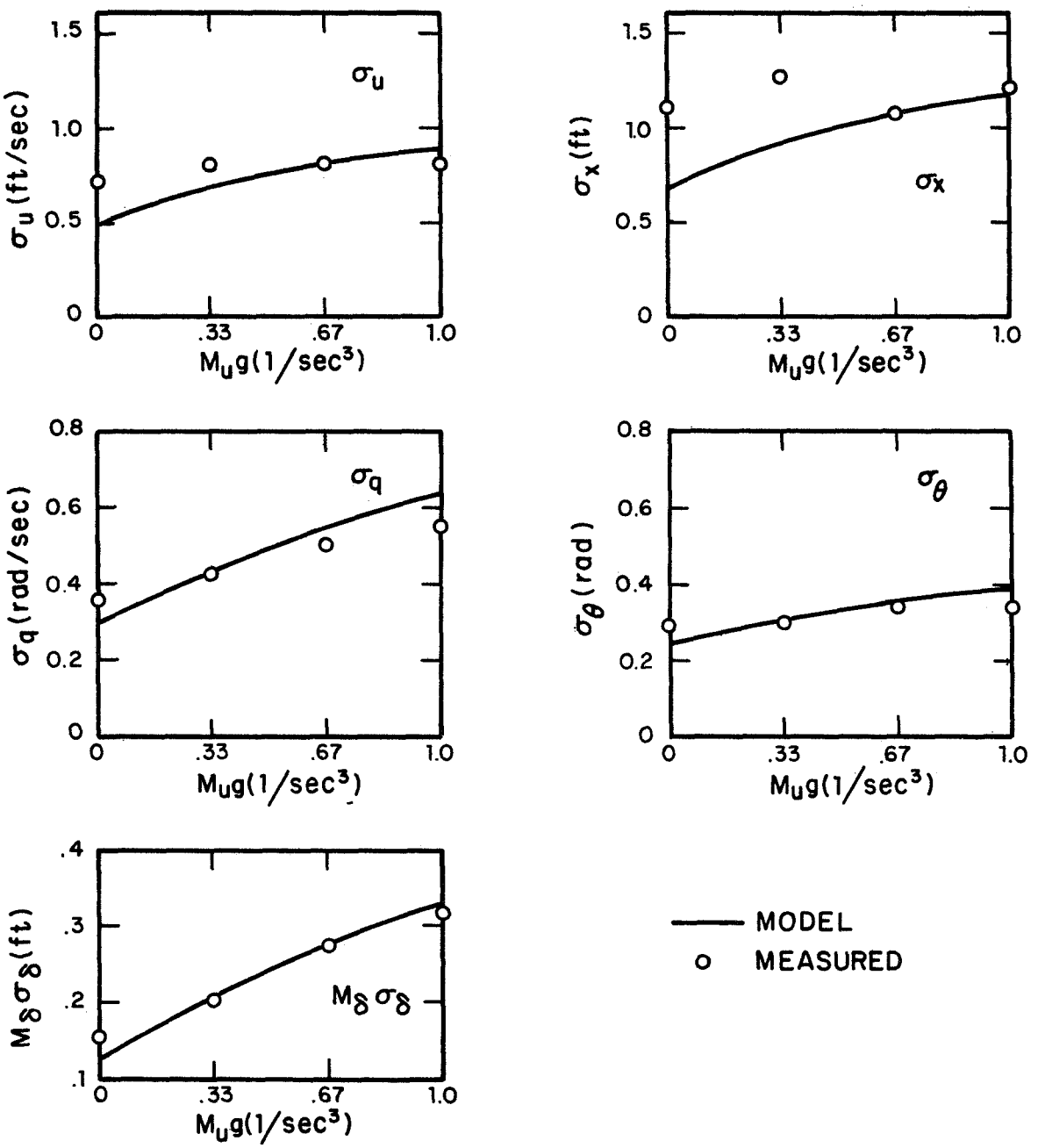

FIG.44 EFFECT OF SPEED STABILITY PARAMETER ON HOVERING PERFORMANCE, (M_q = -3.0, X_u = -.1)

component entering in parallel with the stick so the Kalman filter can obtain very good estimates of q and θ. As we saw in an earlier chapter (and in Reference 17), such a situation may require values of motor noise somewhat greater than -25 dB to model the human operator accurately.†

Equivalent Y_{p_θ} and Y_{p_x} transfers for the cases $M_u g = .33$ and $M_u g = 1.0$ are shown in Figs. 45-46 . Variations in Y_{p_θ} with $M_u g$ take place almost entirely below 1 rad/sec. (The nominal Y_{p_θ} for $M_u g = .667$ falls within those shown.) In the neighborhood of pitch loop crossover (~3 rad/sec), pitch loop gain decreases very slightly with increasing $M_u g$. This was also true for the fixed-form model of Reference 21. The variations in Y_{p_x} (Fig. 46) with $M_u g$ are not very dramatic, with relatively small changes in gain appearing to be the principal effect. It should be noted that the position gain of the optimal control model decreases with increasing $M_u g$, whereas the K_{p_x} of the fixed-form model shows the opposite trend. However, the total variation in position loop gain for the fixed-form model is less than 2 dB and the observed trend may not be significant.

Effects of variations in longitudinal drag parameter, X_u. — Predicted scores were computed for various values of X_u (with M_q and $M_u g$ kept at their nominal values) and are presented along with measured data in Fig. 47.†† Again, the data agree almost

†Note that moderately higher values of motor noise would not increase the scores significantly in the remaining cases examined in this chapter because of the relatively large nominal value for $M_u g$.

††Frequency domain data were also computed but they evidenced similar phenomena as in the other cases and are therefore not presented.

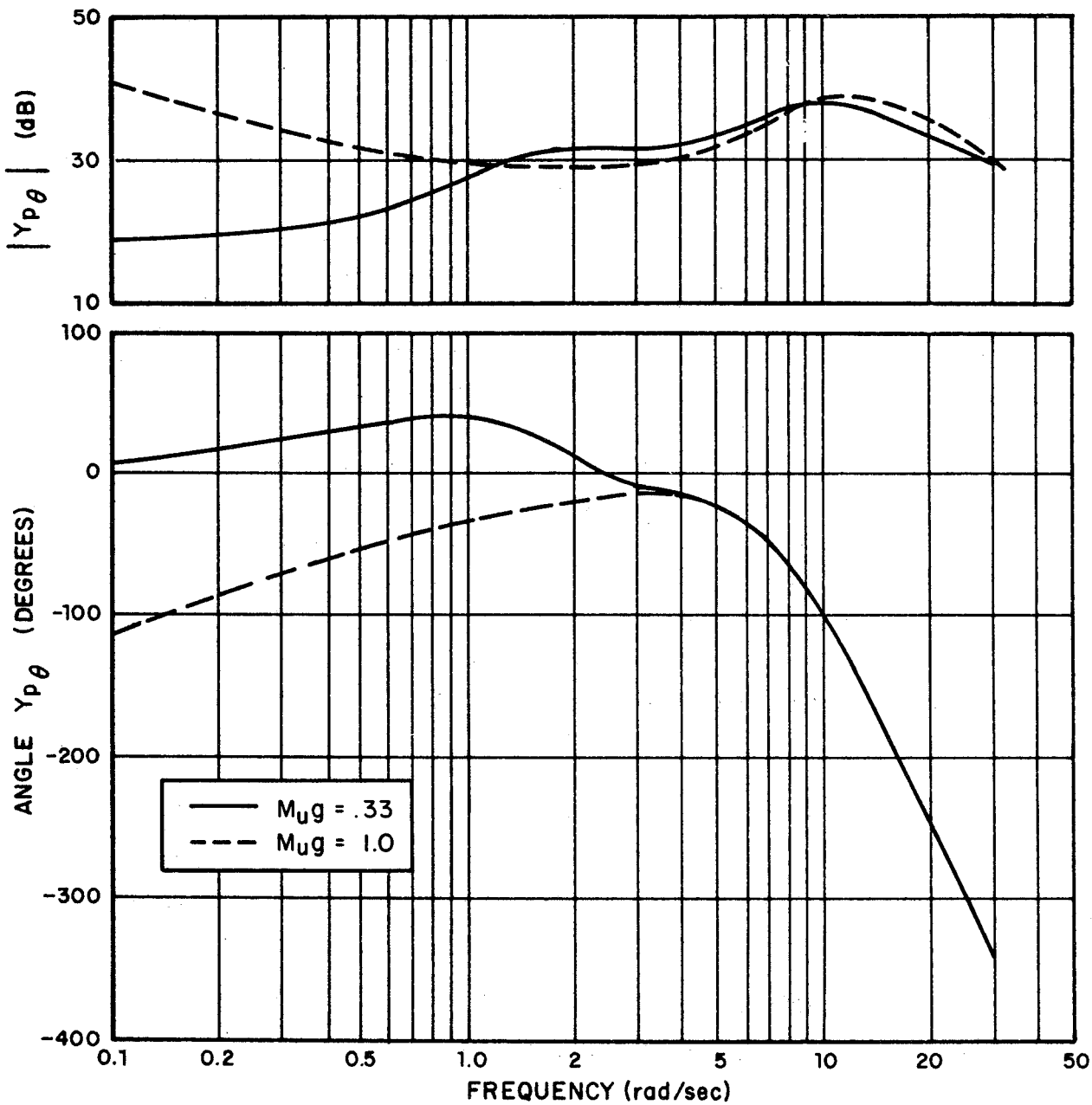

FIG.45 EFFECT OF SPEED STABILITY PARAMETER ON PREDICTED PILOT DESCRIBING FUNCTION FOR PITCH LOOP, (M_q = -3.0, X_u = -.1)

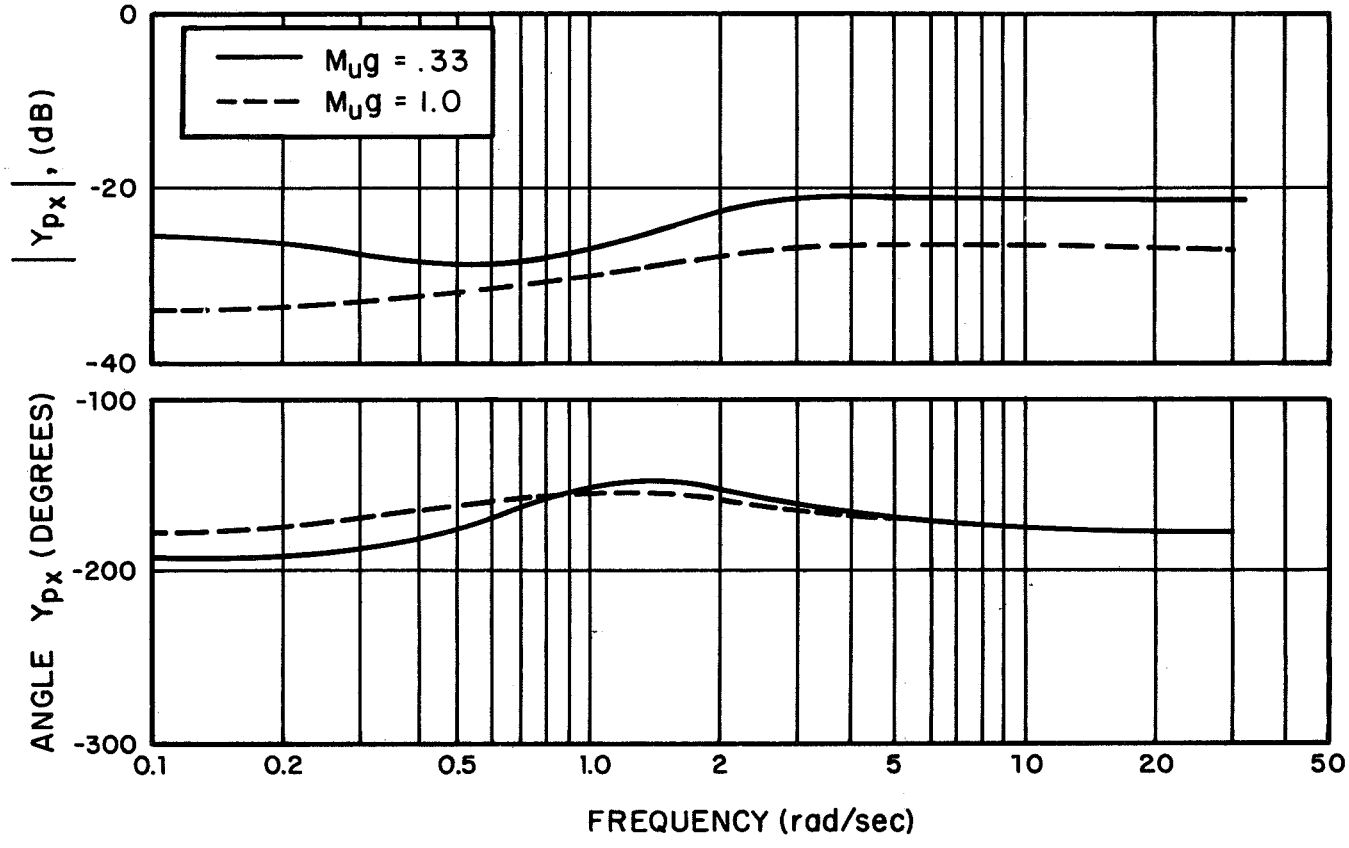

FIG.46 EFFECT OF SPEED STABILITY PARAMETER ON PREDICTED PILOT DESCRIBING FUNCTION FOR POSITION LOOP, (M_q = -3.0, X_u = -.1)

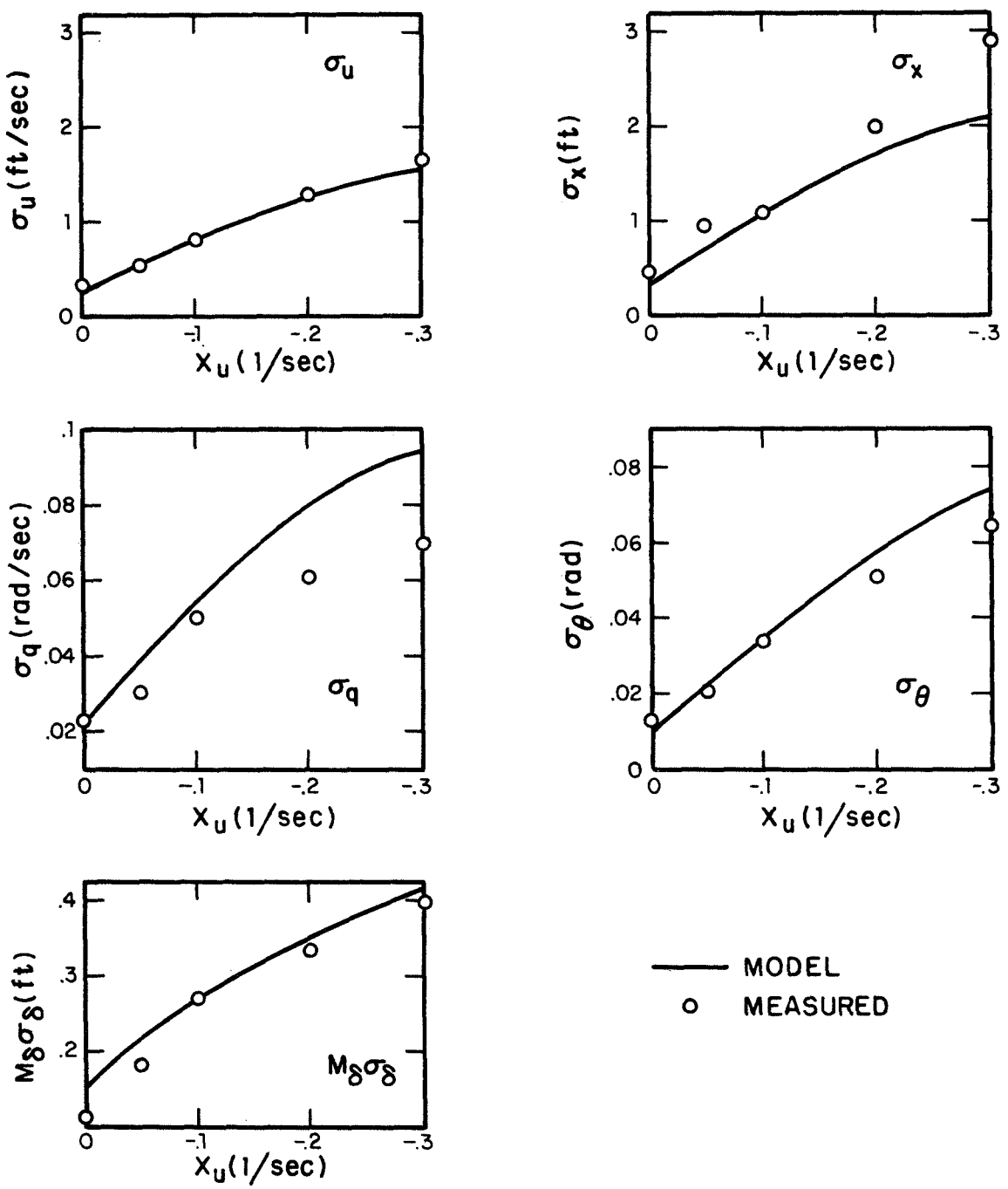

FIG.47 EFFECT OF LONGITUDINAL DRAG PARAMETER ON HOVERING PERFORMANCE, ($M_u g$ = .667, M_q = -3.0)

everywhere; major trends are reproduced and actual values are in close agreement. The only exception is the $X_u = -.3$ case where the model predicts lower position, and higher pitch scores than were actually measured.

Predicted and measured scores could be brought in closer agreement for $X_u = -.3$ by increasing the pitch rate weighting. We therefore obtained model predictions for a weighting of $q_4 = 1000$, a two and one-half-fold increase. The results, along with the measured values and those obtained with the lower weighting, are presented in Table 6.. (Numbers in parentheses are standard deviations.)

Table 6

Score Comparison for Different Pitch Rate Weightings in High Drag Configuration

	σ_u	σ_x	σ_q	σ_θ	σ_δ
Measured	1.67(.20)	2.88(.45)	.069(.005)	.064(.005)	.76(.07)
q_4=400	1.58	2.10	.095	.074	.82
q_4=1000	1.66	2.52	.079	.070	.68

Thus, it would appear from these results that the pilot was unwilling to accept the higher pitch rate scores associated with the larger turbulence (X_u multiplies the input)† and increased his pitch rate weighting accordingly. It is interesting to note that this configuration had the poorest pilot rating of all the cases that we investigated.

†Vinje and Miller also draw the same inference from their data.

Summary and remarks. — We have applied the optimal control model of the human operator to predict performance in a series of longitudinal hovering tasks. The configurational changes that were considered significantly altered the system response to both control and disturbance inputs, yet the model was able to predict performance with exceptional accuracy in almost all cases. Moreover, this was accomplished with a fixed set of model input parameters, whose values were virtually identical to those used in single-axis studies. Also needed in the analysis was a "subjective" weighting on rms pitch-rate error (i.e., a measure of performance in the "additional loop"). Results for all but one case were quite good keeping this parameter invariant and reasonable methods for selecting its value appear to be generally available.

Inasmuch as no frequency domain measurements were available for comparison, the optimal control model was used to predict describing functions that corresponded to the "loop closing" pilot transfer functions that are frequently employed in "classical" multiloop manual control analyses. These "equivalent-optimal" describing functions were compared with fixed-form transfer functions that had been derived in the original analysis of the data [21]. The fixed-form transfer functions were of the "crossover-model" genre, and had some preselected parameters (time delays and neuromotor time constant) and some parameters (gains and lead time constants) that were adjusted to match measured score data.

Invariably, the optimal control and fixed-form describing functions agreed quite well in the neighborhood of loop "crossovers." This is not surprising because the optimal control model predicts the measured scores and the fixed-form model, which is designed primarily for the crossover region, is adjusted to match the

"same" measured scores. For frequencies outside the crossover range, agreement between the differently obtained describing functions is generally not good. This is particularly evident for pitch-loop pilot describing functions. Those describing functions obtained from the optimal control model exhibit much more complex behavior than do the simpler fixed-form transfers. Many of these complex response characteristics are quite similar to those predicted by the model, and also observed experimentally, in single-axis tasks. On this basis we believe that measured describing functions would bear a closer resemblance to those predicted by the optimal control model than to those obtained from the fixed-form model with "measured" parameters.

There were three cases for which the optimal control model did not yield very accurate score predictions. For one of these cases ($M_u g=0$) the discrepancies could be largely attributed to our treatment of motor noise. In the other two cases, more accurate predictions were achieved by changing model input parameters. In one case (lowest pitch rate damping), the observation noise ratio was decreased, and in the other case (highest drag) the pitch-rate weighting was increased. It is interesting and important to note that both of these cases were ones in which significantly poorer pilot ratings were obtained. It would appear to be more than coincidental that a change in the basic model parameters correlated with a substantial degradation in pilot rating. Although, much work remains to be done, we are reasonably convinced that the optimal control model will ultimately provide a versatile and fairly general approach to predicting aircraft flying qualities.

EXTENSIONS AND FURTHER RESEARCH

There are various problems deserving of further research that arise in our modern control approach to human operator modelling. Some of these problems have been mentioned briefly earlier in the report. In this chapter we discuss our preliminary research on several problems of a theoretical nature that relate to the model's development, extensions and practical applications.

A New Characterization of Motor Noise

Recall that motor noise was included in our optimal control model in a somewhat artificial way to prevent the Kalman estimator from knowing perfectly the control signal, u(t). In this section we present a new method for treating motor noise that has more physical and intuitive appeal. In addition, our preliminary results show that this new representation gives model predictions that more accurately reproduce experimental data, especially in the low frequency range, $\omega<1$ rad/sec.

Theoretical development. – Our new approach is to model directly the fact that the human can obtain only imperfect observations of his own outputs. We thus associate with both u(t) and $\dot{u}(t)$ "observation" noises $v_u(t)$ and $v_{\dot{u}}(t)$ with covariances V_u and $V_{\dot{u}}$, respectively. Therefore, the human is assumed to perceive

$$u_p(t) = u(t-\tau) + v_u(t-\tau) \tag{77}$$

$$\dot{u}_p(t) = \dot{u}(t-\tau) + v_{\dot{u}}(t-\tau) \tag{78}$$

and he must estimate u(t) and/or $\dot{u}(t)$ for purposes of control. In this manner we treat motor noise in the same conceptual way as we

treat observation noise $\underline{v}_y(t)$. This imparts a conciseness and uniformity to the model's representation of human limitations.

The "observations" of Eq. (77) are included within the optimization framework as follows. Recall that in developing the human operator model we defined an "augmented" state vector $\underline{\chi} = (\underline{x},u)$ where

$$\begin{aligned} \dot{\underline{\chi}}(t) &= \underline{A}_0\underline{\chi}(t) + \underline{b}_0\dot{u}(t) + \underline{w}(t) \\ \underline{y}(t) &= \underline{C}_1\underline{\chi}(t) = \text{displayed outputs} \end{aligned} \tag{79}$$

$$\underline{A}_0 = \begin{bmatrix} \underline{A} & \underline{b} \\ \underline{0} & \underline{0} \end{bmatrix} \quad ; \quad \underline{b}_0 = \begin{bmatrix} 0 \\ \vdots \\ 0 \\ 1 \end{bmatrix} \quad ; \quad \underline{C}_1 = \left[\begin{array}{c:c} & \\ \underline{C} & \underline{d} \\ & \end{array}\right] \tag{80}$$

It was found that the control law

$$\dot{u}(t) = -\underline{\lambda}\,\hat{\underline{\chi}}(t) \tag{81}$$

minimizes J(u) based on noisy observations. $\hat{\underline{\chi}}(t)$ is the best estimate of $\underline{\chi}(t)$[†] and the gains $\underline{\lambda}$ are given by Eq. (9).

Since $\dot{u}(t)$, and not u(t), is <u>explicitly</u> generated by the feedback controller, we may include the "observations" of Eq. (77) directly within the optimization framework by merely defining an additional output

[†]In the absence of motor noise $\hat{\chi}_{n+1} \equiv u$.

$$y_{m+1}(t) \equiv u(t) \tag{82}$$

with an associated "observation" noise $v_{y_{m+1}}(t) = v_u(t)$. Thus, $u(t)$ is treated as an "observed" or "displayed" output that must be estimated by the feedback controller. Unfortunately, it is not possible to treat $\dot{u}(t)$ in this same simple way. However, we can show that as regards the Kalman estimator, it is possible to represent the model's imperfect perception of $\dot{u}(t)$ by adding a driving noise $\underline{b}_0 v_{\dot{u}}(t)$ in parallel with $\dot{u}(t)$ in Eq. (79).

In order for this latter construct to truly model observational or sensory effects it is necessary that $v_{\dot{u}}(t)$ be much smaller than $\dot{u}(t)$, i.e., its explicit driving effects on the closed-loop system must be negligible. Fortunately, this appears to be the case. We have found, typically, that

$$\frac{V_{\dot{u}}}{\pi\sigma_{\dot{u}}^2} \approx 10^{-4}$$

i.e., $v_{\dot{u}}(t)$ when normalized to $\sigma_{\dot{u}}^2$ has a white-noise power density level of -40 dB. Thus, over the frequency range $0<\omega<30$ rad/sec., $v_{\dot{u}}(t)$ will directly contribute less than 1% to the value of $\sigma_{\dot{u}}^2$. However, $v_{\dot{u}}(t)$ can have a large effect on the Kalman estimator which, in turn, can greatly influence system variances.

Under our new assumptions, the Kalman filter generates the best estimate $\hat{\underline{x}}(t-\tau)$ from the perceived quantities $\tilde{\underline{y}}_p(t) = \text{col}[\underline{y}_p(t), u_p(t)]$ and $\dot{u}_p(t)$ according to

$$\dot{\hat{\underline{x}}}(t-\tau) = \underline{A}_0\hat{\underline{x}}(t-\tau)+\underline{b}_0\dot{u}_p(t)+\tilde{\underline{\Sigma}}\,\tilde{\underline{C}}'\tilde{\underline{V}}_y^{-1}[\tilde{\underline{y}}_p(t)-\tilde{\underline{C}}\,\hat{\underline{x}}(t-\tau)] \tag{83}$$

where the error covariance matrix $\underline{\tilde{\Sigma}}$ satisfies

$$\underline{0} = \underline{A}_0\underline{\tilde{\Sigma}} + \underline{\tilde{\Sigma}}\,\underline{A}_0' + \underline{W}_0 + \underline{b}_0 V_u \underline{b}_0' - \underline{\tilde{\Sigma}}\,\underline{\tilde{C}}'\underline{\tilde{V}}_y^{-1}\underline{\tilde{C}}\,\underline{\tilde{\Sigma}} \tag{84}$$

with

$$\underline{\tilde{C}} = \left[\begin{array}{c|c} \underline{C} & \underline{d} \\ \hline \underline{0} & 1 \end{array}\right] \quad ; \quad \tilde{V}_y = \left[\begin{array}{c|c} \underline{V}_y & \underline{0} \\ \hline \underline{0} & V_u \end{array}\right] \tag{85}$$

The best estimate of the current state, i.e., $\hat{\underline{x}}(t)$ is generated by a least-mean-squared predictor as in Eq. (19).

Once the variance equation (84) is solved for $\underline{\tilde{\Sigma}}$ it is possible to generate predictions of closed-loop response such as in Eqs. (20)-(26). These later equations remain valid in the present context with the replacements $(\tau_N s+1)\to s$, $\hat{\underline{\ell}}\to\underline{\lambda}$, $\underline{A}_1\to\underline{A}_0$, $\underline{b}_1\to\underline{b}_0$, $\underline{\Sigma}\to\underline{\tilde{\Sigma}}$, etc. In addition, the scanning results also remain valid, where the scanning cost $I(\omega)$, (see Eq. 56) is now given precisely by

$$I(\omega) = \left(\underline{\lambda}\, e^{\underline{A}_0\tau}\right)\underline{\tilde{\Sigma}}\left(\underline{\lambda}\, e^{\underline{A}_0\tau}\right)' \cdot g \tag{86}$$

Relationships with earlier method. — In our revised approach for including motor noise it is no longer necessary to single-out the lag network $(\tau_N s+1)^{-1}$ or to define a supposed "commanded" control signal. In our new scheme vehicle outputs and control inputs (i.e., human outputs) are treated as quantities that are perceived by the human.† Time-delay and "observation" noise are associated

†Typically, vehicle outputs are observed visually and control inputs are sensed through muscular feedback. Kinesthetic cues may also be included.

with each perception. Thus, observation noises relate directly to physical quantities that define the nature of the man-machine interface. Figure 48 shows the closed-loop structure of the revised model.

It is worthwhile to point out that there exists a mathematical comparison between the old and new motor noise representations. In the latter case it is possible to show that the error associated with estimating u(t) from the observations (77) is given approximately by

$$\dot{e}_u(t) = -\delta e_u(t) + v_{\dot{u}}(t) + \delta v_u(t) \; ; \; \delta = (V_{\dot{u}}/V_u)^{\frac{1}{2}} \qquad (87)$$

and has power density spectrum,

$$\Phi_{ee_u}(s) = \frac{V_{\dot{u}} + \delta^2 V_u}{s^2 + \delta^2} = \frac{2V_u}{\delta^{-2}s^2 + 1} \; . \qquad (88)$$

This suggests that if we choose V_u and $V_{\dot{u}}$ to satisfy

$$2V_u = V_m$$

$$\delta^{-2} = V_u/V_{\dot{u}} = \tau_N^2 \qquad (89)$$

then the model results that are obtained with our new approach should approximate predictions using the earlier model.† We found this to be true in several cases analyzed.

New model predictions. – The numerical determination of suitable values for V_u and $V_{\dot{u}}$, or the noise ratios

†In the old method a driving noise with power density spectrum $V_m/(\tau_N^2 s^2+1)$ effectively represents the "estimation" error in u(t).

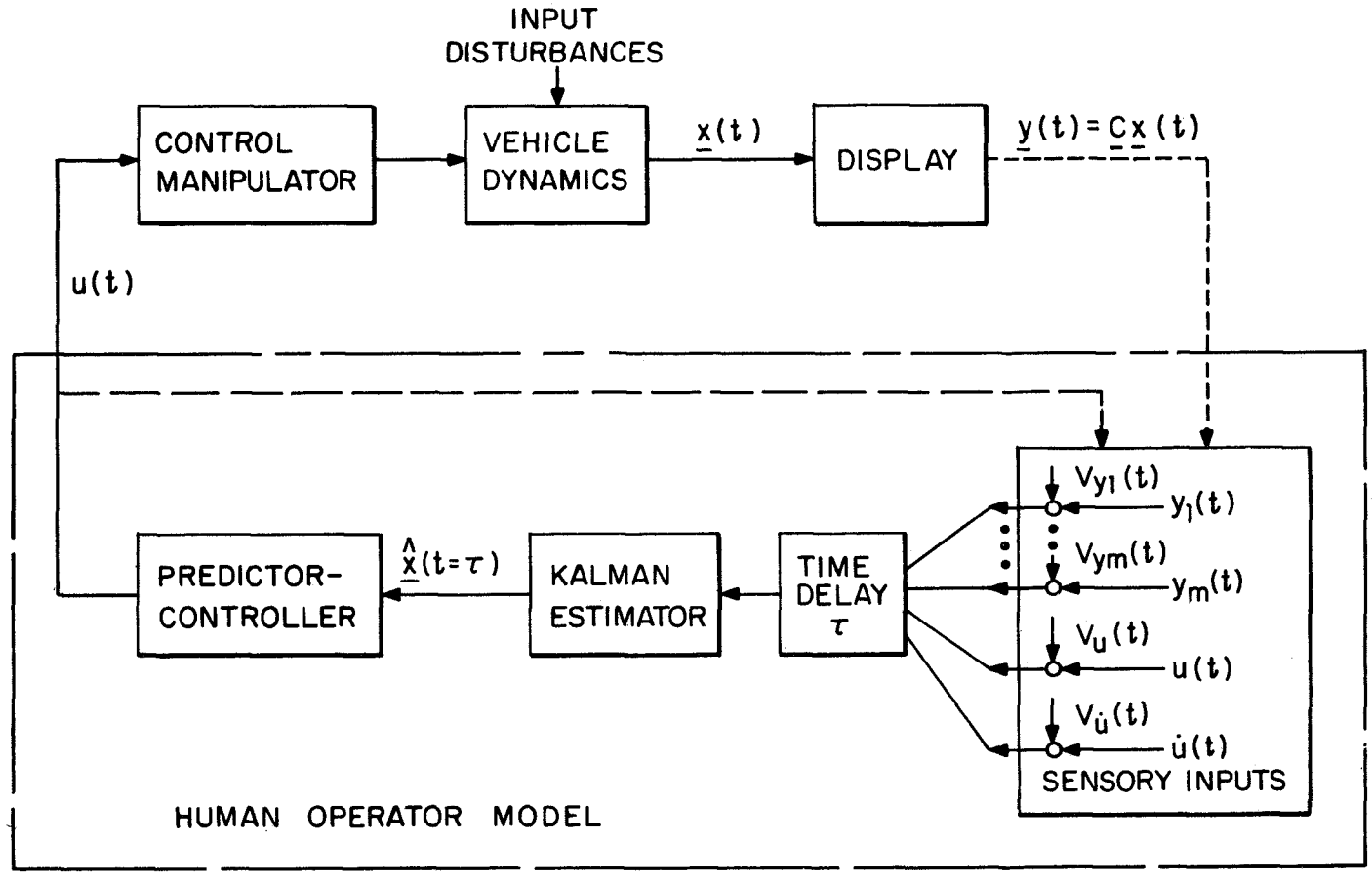

FIG.48 CONCEPTUAL MODEL OF HUMAN ESTIMATION AND CONTROL PROCESSES

$$\rho_u \equiv V_u/\pi\sigma_u^2 \tag{90}$$

$$\rho_{\dot{u}} \equiv V_{\dot{u}}/\pi\sigma_{\dot{u}}^2$$

is a matter for further research.† These quantities depend on the type of control manipulator (e.g., force stick, position stick, etc.) as well as on intrinsic human characteristics. In general, one might expect V_u (or ρ_u) to be large, owing to the difficulty in accurately sensing position through muscular feedback. On the other hand, sensing of movement is more naturally accomplished and $V_{\dot{u}}$ ($\rho_{\dot{u}}$) should be small. Under these conditions (V_u large, $V_{\dot{u}}$ small), the estimation error $e_u(t)$ given by Eq. (87) will have considerable power at only low frequencies i.e., $\omega < \sqrt{\frac{V_{\dot{u}}}{V_u}}$. Thus, our new motor-noise representation would be expected to have its dominant effects on system response in the low frequency range.

Accordingly, we applied the model in a preliminary manner to study the manual control of k, k/s and k/s^2 dynamics. We varied both model parameters V_u and $V_{\dot{u}}$ to give a good match to experimental data. (A force stick manipulator was used in the actual experiments.) The other human response parameters τ_N, τ, V_{y1}, V_{y2} were kept at (approximately) the values used previously. It was found that relatively small values of $V_{\dot{u}}$ (typically $\rho_{\dot{u}} = -40$ to -50 dB), and neglecting the observations of u(t), i.e., $V_u = \infty$, gave model results that were entirely consistent with the data.††

†Model matching techniques, coupled with the results of basic experiments, could prove extremely useful in such a study.

††This seems to verify that motor sensing of position is grossly inaccurate whereas sensing of rate is easily accomplished.

The results for k/s dynamics are shown in Fig. 49. The motor noise parameters are $\rho_{\dot{u}} = -40$ dB, $\rho_u = \infty$. Note that the major difference between the describing function results of Fig. 49 and those obtained earlier (dotted lines in Fig. 49) lies in the low-frequency range as expected. Observed low-frequency phenomena (e.g., phase drooping) are reproduced with an accuracy previously unobtainable. In addition, our results have shown that changing $V_{\dot{u}}$ causes large variations in the low-frequency phase lag but does not greatly affect other system measures. Thus the large variations in low-frequency phase observed experimentally may be related to intersubject variations in the parameter $\rho_{\dot{u}}$.

On the basis of these preliminary studies it appears that our new treatment of motor noise provides a better representation of the human's motor limitations and is capable of duplicating more accurately human response characteristics. Further results are needed to verify these conclusions, however.

Optimal Estimation with Output Related Noise

Recall that in applying the optimal control model of the human operator to foveal viewing conditions, the observation noises $V_{yi}(t)$ are assumed to scale with their associated variances, viz

$$V_{yi} = \rho_i \, E\{y_i^2\} \; ; \; i=1,2,\ldots,m \tag{91}$$

The application of the model thus requires iterating on equations of the form

$$\underline{0} = \underline{P}\,\underline{A}' + \underline{A}\,\underline{P} + \underline{W} - \underline{P}\,\underline{C}'\underline{V}_y^{-1}\underline{C}\,\underline{P} \tag{92}$$

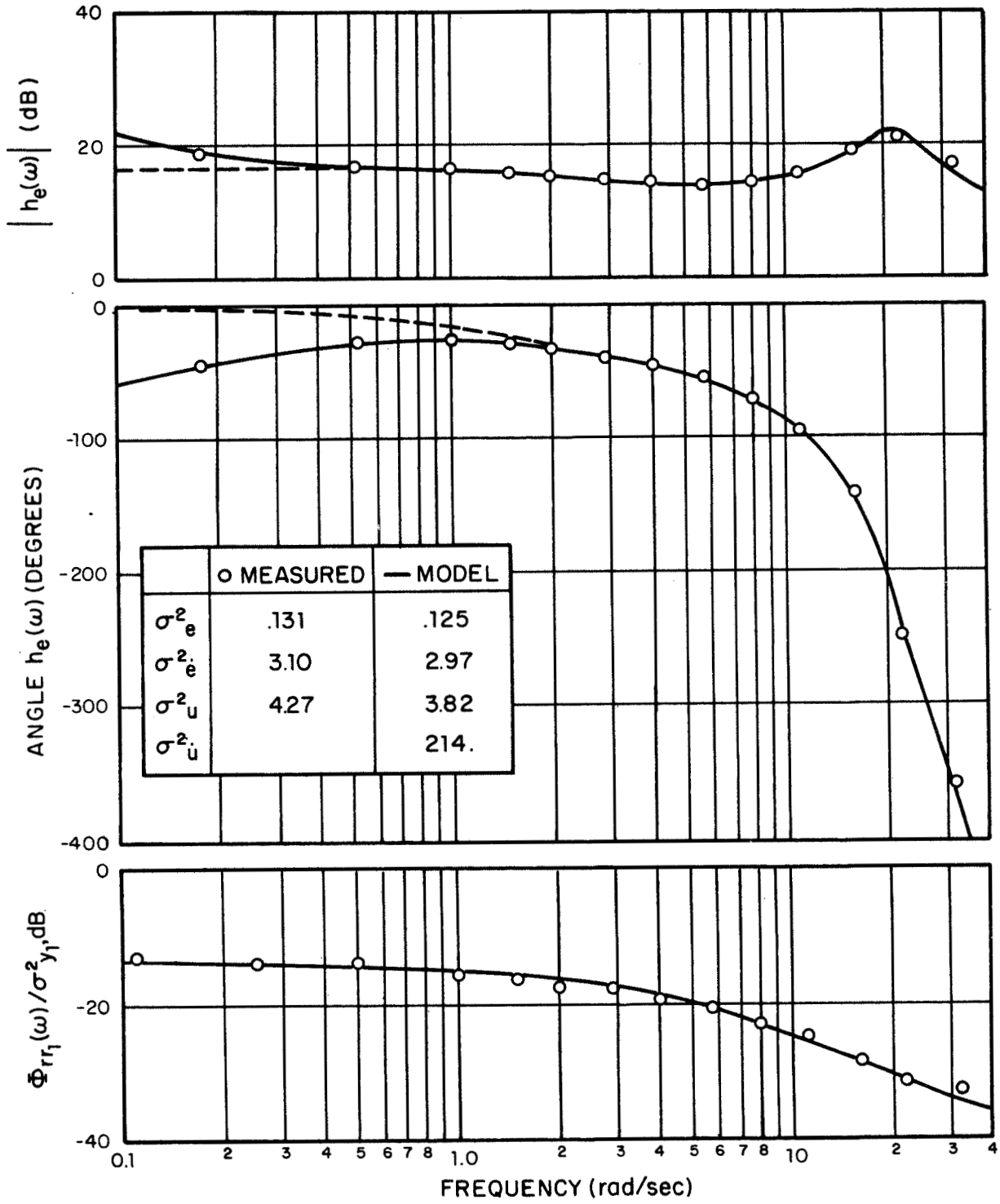

FIG.49 COMPARISON OF FREQUENCY DOMAIN MEASURES, k/s DYNAMICS

and

$$E\{\underline{y}\underline{y}'\} = \underline{C}\left[\int_0^{\tau} e^{\underline{A}\sigma}\underline{W}e^{\underline{A}'\sigma}d\sigma + e^{\underline{A}\tau}\underline{P}e^{\underline{A}'\tau} + \int_0^{\infty} e^{\overline{\underline{A}}\sigma}e^{\underline{A}\tau}(\underline{P}\underline{A}'+\underline{A}\underline{P}+\underline{W})e^{\underline{A}'\tau}e^{\overline{\underline{A}}'\sigma}d\sigma\right]\underline{C}' \tag{93}$$

in order to adjust $\underline{V}_y$ such that Eq. (91) is satisfied.

In this section (and Appendix A) we present a method for solving Eq. (92) directly, given the noise ratios ρ_i, thereby eliminating the bothersome iteration process.

The method we use to solve Eq. (92) is based upon the results of Refs. 24 and 25 . The following theorem is particularly important:

Theorem 1: Let $\underline{P}_k$, k=0,1,... be the (unique) solution of the linear equation

$$\underline{0} = \underline{P}_k\underline{A}_k' + \underline{A}_k\underline{P}_k + \underline{W} + \underline{L}_k[\underline{R} + \underline{\Pi}(\underline{P}_k)]\underline{L}_k' \tag{94}$$

where $\underline{\Pi}(\cdot)$ is a linear matrix function and

$$\begin{aligned} \underline{A}_k &= \underline{A} - \underline{L}_k\underline{C} \\ \underline{L}_k &= \underline{P}_{k-1}\underline{C}'[\underline{R} + \underline{\Pi}(\underline{P}_{k-1})]^{-1} \qquad k=1,2,... \end{aligned} \tag{95}$$

and where $\underline{L}_o$ is chosen such that $\underline{P}_o > \underline{0}$.

Then $\lim_{k\to\infty} \underline{P}_k = \underline{P}$ is the solution of

$$\underline{0} = \underline{P}\,\underline{A}' + \underline{A}\,\underline{P} + \underline{W} - \underline{P}\,\underline{C}'[\underline{R} + \underline{\Pi}(\underline{P})]^{-1}\underline{C}\,\underline{P} \tag{96}$$

Clearly, this algorithm will be of use in solving Eq. (92) since $\underline{V}_y$ is in fact a linear function of $\underline{P}$. The problems are to first define the linear operator $\underline{\Pi}(\underline{P})$ in terms of system parameters and to then develop a simple means for solving Eq. (94).† These problems are solved completely in Appendix A. All necessary equations are included.

In order to use the computational algorithm it is necessary to choose an $\underline{L}_o$ such that $\underline{P}_o$ is positive definite. This is a nontrivial and presently unsolved problem. One scheme that we have found useful is to first choose a (diagonal) matrix $\underline{V}_y$ with

$$V_{yi} = \beta \cdot \rho_i(R_{ii}) \tag{97}$$

where

$$\underline{R} = \underline{C}\left[\int_0^{\tau} e^{\underline{A}\sigma}\underline{W}e^{\underline{A}'\sigma}d\sigma + \int_0^{\infty} e^{\underline{\bar{A}}\sigma}e^{\underline{A}\tau}\underline{W}e^{\underline{A}'\tau}e^{\underline{\bar{A}}'\sigma}d\sigma\right]\underline{C}' \tag{98}$$

and where β is an adjustable parameter (typically β=2-5). We then solve the variance equation

$$\hat{\underline{P}}\,\underline{A}' + \underline{A}\,\hat{\underline{P}} + \underline{W} - \hat{\underline{P}}\,\underline{C}'\underline{V}_y^{-1}\underline{C}\,\hat{\underline{P}} = \underline{0} \tag{99}$$

for $\hat{\underline{P}}$ and set

$$\underline{L}_o = \hat{\underline{P}}\,\underline{C}'\underline{V}_y^{-1} \tag{100}$$

---

†When $\underline{\Pi}(\cdot)=\underline{0}$ the computational algorithm is identical to that used to solve the variance equation. (See Refs. 24 and 26 .)

If this choice of $\underline{L}_o$ does not result in $\underline{P}_o$ being positive definite we increase β in Eq. (97) and repeat the process.

We have developed computer programs for solving Eqs. (91)-(93) directly, given the noise ratios ρ_i. We find typically that the above iterative scheme takes 3-4 times longer to converge than does a single solution of the"standard"variance equation (18). Since several on-line iterations of the standard equation are usually needed before the noise levels are properly adjusted, the direct approach can result in a substantial saving of time and effort.

Manual Control in the Presence of System Nonlinearities

Our optimal control model of the human operator was derived under the assumption that the system being controlled is linear. However, it is possible to extend the optimization framework to include those system nonlinearities that bound and/or limit the control input signal. To be more precise, the linear state equation (1) can be replaced by

$$\dot{\underline{x}}(t) = \underline{A}\,\underline{x}(t) + \underline{b}\,\phi(u(t)) + \underline{w}(t) \tag{101}$$

where $\phi(\cdot)$ is a single-input, single-output, memoryless nonlinear element. An example of $\phi(\cdot)$ is the saturation element

$$\phi(u) = \text{sat}(u) = \begin{cases} a & u > a \\ u & |u| \leq a \\ -a & u < -a \end{cases} \tag{102}$$

which is typical of the characteristics of a limited or "backup" controller.

With the inclusion of a nonlinear element in the control loop, we now assume that the human behaves optimally subject to his own psycho-physical limitations and to the system limitations implied by the nonlinearity. Thus, for the input constrained system of Eq.(101), we assume that the human chooses his output u(t) to minimize the cost functional

$$J(u) = \sum_{i=1}^{n} q_i \sigma_{x_i}^2 + r\, \sigma_{\phi(u)}^2 + g\, \sigma_{\dot{u}}^2 \tag{103}$$

based on displayed information.

There are numerous approaches to the study and optimization of nonlinear systems of the type (101). However, techniques of statistical linearization [27] find particular application in the present context since we assume that the signals circulating in the closed-loop system are Gaussian. (See Wonham and Cashman [28], for example.) The essence of this approach is to approximate the nonlinearity $\phi(\cdot)$ by an equivalent gain or random-input describing function $k(\sigma_u^2)$. Therefore, from a statistical viewpoint we represent the nonlinearity by

$$\phi(u(t)) \doteq k(\sigma_u^2) \cdot u(t). \tag{104}$$

For example, the describing function associated with the saturation element (102)is [29]

$$k(\sigma_u^2) = \operatorname{erf}\left(\frac{a}{\sqrt{2}\,\sigma_u}\right) \tag{105}$$

The above quasi-linear approach is particularly appealing in that the overall control system to be optimized is linear, but with an effective gain $\underline{b}_u = k(\sigma_u^2)\underline{b}$ that depends on the variance of the human's output u(t).† Thus, it is possible to optimize the new system (101) with the same mathematical techniques as were used to develop our basic optimal control model. Furthermore, most of the usual measures of human performance are preserved and the effects of system nonlinearities on the human's gain, phase lag and remnant can be investigated. However, insofar as $k(\cdot)$ is highly dependent on σ_u, an accurate prediction of the control variance is required. Fortunately, our model is capable of making such predictions, even in cases where controller remnant contributes significantly to this variance.

There is an immediate result of coupling linear optimization theory with describing function analysis: If, in the absence of nonlinearity, the control strategy $u^*(\underline{x})$ minimizes a quadratic cost functional of the form (103), it is possible to show that the nonlinear system (101) will be stable with $u = u^*(\underline{x})$ provided

$$k(\sigma_u^2) > 1/2 \tag{106}$$

Thus, it is always possible for the human to control the nonlinear system by means of a linear control strategy, provided the describing function gain is sufficiently large. This is a powerful (and somewhat unexpected) result since it depends only on intrinsic properties of optimal linear systems and not explicitly on the actual system being controlled.

†Clearly the validity of such an approach is highly dependent on the degree to which the nonlinearity can be approximated by an equivalent gain. A good approximation is not always possible [30].

Note that this result can be used to obtain bounds on permissible values of σ_u^2 once the nonlinearity $\phi(\cdot)$ is specified. Alternatively, if a reasonable a priori estimate of σ_u^2 can be found, a priori restrictions can be placed on the degree of the nonlinearity. For example, consider the saturating nonlinearity of Eq.(102). In order for $k(\sigma_u^2) > 1/2$ we require

$$\text{erf}\left(\frac{a}{\sqrt{2} \cdot \sigma_u}\right) > 1/2 \tag{107}$$

or, approximately,

$$a > \frac{\sqrt{2}}{2} \sigma_u \tag{108}$$

When this inequality holds, manual control of the nonlinear system (101)will be feasible.

To illustrate the analysis techniques we applied the above approach, using our optimal control model, to a simple manual tracking task for k/s dynamics. The input disturbance is a first-order noise with a break frequency at 1.0 rad/sec. The control task is to minimize mean-squared tracking error. The controller input nonlinearity $\phi(\cdot)$ is the saturation element (102).

As a first analysis we obtain an a priori bound on the saturation level, a, for which stability is guaranteed. From Eq. (108) we have $a>.707\ \sigma_u$. A reasonable a priori estimate of σ_u^2 is the variance of the human's control signal in the absence of nonlinearity. For this example $\sigma_u^2 = 4.0$, as predicted by our human operator model, (associated mean-squared error = .039), so that if $a>1.4$ the system will be stable.

Theoretical predictions of mean-squared error as a function of saturation voltage are shown in Fig. 50. Also shown are several experimental data points for this same situation, obtained from the results of Duggar, Mannen and Hannen [31]. The vertical line AA' corresponds to a = 1.4. It is clear from the figure that a saturation voltage less than 1.4 rapidly tends to be undesirable. For a = 1.4 there is already a 3-fold increase in mean-squared error over no saturation. However, for a = 1.3 and a = 1.2 there is a 5-fold and 8-fold increase, respectively.

The close agreement between experimental and theoretical results further underscores the potential of this approach to nonlinear system analysis. The major features of the technique are its simplicity, its ability to treat both simple and complex systems within one conceptual framework, and its being a natural extension of our earlier results.

Prediction of Task Interference and Workload

Although techniques for using our model to study task interference and workload have been developed elsewhere (Ref. 12), we feel that it is useful to indicate the underlying concepts here. In this way we can show how the human operator model might be applied to solve higher level problems such as predicting task interference, workload and pilot opinion.

Because the human can exert only a limited amount of physical or mental effort, his performance on a given psychomotor task degrades as he is required to perform more and more tasks simultaneously. The existence of these interference effects requires that we take into consideration the "workload" that is expected to be imposed on a human in any situation where multiple tasks must be performed.

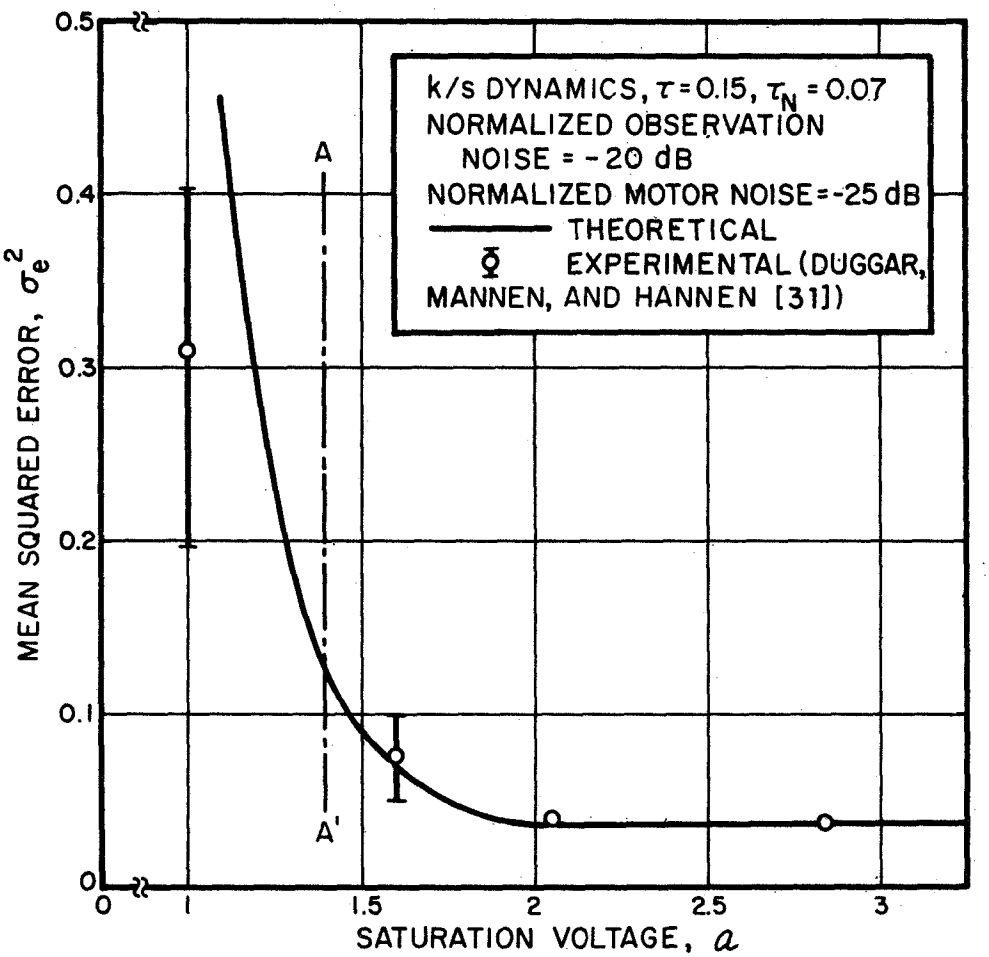

FIG.50 PERFORMANCE CHARACTERISTICS: INTEGRAL CONTROLLER WITH SATURATION

Laboratory studies have led to a model for interference that applies when K independent, continuous control tasks are performed (Refs. 12 and 23). The human operator is assumed to have a fixed amount of central processing capacity (or "attention") that is distributed among the tasks to be performed. This limitation imposed by human capacity is accounted for by modifying the effective observation noise ratios. We associate with the k-th task m_k displayed outputs $y_1, y_2, \ldots, y_{m_k}$ and m_k noise ratios $\rho_1^k, \rho_2^k, \ldots, \rho_{m_k}^k$ that are measured in performing task k alone, i.e., in a single task environment. When the human is required to perform the K tasks simultaneously, these noise ratios are modified according to

$$\hat{\rho}_i^k = \frac{1}{f_k} \rho_i^k \; ; \; i=1,2,\ldots,m_k \; , \; k=1,2,\ldots,K \tag{109}$$

where the f_k's satisfy

$$\sum_{k=1}^{K} f_k = 1 \tag{110}$$

The f_k's are assumed to be adjusted by the human, subject to the constraint of Eq. (110),to optimize system performance. The optimal control model can be used to predict this adjustment as well as to predict the resulting human operator describing functions and system performance measures.

The workload associated with a specific task is often defined as the "attentional demand" of that task. The representation of task interference suggests a metric for operator workload that is consistent with this definition. Since the quantities f_k sum to unity (analogous to a fixed amount of total attention), we associate f_k with the fraction of attention devoted to the k-th subtask.

We then define the workload index of a subtask as the minimum value of f_k that will provide satisfactory system performance. Looked at another way, workload is directly related to the signal-to-noise requirements imposed by the pilot's response strategy.

The optimal-control model has been used to obtain predictions of the workload index for various control situations. These predictions have been tested against pilot opinion data found in the literature, and good agreement has been found between predicted workload and pilot opinion (Ref. 12). However, further experimentation is needed to validate the relationship between noise ratio, workload, and pilot opinion.

CONCLUDING REMARKS

We have seen how modern control and estimation theory can provide a unified approach to the analysis of manual control systems. Within a single optimization hypothesis we can derive mathematical representations for the human operator's control behavior, for his instrument monitoring behavior and even for workload and task interference.

In the preceding chapters we derived an optimal control model of human behavior that is capable of predicting human response characteristics in simple as well as in complex tracking tasks. The techniques for using the model were discussed, model inputs and outputs were delineated and model sensitivities to input parameters were studied. We then took a single set of input parameters obtained from simple experiments, and used the model to accurately predict pilot performance across a wide range of simulated VTOL hovering tasks. This analysis demonstrated convincingly the potential and yet the simplicity of our approach to manual control.

We do not claim that our work on the model is finished. There is much that remains to be accomplished in the manual control field and numerous extensions and improvements of the model are possible (several of which we discussed). However, we do believe that the results presented here provide irrefutable evidence of the value of an optimization approach to manned-vehicle systems analysis.

REFERENCES

1. Russel, L., "Characteristics of the Human as a Linear Servo Element," M.S. Thesis, Elec. Eng. Dept., M.I.T., Cambridge, Mass., (May 1951).

2. Elkind, J.I., "Characteristics of Simple Manual Control Systems," TR111, M.I.T., Lincoln Labs., Lexington, Mass., (April 1956).

3. McRuer, D.T. and Krendel, E.S., "Dynamic Response of Human Operators," Wright Air Dev. Center, WADC TR56-524, Wright-Patterson Air Force Base, Ohio, (October 1957).

4. McRuer, D.T., Graham, D., Krendel, E.S., and Reisener, W.,Jr., "Human Pilot Dynamics in Compensatory Systems: Theory, Models and Experiments with Controlled-Element and Forcing Function Variations," AFFDL-TR-65-15, (July 1965).

5. McRuer, D.T., Ashkenas, I.L., and Pass, H.R., "Analysis of Multiloop Vehicular Control Systems," ASD-TDR-62-1014, (March 1964).

6. Stapelford, R.L., McRuer, D.T. and Magdaleno, R., "Pilot Describing Function Measurements in a Multiloop Task," NASA CR-542, (August 1966).

7. Ashkenas, I.L., and McRuer, D.T., "A Theory of Handling Qualities Derived from Pilot-Vehicle System Considerations," Aerospace Engineering, pp. 83-102, (February 1962).

8. Stapelford, R.L., Wolkovitch, J., et.al., "An Analytical Study of V/STOL Handling Qualities in Hover and Transition," AFFDL-TR-65-73, (October 1965).

9. McRuer, D.T., Hofman, L.G., et.al., "New Approaches to Human Pilot/Vehicle Dynamic Analysis," AFFDL-TR-67-150, (February 1968).

10. Elkind, J.I., Falb, P.F., et.al., "An Optimal Control Method for Predicting Control Characteristics and Display Requirements of Manned-Vehicle Systems," AFFDL-TR-67-187, (April 1968).

11. Burchfiel, J.D., Elkind, J.I., and Miller, D.C., "On the Optimal Behavior of the Human Controller: A Pilot Study Comparing the Human Controller with Optimal Control Models," Bolt Beranek and Newman Inc., Rept. 1532, (August 1967).

12. Levison, W.H., Elkind, J.I. and Ward, J.L., "Studies of Multivariable Manual Control Systems: A Model for Task Interference," Bolt Beranek and Newman Inc., Rept. No. 1892, (December 1969).

13. Kleinman, D.L., Baron, S., and Levison, W.H., "An Optimal Control Model of Human Response, Part I: Theory and Validation," Automatica, Vol.6, No.3, (May 1970).

14. Levison, W.H., Baron, S., and Kleinman, D.L., "A Model for Human Controller Remnant," IEEE, Trans. Man-Machine Systems, Vol.MMS-10, No.4, (December 1969).

15. Rynaskii, E.G., and Whitbeck, R.F., "The Theory and Application of Linear Optimal Control," AFFDL-TR-65-28, (January 1966).

16. Kleinman, D.L., "Optimal Control of Linear Systems with Time-Delay and Observation Noise," IEEE, Trans. Auto. Control, Vol.AC-14, No.5, (October 1969).

17. Baron, S., Kleinman, D.L., et.al., "Application of Optimal Control Theory to the Prediction of Human Performance in a Complex Task," AFFDL-TR-69-81, (March 1970).

18. Baron, S., and Kleinman, D.L., "The Human as an Optimal Controller and Information Processor," IEEE, Trans. Man-Machine Systems, Vol.MMS-10, No.1, (March 1969). Also NASA CR-1151, (September 1968).

19. Chang, S.S.L., Synthesis of Optimum Control Systems, McGraw-Hill Book Co., New York, (1961).

20. Vinje, E.W., and Miller, D.P., "Interpretation of Pilot Opinion by Application of Multiloop Models to a VTOL Flight Simulator Task," NASA SP-144, (March 1967).

21. Vinje, E.W. and Miller, D.P., "An Analysis of Pilot Adaptation in a Simulated Multiloop VTOL Hovering Task," NASA SP-192, (March 1968).

22. Anderson, R.O., "A New Approach to the Specification and Evaluation of Flying Qualities," AFFDL-TR-69-120, (November 1969).

23. Levison, W.H., "A Model for Task Interference," Proc. IEEE, International Symposium on Man-Machine Systems, Vol.3, (September 1969).

24. Kleinman, D.L., "Optimal Stationary Control of Linear Systems with Control-Dependent Noise," IEEE, Trans. Auto. Control, Vol.AC-14, No.6, (December 1969).

25. Wonham, W.M., "Random Differential Equations in Control Theory," in Probabalistic Methods in Applied Mathematics, Vol.2, A.T. Bharucha-Reid, Ed., Academic Press, New York, (to be published).

26. Kleinman, D.L., "On an Iterative Technique for Riccati Equation Computations," IEEE, Trans. Auto. Control, Vol.AC-13, No.1, (February 1968).

27. Booton, R.C., "Nonlinear Control Systems with Random Inputs," IRE, Trans. Circuit Theory, Vol.CT-1 (1954).

28. Wonham, W.M. and Cashman, W.F., "A Computational Approach to Optimal Control of Stochastic Saturating Systems," Preprints 1968 Joint Automatic Control Conference, Ann Arbor, Michigan.

29. Graham, D., and McRuer, D., Analysis of Nonlinear Control Systems, John Wiley and Sons, Inc., New York, (1961).

30. Fitts, R.E., "Linearization of Nonlinear Feedback Systems," PhD Dissertation, M.I.T., Cambridge, Mass., (June 1966).

31. Duggar,L.C., Mannen, J.T., and Hannen, R.A., "Pilot Describing Function Models for Nonlinear Controlled Elements," NASA SP-215, (March 1969).

32. Bellman, R., Introduction to Matrix Analysis, McGraw-Hill, New York, (1960).

33. Levison, W.H., "The Effects of Display Gain and Signal Bandwidth on Human Controller Remnant," Bolt Beranek and Newman Inc. Report No. 1968, (June 1970).

APPENDIX A

USE OF THEOREM 1 TO FIND THE KALMAN ESTIMATOR

In order to use the algorithm of Theorem 1 to solve the optimal estimation problem, when the noises are output dependent, it is necessary to define the noise covariance matrix in the form

$$\underline{V}_y = \underline{R} + \underline{\Pi}(\underline{P}) \tag{A1}$$

and to develop a means for solving repeatedly the linear matrix equation

$$\begin{aligned} \underline{O} &= \underline{P}_k\underline{A}_k' + \underline{A}_k\underline{P}_k + \underline{W} + \underline{L}_k[\underline{R} + \underline{\Pi}(\underline{P}_k)]\underline{L}_k' \\ \underline{A}_k &= \underline{A} - \underline{L}_k\underline{C} \\ \underline{L}_k &= \underline{P}_{k-1}\underline{C}'[\underline{R} + \underline{\Pi}(\underline{P}_{k-1})]^{-1} \qquad k=1,2,\ldots \end{aligned} \tag{A2}$$

with $\underline{L}_0$ given. In this appendix we use matrix algebra to arrive at the desired results.

The identification of $\underline{V}_y$ in the form (A1) is relatively straightforward by combining Eqs. (91) and (93) to obtain

$$\underline{R} = \sum_{i=1}^{m} \rho_i \underline{e}_i \left[\underline{C} \left(\int_0^{\tau} e^{\underline{A}\sigma} \underline{W} e^{\underline{A}'\sigma} d\sigma + \int_0^{\infty} e^{\underline{\bar{A}}\sigma} e^{\underline{A}\tau} \underline{W} e^{\underline{A}'\tau} e^{\underline{\bar{A}}'\sigma} d\sigma \right) \underline{C}' \right]_{ii} \underline{e}_i' \tag{A3}$$

= part of $\underline{V}_y$ independent of $\underline{P}$

where $\underline{e}_i$ is an m-dimensional unit vector in the i-th direction. The part of $\underline{V}_y$ related to $\underline{P}$ is given by

$$\underline{\Pi}(\underline{P}) = \sum_{i=1}^{m} \rho_i \underline{e}_i \left[\underline{C}\ e^{\underline{A}\tau} \underline{P}\ e^{\underline{A}'\tau} \underline{C}' \right]_{ii} \underline{e}_i'$$

$$+ \sum_{i=1}^{m} \rho_i \underline{e}_i \left[\underline{C} \int_0^{\infty} e^{\overline{\underline{A}}\sigma} e^{\underline{A}\tau} (\underline{P}\ \underline{A}' + \underline{A}\ \underline{P}) e^{\underline{A}'\tau} e^{\overline{\underline{A}}'\sigma} d\sigma\ \underline{C}' \right]_{ii} \underline{e}_i' \quad (A4)$$

It is possible to show, by matrix and vector manipulations, that $\underline{\Pi}(\underline{P})$ may be written as

$$\underline{\Pi}(\underline{P}) = \sum_{i=1}^{m} \rho_i \underline{e}_i \hat{\underline{c}}_i' \underline{P}\ \hat{\underline{c}}_i \underline{e}_i' + \sum_{i=1}^{m} \sum_{j=1}^{n} \rho_i \underline{e}_i \underline{\xi}_j' \underline{P}\ \underline{H}^i \underline{\xi}_j \underline{e}_i'$$

where $\hat{\underline{c}}_i'$ is the i-th row of $\hat{\underline{C}} = \underline{C}\ e^{\underline{A}\tau}$, $\underline{\xi}_j$ is an n-dimensional unit vector and

$$\underline{H}^i = 2\underline{A}' e^{\underline{A}'\tau} \int_0^{\infty} e^{\overline{\underline{A}}'\sigma} \underline{c}_i \underline{c}_i' e^{\overline{\underline{A}}\sigma} d\sigma e^{\underline{A}\tau}$$

Equation (A5) clearly shows the relationship between $\underline{\Pi}(\underline{P})$, or equivalently $\underline{V}_y$, and $\underline{P}$. Note that since $\underline{\xi}_j' \underline{P}\ \underline{H}^i \underline{\xi}_j$ is a scalar, $\underline{\Pi}(\cdot)$ is symmetric, i.e., $\underline{\Pi}(\cdot) = \underline{\Pi}'(\cdot)$.

Having obtained an expression for $\underline{\Pi}$ we can turn to the solution of Eq. (A2) for $\underline{P}_k$. We first write, dropping the k subscript, for notational ease

$$\underline{L}[\underline{R}+\underline{\Pi}(\underline{P})]\underline{L}' = \underline{L}\ \underline{R}\ \underline{L}' + \underline{L}\ \underline{\Pi}(\underline{P})\underline{L}' \tag{A7}$$

Substituting Eq. (A5) for $\underline{\Pi}(\cdot)$, the second term becomes

$$\underline{L}\ \underline{\Pi}(\underline{P})\underline{L}' = \sum_{i=1}^{m} \rho_i (\underline{\ell}_i \hat{\underline{c}}_i')\underline{P}(\underline{\ell}_i \hat{\underline{c}}_i')' \tag{A8}$$

$$+ \sum_{i=1}^{m}\sum_{j=1}^{n} \rho_i (\underline{\ell}_i \underline{\xi}_j')\underline{P}(\underline{\ell}_i \underline{h}_j^i)' \tag{A8}$$

where $\underline{\ell}_i$ is the i-th column of $\underline{L}$ and $\underline{h}_j^i$ is the j-th row of $\underline{H}^{i\,\prime}$. Thus, Eq. (A7) may be written in the form

$$\underline{L}[\underline{R}+\underline{\Pi}(\underline{P})]\underline{L}' = \underline{L}\ \underline{R}\ \underline{L}' + \sum_{i=1}^{m} \underline{G}_i \underline{P}\ \underline{G}_i' + \sum_{i=1}^{m}\sum_{j=1}^{n} \underline{E}_{ij} \underline{P}\ \underline{F}_{ij}' \tag{A9}$$

where $\underline{G}_i = \sqrt{\rho_i}\ \underline{\ell}_i \hat{\underline{c}}_i'$, $\underline{E}_{ij} = \sqrt{\rho_i}(\underline{\ell}_i \underline{\xi}_j')$, $\underline{F}_{ij} = \sqrt{\rho_i}\ \underline{\ell}_i \underline{h}_j^i$

Consequently, the solution of Eq. (A2) is tantamount to solving a linear equation of the form

$$\underline{P}\ \underline{A}' + \underline{A}\ \underline{P} + \underline{W} + \underline{L}\ \underline{R}\ \underline{L}' + \sum_{i=1}^{m} \underline{G}_i \underline{P}\ \underline{G}_i' + \sum_{i=1}^{m}\sum_{j=1}^{n} \underline{E}_{ij} \underline{P}\ \underline{F}_{ij}' = \underline{0} \tag{A10}$$

This equation may be solved with the help of Kroneker product notation (see Ref.[32]). We define the n^2-vector, $\underline{P}_v$, as

$$\underline{P}_v = (p_{11}, p_{21}, \ldots, p_{n1}, p_{12}, \ldots, p_{n2}, \ldots, p_{nn}) \tag{A11}$$

and make a similar definition for $(\underline{W}+\underline{L}\ \underline{R}\ \underline{L}')_v$. It is then possible to show that

$$P_v = -\mathcal{A}^{-1}(\underline{W} + \underline{L}\ \underline{R}\ \underline{L}')_v$$

where

$$\mathcal{A} = \underline{I}\,\textcircled{X}\,\underline{A}' + \underline{A}'\,\textcircled{X}\,\underline{I} + \sum_{i=1}^{m} \underline{G}_i\,\textcircled{X}\,\underline{G}_i + \sum_{i=1}^{m}\sum_{j=1}^{n} \underline{E}_{ij}\,\textcircled{X}\,\underline{F}_{ij} \tag{A12}$$

Consequently, for a given iterate k, the solution of Eq. (A2) for $\underline{P}_k$ is equivalent to the solution of a set of n^2 simultaneous linear equations. The use of Theorem 1 to solve for the optimal estimator, given the noise ratios ρ_i, is thus easily accomplished using the same iterative technique as is used to solve the "standard" estimation problem (i.e., given the noise covariances $\underline{V}_y$).

APPENDIX B

AN OPTIMAL CONTROL MODEL FOR PREDICTING HUMAN RESPONSE

A MANUAL FOR THE USE OF COMPUTER PROGRAMS

This Appendix is a guide for using the computer programs that have been developed to solve the optimization problems associated with our human operator model. This appendix is included as a separate section, independent of the main body of the report, in order to facilitate its use. As a matter of convenience we have restated the basic assumptions of the model, which results in some repetition of the results already presented.

INTRODUCTION

This manual is a guide for using on-line interactive computer programs that predict human operator performance and response characteristics in tracking tasks. The human operator model is based on optimal control and estimation theory coupled with a mathematical description of the human's limitations. The basic underlying assumption is that the well-motivated, well-trained human operator behaves in a near optimal manner subject to his inherent limitations and constraints, and his control task. The details of the theoretical development appear in Kleinman, Baron and Levison [1] where the model was described in detail and was applied to study several simple manual tracking tasks.

Herein we present a thoroughly detailed and documented guide for using computer programs associated with the optimal control model. Input quantities are clearly described as are the various options for model outputs. The computer programs are written in Fortran IV for use on a Digital Equipment PDP-10 time-shared computer with disk storage.†

Finally, an example is presented that demonstrates the on-line use of the model with sample print-outs.

† The modifications to a DEC-TAPE system are trivial.

MODEL SUMMARY

Controlled Element Dynamics

The human operator's basic task is to control in some prescribed way, a dynamical system. The vehicle dynamics are assumed to be represented adequately by the linearized state equations

$$\dot{\underline{x}}(t) = \underline{A}\ \underline{x}(t) + \underline{b}\ u(t) + \underline{w}(t) \tag{1}$$

where $\underline{x}(t)$ is an n-vector that describes the state of the vehicle and $u(t)$ is the human's scalar control. $\underline{w}(t)$ is a vector of (zero-mean) independent "white" driving noise processes with autocovariance

$$E\{w_i(t)w_i(\sigma)\} = W_i\delta(t-\sigma) \tag{2}$$

If the external forcing functions have rational power density spectra of first order or higher, the resulting "shaping filter" dynamics are incorporated into Eq. (1). We assume that the states are ordered such that the first n_c states $x_1, x_2, \ldots, x_{n_c}$ are associated with the noise dynamics (n_c=1 for first order noise, etc.)

The pertinent system outputs $\underline{y}(t) = (y_1, y_2, \ldots, y_m)$ are linear combinations of system states and control, namely

$$\underline{y}(t) = \underline{C}\ \underline{x}(t) + \underline{d}\ u(t) \tag{3}$$

and are presented to the human by way of some display.

Thus the external system, S to be controlled by the human is described by the quantities

$$S:(n, n_c, m, \underline{A}, \underline{b}, \underline{W}, \underline{C}, \underline{d}) \tag{4}$$

Human's Limitations

The various psycho-physical limitations inherent in the human are represented by a lumped equivalent perceptual time delay τ and a model for remnant consisting of an equivalent observation noise vector $\underline{v}_y(t)$. A separate (white) observation noise $v_{y_i}(t)$ is associated with each displayed output $y_i(t)$. The autocovariance of $v_{y_i}(t)$ is

$$E\{v_{y_i}(t)v_{y_i}(\sigma)\} = V_{y_i}\cdot\delta(t-\sigma) \tag{5}$$

Thus, the human perceives

$$\underline{y}_p(t) = \underline{y}(t-\tau) + \underline{v}_y(t-\tau) \ , \tag{6}$$

a delayed, noisy replica of the displayed system output.

In order to model certain control situations adequately, we have found it necessary to include a motor noise term $v_u(t)$ in addition to the observation noise vector. This is helpful primarily when the input disturbance is not applied in parallel with the pilot's control signal. In this situation, motor noise serves to prevent the model from acquiring perfect knowledge of various system inputs or outputs which, in fact, are not known perfectly by the human. Use of motor noise here is strictly a mathematical convenience and does not imply that we are able to distinguish experimentally the various sources of remnant, which we cannot do at present. The motor noise is assumed to be white with autocovariance

$$E\{v_u(t)v_u(\sigma)\} = V_u\cdot\delta(t-\sigma) \tag{7}$$

Control Task

It is assumed that the overall control task is adequately reflected in the human's choice of a control input $u^*(t)$ that minimizes a weighted sum of averaged state and control variances

$$J(u) = \sum_{i=1}^{n} q_i \sigma_{x_i}^2 + r\sigma_u^2 + g\sigma_{\dot{u}}^2 \tag{8}$$

conditioned on the human's observations $\underline{y}_p(\cdot)$.

The weightings in J(u) satisfy $q_i \geq 0$, $r \geq 0$, $g > 0$ and may be objectively and/or subjectively determined.

Note that neuro-motor dynamics have not been included among the human's inherent limitations. However, included in J(u) is a cost which depends on control rate. This term can represent an actual cost on $\dot{u}(t)$ or it can be used to account indirectly for the physiological limitations on the rate at which a human effects control action. It can be shown that the inclusion of such a term results in a first-order lag (often associated with the neuromuscular system) being generated in the optimal controller.

Model Structure

With the above assumptions, the human's control characteristics are determined by the solution of an optimal regulator problem with time-delay and observation noise. It has been shown (Ref.1) that the resultant optimal closed-loop system has the general structure shown in Fig. 1. The human operator model consists of the cascade combination of a Kalman estimator, a least-mean-squared predictor and a set of gains acting on $\hat{\underline{x}}(t)$, the best estimate of the system

state $\underline{x}(t)$.[†] The lag factor τ_N depends on the choice of control rate weighting, g. For given values of q_i and r there is a one-to-one correspondence between g and τ_N: the smaller g, the smaller is τ_N. Thus, a prespecified value of τ_N may be obtained by suitably adjusting g.

Since the optimal feedback controller is linear and time-invariant, the human can also be modelled in the frequency domain by a (vector) transfer function

$$u(s) = \underline{h}(s)\underline{y}(s) \tag{9}$$

Therefore, in a straightforward manner, one can predict human operator describing functions (and injected remnant) that are equivalent to those that are normally measured in an experiment. Furthermore, the model allows us to predict the power spectrum (input and remnant related) of any system state, of any output, or of the human's control. Also available is a prediction of closed-loop performance, i.e., state, output and control variances.

Summary - Model Inputs and Outputs

As we have seen, the use of the optimal control model in a predictive manner requires the specification of various input parameters relating to the fixed vehicle configuration, the task description and the human's limitations. Various human operator characteristics can then be computed as outputs. For reference and convenience, Fig. 2 summarizes these model inputs and outputs.

[†]The detailed structure of the optimal feedback system is given in Ref.1.

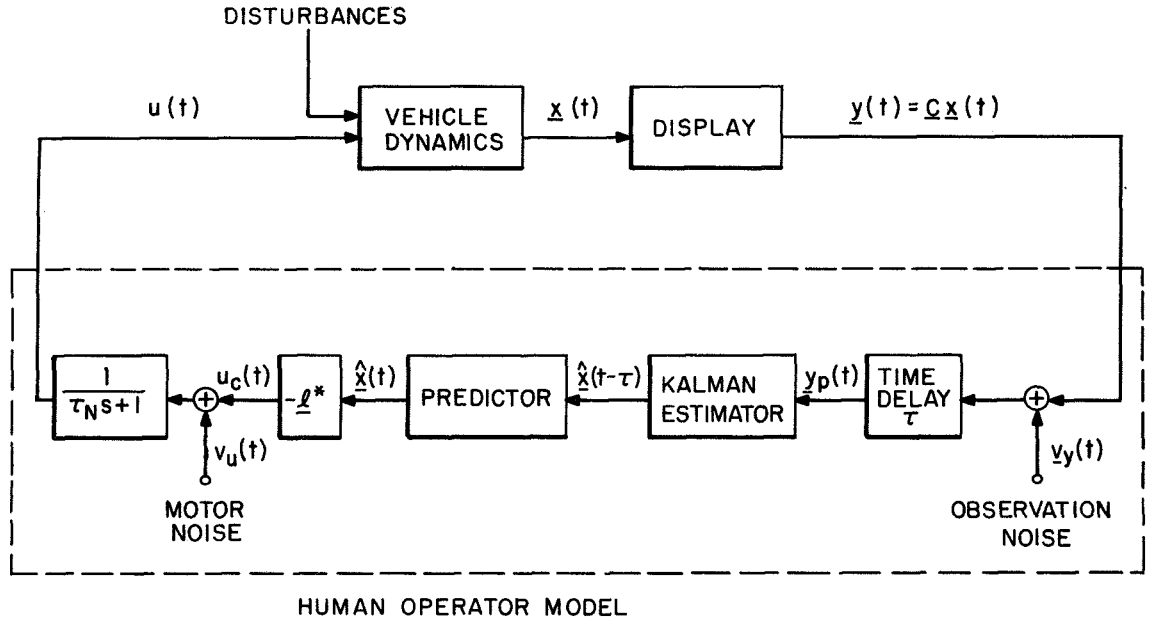

FIG.1 CONTROL THEORETIC MODEL OF OPTIMAL HUMAN BEHAVIOR

INPUTS

- VEHICLE DESCRIPTION
  - (a) System Dynamics and Input Shaping
  - (b) Displayed Variables
- TASK DESCRIPTION
  - (a) Cost Functional Weightings
- HUMAN DESCRIPTION
  - (a) Subjective Weightings
  - (b) "Neuromotor" Time Constant, τ_N
  - (c) Time Delay
  - (d) Motor Noise
  - (e) Observation Noise

OUTPUTS

- STATE, OUTPUT, AND CONTROL VARIANCES
- PILOT DESCRIBING FUNCTION AND REMNANT SPECTRA
- STATE, OUTPUT, AND CONTROL POWER SPECTRA (INPUT CORRELATED AND REMNANT CORRELATED)

FIG.2 MODEL INPUTS AND OUTPUTS

COMPUTER PROGRAMS

Two main programs have been written for using the optimal control model. The first program enables the user to specify the fixed system parameters. The second program solves the optimization problems associated with the model and provides human response prediction. Both programs are discussed below.

Fixed Parameter Specification

The quantities $\underline{A}, \underline{b}, \underline{W}, \underline{C}, \underline{d}$ are assumed to be fixed and parametrize the configuration of the system to be controlled. A computer program, INPUT, has been written to allow on-line user specification of these quantities. The parameters are outputed to a user specified file for subsequent reading by later programs. It is therefore possible (and in many cases convenient) to establish numerous such data files, each of which is associated with a different set of vehicle dynamics.

The program is initiated from the PDP-10 time-sharing monitor by typing

RUN DSK:INPUT↵

The program may be aborted at any time by typing successive ↑C (CONTROL-C), which then returns control to the time-sharing monitor. The INPUT program can then be reinitiated by typing .START↵

A flow chart for the INPUT program is shown in Fig. 3. Various features have been included for the user's benefit and for operational ease. Specifically,

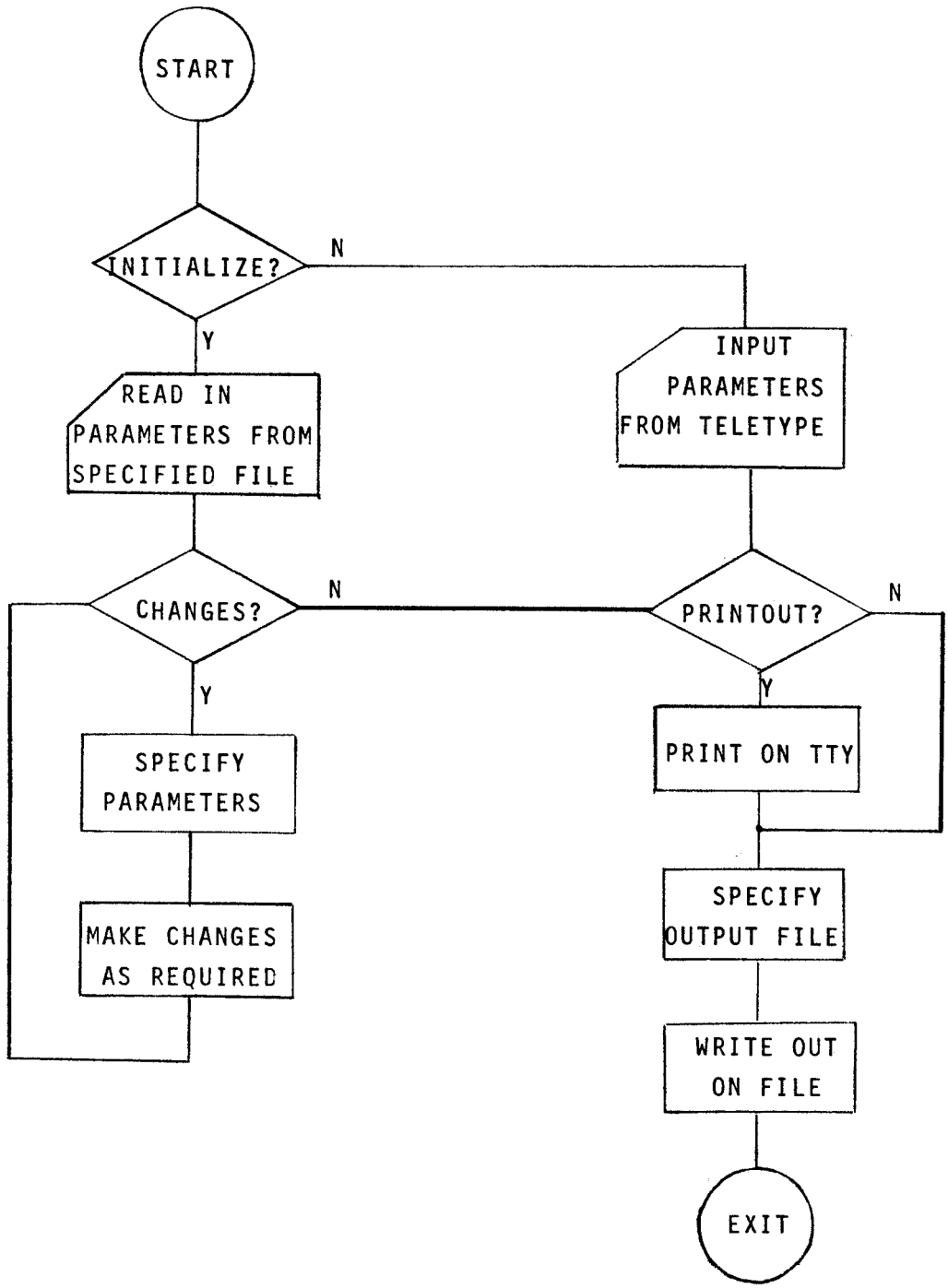

FIG. 3 FLOW CHART FOR PARAMETER SPECIFICATION PROGRAM

1. Initialization of parameters from Teletype

This is the usual way for first specifying input parameters. The program requests, in order, the parameters

n = number of states

n_c = number of noise shaping filter states

$\underline{A} = (a_{ij})$; i=1,2,...,n , j=1,2,...,n

$\underline{b} = (b_i)$; i=1,2,...,n

$\underline{W} = (w_i)$; i=1,2,...,n

m = number of outputs

$\underline{C} = (c_{ij})$; i=1,2,...,m , j=1,2,...,n

$\underline{d} = (d_i)$; i=1,2,...,m

Type-in errors can be immediately deleted by typing successive (RUBOUTS). Each (RUBOUT) deletes one preceding character which is then echoed for verification on the teletype. All user type-ins are actuated by a CARRIAGE RETURN (↵).

After all of the components of a matrix or vector (say $\underline{A}$) are typed in, an opportunity is given the user to make any final corrections.

2. Initialization of parameters from an existing file

This enables the user to change (or examine) any number of specific parameters on an existing file without having to retype all quantities. If this option is elected, the user must supply the name of the data file that contains $\underline{A}$,$\underline{b}$, etc. The parameters are read and changes are requested.

3. Parameter printout

When all of the parameters have been specified by the user (or read from a data file and subsequent changes made), a printed teletype listing may be obtained if so desired.

4. Frequencies

A preselected set of 15 frequencies from .05 to 40.0 rad/sec is generated for later use by the model. Subsequent frequency domain predictions will be made at these 15 values only. The preset frequencies are:

$$\omega = .05,.18,.52,1.0,1.5,2.0,2.9,4.0,5.7,8.,11.,16.,22.,32.,40$$

5. Output to data file

The user specifies the name of a data file on which all of the parameters are to be stored. This may be an existing file or a new file. File names are arbitrary, except that they must be five characters or less. After outputing, control is automatically transferred to the time-shared monitor.

Model Use

A computer program HRA3 (Human Response Analyzer - 3) as well as numerous subroutines has been written† to solve the optimization problems associated with our modelling approach. The main program consists of seven different but interactive parts. These parts involve parameter specifications, computations and type-out options. The specific function of each part is listed in Table 1.

HRA3 is actuated from the monitor system by typing

. RUN DSK:HRA3↵

†In Fortran IV for use on the PDP-10.

The program begins by requesting the name of the data file that contains the vehicle parameters (Part 1).

Computer control proceeds automatically from one part to the next in a sequential manner. However, it is possible for the user to interrupt and then (re)start the program at any part in order to respecify parameters and/or recompute model outputs.

TABLE 1

Part Functions and I-O of HRA3

Part No.	User Type-In	Computer Operation	Program Type-Outs
1	Name of Data file.	Read fixed system parameters from file.	
2	Cost functional weights q_i, r		
3	Control rate weighting, g	Obtain optimal feedback gains, τ_N.	value of τ_N
4	Humans time delay, τ	Compute $e^{A\tau}$.	
5	Motor noise covariance, V_u	Obtain portion of optimal cost.	
6	Observation noise covariances, $\underline{V}_y$.	Solve variance equation; compute optimal costs and noise ratios.	Normalized noise ratios (dB). System variances.
7	Transfer function, reflected remnant and spectra specification.	Obtain frequency domain representation.	Transfer function-Mag. and Phase. Reflected normalized obs. noise. Spectra-correlated and uncorrelated in dB.

The procedure for controlling program flow is quite simple. The user first interrupts the program by typing successive ↑C (which returns control to the time-sharing monitor), followed by .START↵. The computer responds by typing

TO PART:

and the user then types the desired part number. Before control is transferred to the specified part, a validity test is made – it is illegal to begin Part i if all preceding parts have not been completed.

A flow chart for HRA3 is presented in Fig. 4. Here we give a concomitant discussion of the I-O operation of each program part.

1. Vehicle parameters --- User specifies data file (created at some earlier time by INPUT) from which vehicle parameters are read. Data is read.

2. State and control weightings --- User specifies q_i, i=1,...,n and r.

3. Control rate weighting --- User specifies g. The optimal feedback gains are computed and τ_N is printed. The user then verifies if this value of τ_N is acceptable. If unacceptable, part 3 is repeated automatically.

4. Human's time delay --- User specifies τ.

5. Motor noise --- User specifies the motor noise covariance V_u. This quantity may be set to zero.

6. Observation noise --- User specifies the observation noise covariances V_{yi}, i=1,2,...,m. These numbers must be greater than zero. The optimal feedback structure as well as system performance is computed. The normalized motor noise and observation noises are printed.† An option is then given for printing all system variances (i.e., closed-loop performance). The user responds by typing Y or N, followed by ↵.

7. Frequency domain results --- Requests are made for outputing frequency domain data as predicted by the model. The user can output internal or equivalent transfer functions between u and any displayed quantity y_i. The internal transfer (I) is the associated component of $\underline{h}(s)$ in Eq. (9). The equivalent transfer (E) is the ratio of the transforms $y_i(s)$ and u(s). The equivalent transfer is what one normally measures in an experiment.

   Available is a prediction of remnant. The program combines all sources of remnant into a single equivalent noise source injected onto any specified output y_i and then normalized by σ^2_{yi}.

   Finally, the user can obtain the spectrum (both correlated and uncorrelated portions) of any single state (X), output (Y) or of the control (U). The printed spectra are one sided - i.e., for positive frequencies only.

   In all cases, predictions are made at a preselected set of 15 frequencies ranging from .05 to 40. rad/sec. The specific frequencies are read from the original data file that contains the parameters $\underline{A}$,$\underline{b}$,$\underline{C}$, etc.

As we have mentioned earlier, the user may restart the program at any specified part.

---

†These noise ratios are often more fundamental in human response analysis than are the noise magnitudes themselves, (e.g., see Ref. [2]).

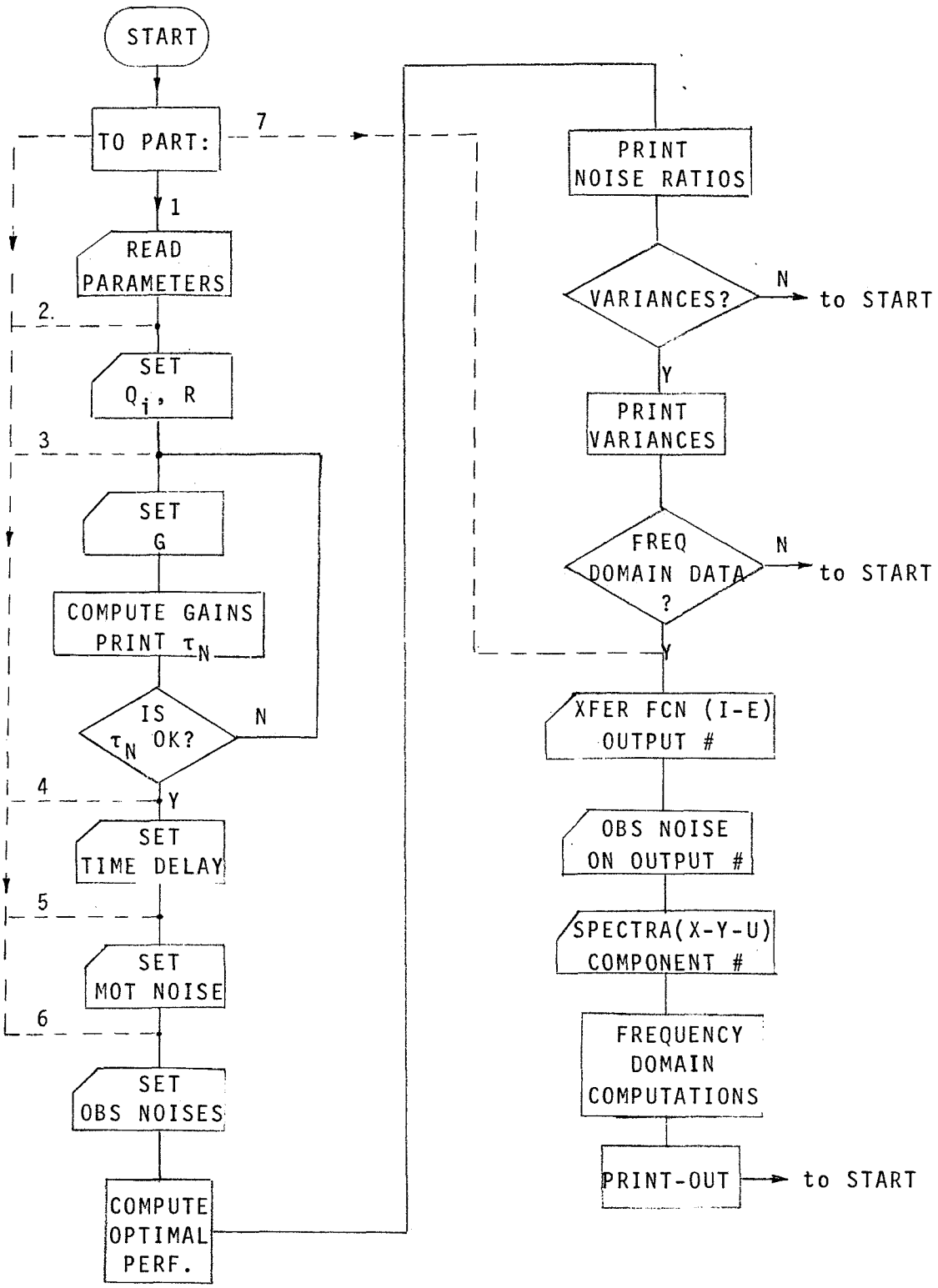

FIG.4 COMPUTER FLOW CHART FOR HUMAN RESPONSE ANALYSIS

AN EXAMPLE

System Inputs and Outputs

In this section we illustrate, by means of a simple example, the step by step procedure for using the described programs. We examine a compensatory tracking task of 1/s dynamics in which the human is given an explicit display of system error (e). We assume that the human also perceives directly the rate of change of error ($\dot{e}$). The system input disturbance is taken to be a first-order noise having a break frequency of 2 rad/sec and a variance of 1.0. Fig. 5 contains a block diagram of the system configuration.

The system state equations are first obtained in the required form. If $x_1(t)$ denotes the noise disturbance (which is added to control input) and $x_2(t)$ denotes the system error, e, then

$$\dot{x}_1(t) = -2x_1(t) + w_1(t)$$

$$\dot{x}_2(t) = x_1(t) + u(t)$$

(i.e. n=2 and n_c=1) where $w_1(t)$ is white noise with covariance $w_{11} = 4.0$ (so as to yield a required value of $E\{x_1^2\} = 1.0$). Thus, in matrix notation

$$\dot{\underline{x}}(t) = \underline{A}\ \underline{x}(t) + \underline{b}\ u(t) + \underline{w}(t)$$

where

$$\underline{A} = \begin{vmatrix} -2. & 0. \\ 1. & 0. \end{vmatrix}; \quad \underline{b} = \begin{vmatrix} 0. \\ 1. \end{vmatrix}; \quad \underline{W} = \begin{vmatrix} 4. & 0. \\ 0. & 0. \end{vmatrix}$$

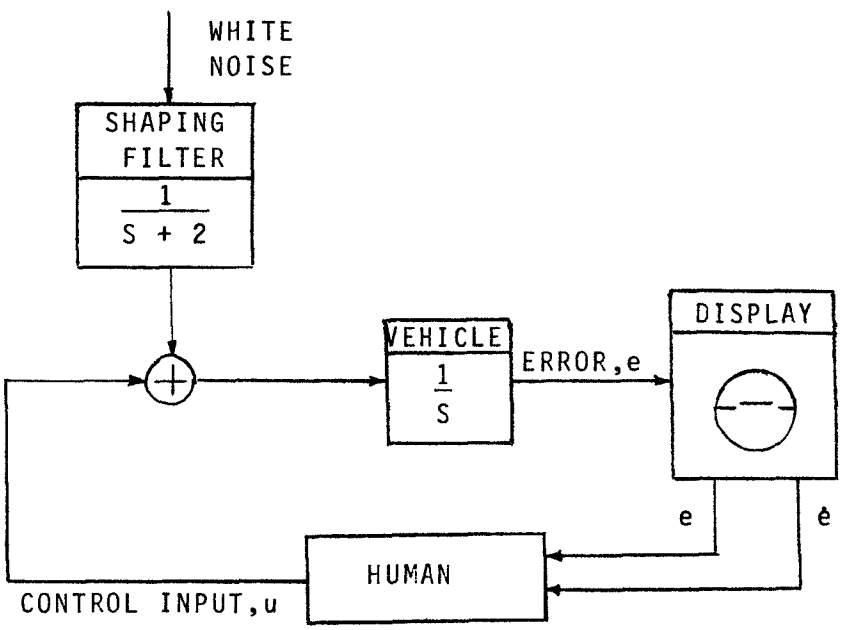

FIG.5 MANUAL TRACKING OF 1/S DYNAMICS WITH FIRST-ORDER NOISE DISTURBANCE

The system outputs (i.e. "displayed" quantities) y_1 and y_2 are respectively error (x_2) and error rate ($\dot{x}_2$). Thus m=2 and $\underline{y} = \underline{C}\,\underline{x} + \underline{d}u$ where

$$\underline{C} = \begin{vmatrix} 0 & 1 \\ 1 & 0 \end{vmatrix} ; \qquad \underline{d} = \begin{vmatrix} 0 \\ 1 \end{vmatrix}$$

The human's objective control task is to minimize mean-squared error. Thus, the cost functional J(u) is simply assumed to be

$$J(u) = \sigma^2_{x_2} + g\sigma^2_{\dot{u}}$$

i.e. $q_1 = 0$, $q_2 = 1$, $r = 0$. The control rate weighting g is, for the moment, arbitrary.

For the human's parameters we shall take $\tau = .20$, and we shall adjust the control rate weighting g to give a value of $\tau_n \approx .1$. Finally, we wish to choose values for the motor noise convariance V_u and the observation noise covariances V_{y_1}, V_{y_2} such that the resultant normalized notor noise is -25db and the resultant normalized observation noises are both -20 dB.† Clearly this will require on-line adjustment of the values V_u, V_{yi}.

We wish to predict a) the closed-loop performance, b) the closed-loop describing function relating control to error, c) remnant spectrum viewed as a single noise source injected onto system error, d) the human's control spectrum.

---

† These values are typical of those measured in single-axis tracking tasks.

Program Use

a. Data Specification

As discussed earlier, the first step in our analysis procedure is the creation of a data file that contains the fixed system parameters n, n_c, A, b, etc. The computer printout showing the initialization procedure is given in Fig. 6 . The underlined quantities are the user type-ins. Various type-in mistakes have been made intentionally in order to demonstrate the versatility of the program in making parameter corrections and changes. The various corrective features are shown with numbered tags. A corresponding description of each feature is given below.

(1) The letter "N" was inadvertantly struck while typing a_{12}. It was immediately deleted by typing RUBOUT. The computer responded by printing /N.

(2) b_2 was erroneously typed as 2.0. The error was immediately realized and corrected by typing 3 successive RUBOUT's (deleting the 3 characters 2.0 which are delimited by the computer) and then typing the correct value of 1.0.

(3) w_1 and w_2 were mistakenly interchanged. This error was not noticed by the user. Later corrections will have to be made here.

(4) c_{21} was erroneously typed as 2.0. The error was fixed using the program's internal correction routine.

(5) d_1 and d_2 were mistakenly interchanged. They were reversed using the correction routine.

(6) A parameter listing was obtained. The user realized the interchange of w_1 and w_2.

```
.RUN DSK:INPUT )

FIXED PARAMETERS FOR DX/DT=AX+BU+W, Y=CX+DU
INITIALIZE FROM FILE? N )

NO. OF STATES=2 )

 NO. OF NOISE STATES=1 )

 A( 1, 1)=-2.0 )
 A( 1, 2)=0N\N\.0 )
 A( 2, 1)=1.0 )
 A( 2, 2)=0.0 )
ANY CORRECTIONS? N )
   *****

 B( 1)=0.0 )
 B( 2)=2.0\0.2\1.0 )
ANY CORRECTIONS? N )
   *****

THE NOISE COVARIANCES:
 W( 1)=0.0 )
 W( 2)=4.0 )
 ANY CORRECTIONS? N )
   *****

NO. OF OUTPUTS=2 )

 C( 1, 1)=0.0 )
 C( 1, 2)=1.0 )
 C( 2, 1)=2.0 )
 C( 2, 2)=0.0 )
ANY CORRECTIONS? Y )
TYPE INDICES
I=2 )
J=1 )
 C( 2, 1)=1.0 )
ANY MORE?N )
    *****

 D( 1)=1.0 )
  D( 2)=0.0 )
 ANY CORRECTIONS? Y )
TYPE INDICES
I=1 )
 D( 1)=0.0 )
ANY MORE?Y )
 I=2 )
 D( 2)=1.0 )
 ANY MORE?N )
    *****

TYPEOUT PARAMETERS ON TELETYPE? Y )


A MATRIX:
  -2.000E+00   0.000E-01
   1.000E+00   0.000E-01


B MATRIX:
   0.000E-01
   1.000E+00


W MATRIX:
   0.000E-01
   4.000E+00


C MATRIX:
   0.000E-01   1.000E+00
   1.000E+00   0.000E-01


D MATRIX:
   0.000E-01
   1.000E+00

OUTPUT ON FILE: ABC )

FINISHED.
EXIT
 *C
```

FIG.6 SAMPLE PRINT-OUT OF INPUT PROGRAM

```
•RUN DSK:INPUT)

FIXED PARAMETERS FOR DX/DT=AX+BU+W, Y=CX+DU
INITIALIZE FROM FILE? Y)
FILE NAME: ABC)

PARAMETERS READ. ANY CHANGES? Y)
WHICH PARAMETER? W)
TYPE INDICES
I=1)
 W( 1)=      0.0000 CHANGE TO: 4.0)
ANY MORE?Y)
 I=2)
 W( 2)=      4.0000 CHANGE TO: 0.0)
ANY MORE?N)
    *****

 OTHER PARAM. CHANGES? Y)
WHICH PARAMETER? A)
TYPE INDICES
I=1)
J=1)
 A( 1, 1)=     -2.0000 CHANGE TO: -2.0)
ANY MORE?N)
    *****

OTHER PARAM. CHANGES? N)

TYPEOUT PARAMETERS ON TELETYPE? N)

OUTPUT ON FILE: ABC)

FINISHED.
EXIT
↑C
```

FIG. 7 AN EXAMPLE OF CHANGING PARAMETERS ON AN EXISTING FILE

(7) The parameters are outputed to a file named ABC.

In order to change parameters on the file ABC the same procedure as above is followed except that the parameters are now initialized from the pertinent file. The process by which w_1 and w_2 are changed is shown in the type-out of Fig. 7. Also shown is an examination of the quantity a_{11}.

b. Model Predictions

Having typed in the fixed parameters and stored them on a disk file, the user is now prepared to use the Human Response Analyser. Below we give the results of the step-by-step procedure in using HRA3.

1. Initializing and reading input parameters from file

```
.RUN DSK:HRA3)

 READ FIXED PARAMETERS FROM FILE:ABC)
FINISHED.
```

2. Specify q_i,r

```
STATE WEIGHTINGS, Q:
 Q( 1)=0.0)
 Q( 2)=1.0)
ANY CORRECTIONS? N)
   *****

 CONTROL WEIGHTING, R=0.0)
```

3. Choose g, compute τ_n

```
 CONTROL RATE WEIGHTING, G=.001)

TN= 0.126  IS THIS OK? N)
```

Since the computed value of $\tau_n \neq .1$, new values of g are requested until τ_n is suitably close to the desired

value:

```
CONTROL RATE WEIGHTING, G=.0004)

TN= 0.100  IS THIS OK? Y)
```

4. Specify τ

```
HUMAN"S T.D.=.2)
```

5. Choose V_u

```
MOTOR NOISE, VU:
VU( 1)=.01)
```

6. Choose V_y, compute noise ratios

```
OBS. NOISE, VY:
VY( 1)=.01)
VY( 2)=.01)
ANY CORRECTIONS? N)
   *****

  3 X 3 M: RANK 2 ←(This typeout is part of an
                    initialization routine only)
NOISE RATIOS:
VU( 1)=-27.8DB
VY( 1)=-13.0DB
VY( 2)=-25.7DB

VARIANCES? N)

TO PART:5)
```

Since the noise ratios are not as desired, the user decides not to type-out the system variances. Control can then be transferred to part 5 (respecify V_u) or part 6 (respecify V_y) in order for the user to readjust the noise values to give the proper ratios:

```
MOTOR NOISE,VU:
VU( 1)=.015)

OBS. NOISE,VY:
VY( 1)=.002)
 VY( 2)=.03)
 ANY CORRECTIONS? N)
   *****

 3 X 3 M: RANK 2

NOISE RATIOS:
VU( 1)=-26.3DB
VY( 1)=-20.6DB
VY( 2)=-21.5DB

VARIANCES? N)


TO PART:5)


MOTOR NOISE,VU:
VU( 1)=.02)

OBS. NOISE,VY:
VY( 1)=.0025)
 VY( 2)=.045)
 ANY CORRECTIONS? N)
   *****

 3 X 3 M: RANK 2

NOISE RATIOS:
VU( 1)=-25.2DB
VY( 1)=-20.2DB
VY( 2)=-20.1DB
```

Since the noise ratios are sufficiently close to the desired ratios, the user can stop iterating on V_u and V_y and obtain the resultant closed-loop system variances (if so desired)

```
VARIANCES? Y )

 X( 1) : 1.000E+00
 X( 2) : 8.284E-02
 U( 1) : 1.636E+00
 DU/DT : 6.767E+01
 Y( 1) : 8.284E-02
 Y( 2) : 1.451E+00
```

7. Frequency domain Results

The desired frequency domain representation is next obtained

```
FREQUENCY DOMAIN REPRESENTATION? Y )

XFER FCN: INTERNAL OR EQUIVALENT? E )
BETWEEN CONTROL AND OUTPUT #1 )

NORM. REMNANT: REFLECTED ON OUTPUT # 1 )

SPECTRAL DENSITY: X,Y,U? U )
COMPONENT # 1 )
```

FREQ	MAG	PHASE	REMN	CORR	UNCORR
0.05	13.8	-0.9	-14.5	-5.0	-51.3
0.18	13.8	-3.4	-14.5	-5.0	-40.2
0.52	13.6	-9.5	-14.6	-5.1	-31.0
1.00	13.3	-17.3	-14.9	-5.6	-25.4
1.50	12.9	-24.1	-15.4	-6.1	-21.9
2.00	12.5	-29.8	-15.9	-6.8	-19.4
2.90	12.1	-38.4	-16.9	-7.8	-16.4
4.00	11.6	-47.9	-18.2	-9.2	-14.2
5.70	11.2	-62.8	-20.0	-11.7	-12.8
8.00	12.7	-84.4	-22.2	-16.0	-13.7
11.00	14.5	-116.7	-25.0	-21.9	-17.0
16.00	18.8	-192.6	-29.2	-30.2	-23.1
22.00	16.8	-310.7	-31.2	-37.9	-27.2
32.00	11.0	-70.6	-31.1	-47.2	-30.0
40.00	10.0	-161.1	-32.2	-52.9	-32.9

```
TO PART: 4 )

HUMAN"S T.D.=.15 )
```

After completing the type-out the program control is transferred to the part director. The user can then start the program at any part. For example, to change τ, restart at part 4.

The user can stop the computer type-out at any time by stopping successive ↑C (which returns control to the monitor and then typing .START) which allows user part specification, e.g.

```
TO PART:7)

XFER FCN: INTERNAL OR EQUIVALENT? E)
BETWEEN CONTROL AND OUTPUT #1)

NORM. REMNANT: REFLECTED ON OUTPUT # 1)

SPECTRAL DENSITY: X,Y,U? Y)
COMPONENT # 1)

 FREQ     MAG      PHASE     REMN     CORR     UNCORR
 Ø.Ø5     13.8      -Ø.9    -14.5    -18.8    -25.3
 Ø.18     13.8      -3.4    -14.5    -18.8    -25.3
 Ø.52     13.6      -9.5↑C

.START)


TO PART:3)

CONTROL RATE WEIGHTING, G=
```

REFERENCES

1. Kleinman, D.L., Baron, S., and Levison, W.H., "An Optimal Control Model of Human Response, Part I: Theory and Validation," Automatica, Vol. 6, May 1970.

2. Levison, W.H., Baron, S., and Kleinman, D.L., "A Model for Human Controller Remnant," IEEE, Trans. on Man-Machine Systems, Vol. MMS-10, December 1969.

NASA-Langley, 1971 —— 10 CR-1753

NATIONAL AERONAUTICS AND SPACE ADMINISTRATION
WASHINGTON, D.C. 20546

OFFICIAL BUSINESS
PENALTY FOR PRIVATE USE $300

FIRST CLASS MAIL

POSTAGE AND FEES P
NATIONAL AERONAUTIC
SPACE ADMINISTRATI

POSTMASTER: If Undeliverable (Sectio
Postal Manual) Do Not

"The aeronautical and space activities of the United States shall be conducted so as to contribute . . . to the expansion of human knowledge of phenomena in the atmosphere and space. The Administration shall provide for the widest practicable and appropriate dissemination of information concerning its activities and the results thereof."

—NATIONAL AERONAUTICS AND SPACE ACT OF 1958

NASA SCIENTIFIC AND TECHNICAL PUBLICATIONS

TECHNICAL REPORTS: Scientific and technical information considered important, complete, and a lasting contribution to existing knowledge.

TECHNICAL NOTES: Information less broad in scope but nevertheless of importance as a contribution to existing knowledge.

TECHNICAL MEMORANDUMS: Information receiving limited distribution because of preliminary data, security classification, or other reasons.

CONTRACTOR REPORTS: Scientific and technical information generated under a NASA contract or grant and considered an important contribution to existing knowledge.

TECHNICAL TRANSLATIONS: Information published in a foreign language considered to merit NASA distribution in English.

SPECIAL PUBLICATIONS: Information derived from or of value to NASA activities. Publications include conference proceedings, monographs, data compilations, handbooks, sourcebooks, and special bibliographies.

TECHNOLOGY UTILIZATION PUBLICATIONS: Information on technology used by NASA that may be of particular interest in commercial and other non-aerospace applications. Publications include Tech Briefs, Technology Utilization Reports and Technology Surveys.

Details on the availability of these publications may be obtained from:

SCIENTIFIC AND TECHNICAL INFORMATION OFFICE

NATIONAL AERONAUTICS AND SPACE ADMINISTRATION

Washington, D.C. 20546